Norwegian University of Life Sciences

Master's Thesis 2022 60 ECTS
Faculty of Environmental Sciences and Natural Resource Management

Detection of tire and road wear particles in duck mussels (*Anodonta anatina)* from a road-near lake in Norway using various analytical techniques

Ole-Johan Næss Holm
Environment and natural resources

Acknowledgements

In January 2020 I was scoping out possibilities for my MSc thesis. It became clear that I wanted to write about something I did not have a lot of knowledge about through my study program, but rather test the transferability of environmental sciences through a topic of personal interest. Microplastics were something I wanted to learn more about, and after a deep dive into the topic, I am pleased with all I have learned. I am happy to have contributed with knowledge in this field, and hopefully my work will fill a small part of the knowledge gap that exists within microplastics as an environmental problem.

After five years of studying environment and natural resources at the Norwegian university of life sciences (NMBU), this thesis marks the end of my MSc degree. It has been challenging, in a good way, and the knowledge gained by this process will follow me throughout my life.

My thesis is a part of the phD-project microROAD, funded by the Norwegian Public Roads Administration (NPRA) (through NordFoU) and the Norwegian Institute of Water Research (NIVA). The project is a collaboration between NIVA, NMBU and NPRA.

Firstly, I would like to thank my supervisors Sondre Meland (NMBU, NIVA), Ole Christian Lind (NMBU) and Elisabeth Rødland (NIVA) for great guidance, discussions and proof reading. Marit Nandrup Pettersen (NMBU) and Ian Byrnes (NMBU) also deserves to be thanked, for helping me at the lab and for discussions of results. Lastly, I would like to thank everyone else who has contributed to this work, both scientifically and socially.

Abstract

Microplastic particles (MP) in the environment are an emerging problem, and the environmental impacts are still to be completely understood. It is known that small plastic particles have been in the environment for a long time, and recent research on the topic has increased drastically. Tire and road wear particles (TRWP) are assumed to be one of the largest sources of microplastics to the environment. Thus, the United Nations (UN) has called out MP as an environmental emergency and included microplastics in their sustainable development goals (SDG). Although the knowledge base on the topic is increasing, a common challenge faced by researchers is the lack of standardized quantification methods, making comparisons of studies challenging, especially in regards of TRWP.

TRWP are reported to have high contents of sulfur (S), silicon (Si) and zinc (Zn) along with a recognizable morphology. It was hypothesized that micro-X-ray fluorescence (μ-XRF) could detect these elements and, thus be a novel method to identify TRWP in biological samples. Hence, an approach based on μ-XRF and image analysis techniques with ImageJ were developed. Reference tire particles (TP_{ref}) were analyzed, both as free particles and on different sample media. Secondly, it was hypothesized that mussels found close to a road, would have a higher content of TRWP than mussels found farther from a road. For this purpose, duck mussels (*Anodonta anatina*) from the road-near lake Padderudvann were acquired. Samples were taken from the roadside (L1) and a reference site (L2) on the far side of the lake. The mussels were digested using sodium hypochlorite (NaClO) and filtered. Filters were analyzed with light microscopy and μ-XRF.

Measurements of TP_{ref} using inductively coupled plasma mass spectrometry (ICP-MS) and μ-XRF are in line with reported amounts of signature elements from the literature. TP_{ref} were detected with μ-XRF in and on top of sample material. Principal component analysis (PCA) shows that mussels from L1 had a higher content of zinc and copper (Cu) than mussels from L2. There was a statistically significant difference in potential TRWP found through microscopy between the mussels from the two locations, with mussels from L1 having the highest number of potential TRWP. With the developed approach using μ-XRF it was found one potential TRWP.

Performed analyses in this thesis suggests that μ-XRF could be a way of quantifying TRWP in mussels, hence first hypothesis is supported. The challenge faced with this approach was the residues on the filters hampering excitation of metals in potential TRWP, as well as causing self-absorption of fluorescent X-rays. If the digestion process is optimized, μ-XRF has the potential of being a robust approach to identify TRWP in biological samples. The second hypothesis is also supported based on the content of metals related to road runoff, as well as content of potential TRWP. However, neither of the hypotheses can be confirmed, nor denied by the results of this present thesis.

Sammendrag

Mikroplastpartikler (MP) i miljøet er et stadig fremtredende problem. Små plastpartikler har sirkulert i miljøet lenge og de miljømessige konsekvensene er fortsatt usikre. Det har vært en kraftig økning i forskning innenfor dette feltet de siste årene. Dekk- og veislitasjepartikler (TRWP) er antatt å være blant de største kildene til mikroplastforurensning. De Forente Nasjoner (FN) har utpekt MP som en miljømessig krise, og dermed inkludert mikroplastforurensning i sine bærekraftsmål (SDG). En stor utfordring i forskningsmiljøet er mangelen på standardiserte kvantifiseringsmetoder, noe som gjør sammenligning av studier utfordrende, spesielt med tanke på TRWP.

TRWP har et høyt innhold av svovel (S), silisium (Si) og sink (Zn) i tillegg til å ha en gjenkjennelig morfologi. Den første hypotesen ble derfor at mikro røntgenfluorescens (µ-XRF) kan oppdage disse grunnstoffene, og at TRWP kan identifiseres i biologiske prøver. En metode basert på µ-XRF og bildeanalyse med ImageJ ble utviklet. Referansebildekkpartikler (TP_{ref}) ble analysert på og i ulikt prøvemateriale, og som selvstendige partikler. Den andre hypotesen omhandler at muslinger som er funnet i nærheten av en vei vil inneholde mer TRWP enn muslinger som er funnet lenger unna. I forbindelse med dette ble andemuslinger (*Anodonta anatina*) fra den veinære innsjøen Padderudvann undersøkt. Muslingene ble samlet inn fra veisiden (L1) av innsjøen, og fra en referanselokalitet (L2) på den andre siden av innsjøen. Muslingene ble løst opp med natriumhypokloritt (NaClO) og deretter filtrert. Filtrene ble analysert med lysmikroskop og µ-XRF.

Målinger av referansebildekkpartikler (TP_{ref}) som ble gjort med induktivt koblet plasma massespektrometri (ICP-MS) og µ-XRF samsvarte med de rapporterte mengdene av signaturgrunnstoffene fra litteraturen. TP_{ref} ble påvist både i og på prøvematerialet med µ-XRF. Hovedkomponentanalyse (PCA) tyder på at muslingene fra L1 hadde et høyere innhold av sink og kobber (Cu) enn muslinger fra den L2. Det var en statistisk signifikant forskjell i potensielle TRWP funnet med mikroskop i muslinger fra de to lokalitetene. Muslinger fra L1 hadde den største mengden potensielle TRWP. Ved bruk av den nyutviklede µ-XRF-metoden ble det funnet én potensiell TRWP.

Analyser som er gjort i denne masteroppgaven antyder at μ-XRF kan identifisere TRWP i muslinger, noe som støtter den første hypotesen. En utfordring med denne metoden var at rester på filtrene hindret eksitering av metaller i potensielle TRWP i tillegg til å føre til selv-absorpsjon av fluoriserende røntgenstråler. Dersom oppslutningsprosessen optimaliseres, har μ-XRF potensiale til å bli en robust metode for å identifisere TRWP i biologiske prøver. Hypotese 2 støttes også, på bakgrunn av det det målte innholdet metaller som kan relateres til veiavrenning i muslingene, i tillegg til innhold av potensielle TRWP. Ingen av hypotesene kan bekreftes eller avkreftes på bakgrunn av resultatene i denne masteroppgaven.

Table of contents

List of abbreviations

Abbreviation	Meaning
6-PPDQ	N-(1,3-dimethylbutyl)-N´-phenyl-p-phenylenediamine quinone
BR	Butadiene Rubber
CN	Cellulose Nitrate
DI H2O	Deionized water
E18	European highway 18
ICP-MS	Inductively Coupled Plasma Mass Spectroscopy
KOH	potassium hydroxide
L1	Roadside location
L2	Reference site
MP	Microplastic particles
NaClO	Sodium hypochlorite
NR	Natural rubber
PAH	Polycyclic aromatic hydrocarbons
PBDE	Polybrominated diphenyl ethers
PCA	Principal component analysis
PCB	Polychlorinated biphenyls
PE	Polyethylene
PM_{10}	Particulate Matter < 10 µm
$PM_{2.5}$	Particulate Matter < 2.5 µm
PMB	Polymer modified bitumen
POPs	Persistent organic pollutants
PP	Polypropylene
PS	Polystyrene
Pyr-GC-MS	Pyrolysis gas chromatography mass spectroscopy
RM	Road markings
ROI	Regions of interest
RWP	Road wear particles
SBR	Styrene butadiene rubber
SS	Suspended solids
TP	Tire particles
TP_{ref}	Reference tire particles
TRWP	Tire and road wear particles
TWP	Tire wear particles
TWW	Tunnel wash water
W-probe	Tungsten probe
AADT	Annual average daily traffic
µ-XRF	Micro-X-ray fluorescence
µFT-IR	Micro Fourier transform infrared spectroscopy

List of Figures

List of tables

1 Introduction

Microplastics (MP) is an emerging problem globally, however, the effects and amplitude of this problem is yet to be fully understood. The United Nations Environmental Programme (UNEP) have released a report calling plastic pollution an urgent environmental emergency (Tsakona et al., 2021), and this year it was reported findings of MP in human blood (Leslie et al., 2022). Plastics are found in all types of surface waters. It is estimated that 14 million tons of plastic enters the ocean every year (IUCN, 2021).

Small plastic particles have been circulating in the environment for a long time. The first report on small plastic particles was released by Carpenter et al. (1972). In the early 2000s it was reported that plastic particles were accumulating in the oceans by Thompson et al. (2004). Research on the topic has since then received a lot of attention, and new research is released in a high frequency (Lusher et al., 2017). In the mid 2010s the first reports about national microplastic budgets were released. These early reports contained a lot of assumptions since not many countries had made these budgets at the time. Since then, there has been a lot of focus on the matter, and more reports about national and international microplastic emissions have been released (Hann et al., 2016; Lassen et al., 2015; Sundt et al., 2016). This has led to more understanding around national and international emissions, thus expanding the knowledge base on the topic.

In recent years tire and road wear particles, often referred to as TRWP, have been included in the category of microplastics. Although it does not match the common description of microplastics, the rubber in tires, road paving, and road markings (RM) contain several polymers (Kole et al., 2017; Rochman et al., 2019; Rødland et al., 2022c; Wagner et al., 2018). Many countries are reporting that the biggest contributor to microplastic emissions are related to roads and traffic. In Norway it is estimated that roads and traffic is the source of 41,6% of all microplastic emissions (Sundt et al., 2020; Vogelsang et al., 2020).

The United Nations sustainable development goal (SDG) 14, life below water, is taken into consideration in this thesis. Specifically target 14.1: *By 2025, prevent and significantly reduce marine pollution of all kinds, in particular from land-based activities, including marine debris*

and nutrient pollution. Indicator 14.1.1 specifies further: *(a) Index of coastal eutrophication; and (b) plastic debris density* (UN, 2015). According to Walker (2021) there are at least 11 other SDG that are directly or indirectly impacted by microplastic pollution. This illustrates the amplitude of microplastics as a problem to a sustainable future.

The methods being used to quantify and analyze MP contamination varies greatly. As of now there is no standardized procedure for detection and quantification of MP. Different methods are being used, such as pyrolysis gas chromatography mass spectroscopy (pyr-GC-MS) (Rødland et al., 2022c), micro Fourier transform infrared spectroscopy (μFT-IR) (Bråte et al., 2020) and more (Atici, 2022; Kovochich et al., 2021; Van Cauwenberghe et al., 2015). If results from different reports are to be comparable, there should be a standard way of analyzing as stated by Hartmann et al. (2019). Thus, addressing the importance of analytical approaches being used and strive for a standardized procedure is an important matter in this field of environmental science.

Objectives and hypotheses

There are two main objectives in this present thesis. The first addresses the need for expanding the knowledge base on analytical approaches used for identification and quantification of TRWP in biological samples. This will be done through developing an approach using micro-X-ray fluorescence (μ-XRF). The second objective was to apply this developed approach to identify TRWP in duck mussels (*Anodonta anatina*) from Padderudvann.

The following hypotheses were formed:

Hypothesis 1: μ-XRF can be applied to identify and quantify TRWP in biological samples.

Hypothesis 2: Mussels found close to a road have a higher content of TRWP than mussels found farther from a road.

2 Background

2.1 The beginning of the "plastic age"

Plastics has been widely used for a long time. The first polymers were created by accident or ruled not useful for further research. The first mass produced polymer was made because of a lack of ivory, mainly used in the making of billiard balls. A billiards supplier started a contest in 1863 with a ten-thousand-dollar reward for whoever that could make a replacement substance for ivory. After years of trial-and-error John Wesley Hyatt made the discovery of a cellulose material, which him and his brother called "celluloid". This material was not perfect for billiards, but for production of hair combs it was very good (Freinkel, 2011). This marks the starting point of the "plastic Age" (Wagner et al., 2014).

Since then, plastics has become one of the most used materials in the world. Plastics can be used to almost anything and take most forms and shapes. But there is no ordinary plastic. Over the years a plethora of different polymers have been developed (Table 2.1), and their respective versatility and usability have made them necessary in our everyday life.

Table 2.1: Different polymers, discovery year and discoverer. Based on Lambert (2013).

YEAR	POLYMER TYPE	INVENTOR
1839	Natural rubber latex	Charles Goodyear
1839	Polystyrene	Discovered by Eduard Simon
1862	Parkesine	Alexander Parkes
1865	Cellulose acetate	Paul Schützenberger
1869	Celluloid	John Wesley Hyatt
1872	Polyvinyl chloride	First created by Eugen Baumann
1909	Bakelite	Leo Hendrik Baekland
1926	Plasticized PVC	Walter Semon
1933	Polyvinylidene chloride	Ralph Wiley
1935	Low-density polyethylene	Reginald Gibson and Eric Fawcett
1936	Acrylic or polymethyl methacrylate	Unknown
1937	Polyurethane	Otto Bayer and co-workers
1938	Polystyrene	As a commercially viable polymer
1938	Polyethylene terephthalate	John Whinfield and James Dickson
1942	Unsaturated polyester	John Whinfield and James Dickson
1951	High density polyethylene	Paul Hogan and Robert Banks
1951	Polypropylene	Paul Hogan and Robert Banks
1953	Polycarbonate	Hermann Schnell
1954	Styrofoam	Ray McIntire
1960	Polylactic acid	Patrick Gruber
1978	Linear low-density polyethylene	DuPont

2.2 Plastics in the environment

The versatile use of plastics, along with the vast amount of one-time plastic products, plastic pollution is a common sight all over the world. Many countries lack the infrastructure to properly manage plastic waste, or lack the funds to create sanitary landfills or facilities for incineration or recycling (IUCN, 2021). The most common polymers found in the environment are polyethylene (PE), polypropylene (PP), and polystyrene (PS) (Figure 2.1) (Cózar et al., 2015; Fischer et al., 2019; GESAMP, 2016; La Nasa et al., 2020; PlasticsEurope, 2019; SAPEA, 2019; Suaria et al., 2016; Zhang et al., 2019).

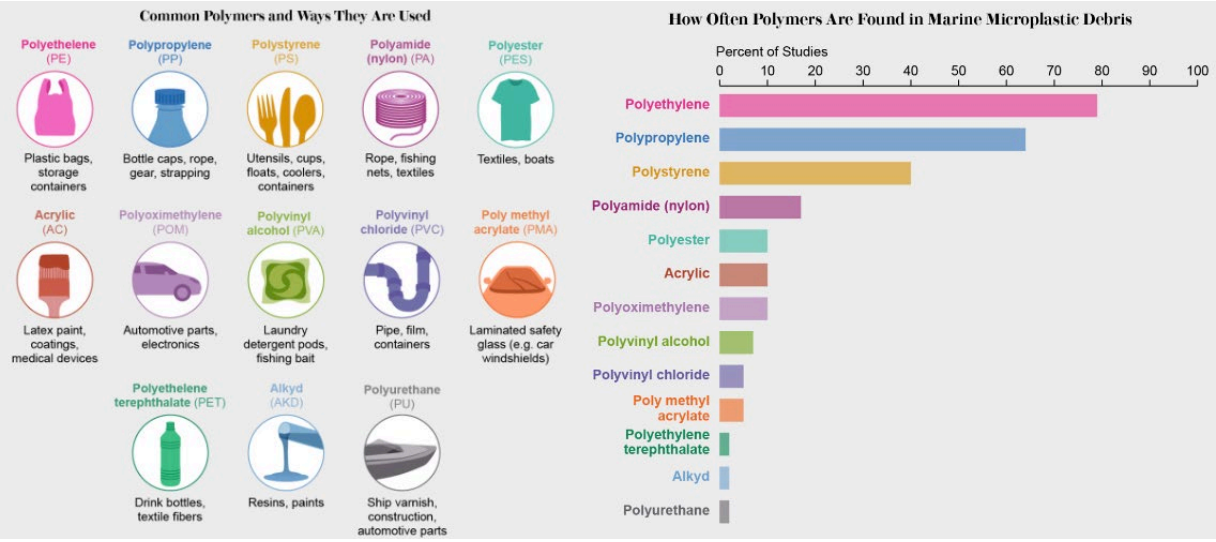

Figure 2.1: Products containing common polymers (left), and how often the polymers are found in the environment as microplastics in marine environment (right). Copied from Thompson (2018). Data is collected from GESAMP (2016).

Microplastics are defined by their size, which is in the microscopic scale. The common definition to use today was agreed upon in a workshop arranged by the National Oceanic and Atmospheric Administration (NOAA). At this workshop scientists agreed that the defined size range for microplastics should be particles smaller than 5 mm in the longest diameter (Arthur et al., 2009). In later years there have been discussions and proposals to find more accurate definitions of size distribution. This has led to newer definitions in size categorization of plastic litter. Four different categories are now being used. These

categories are, in descending size order; macroplastics, mesoplastics, microplastics and nanoplastics. However, there is not yet agreed upon a standard size definition on the four categories as of 2019 (Hartmann et al., 2019), and over time there has been proposed many different classification systems (Figure 2.2).

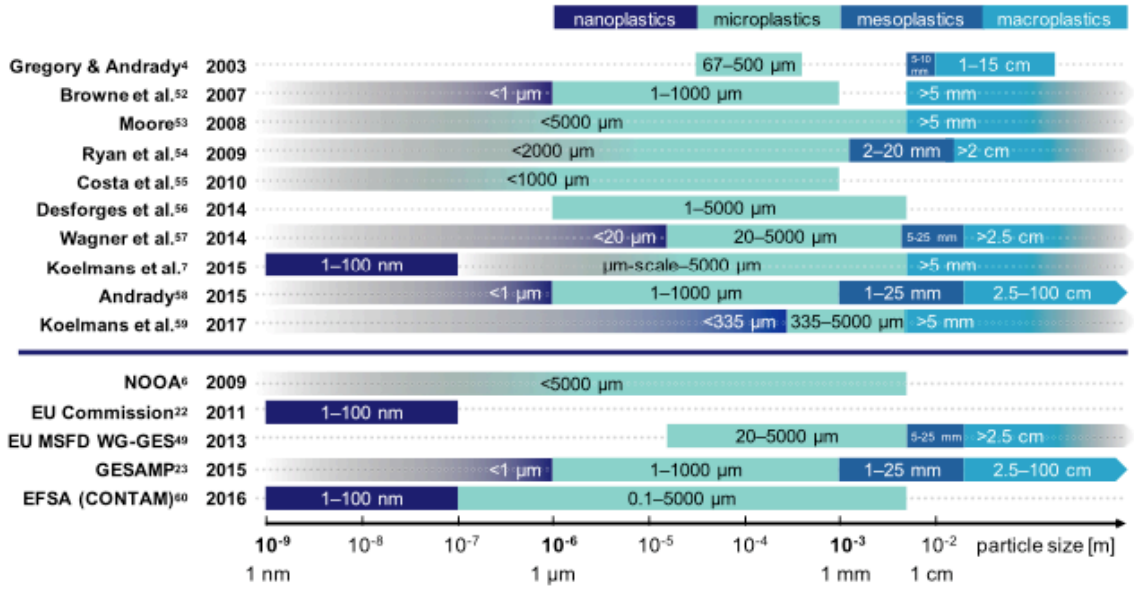

Figure 2.2: Examples and differences of size fraction categorization of plastic debris. Examples from scientific literature are found above the blue line, and examples from institutional reports are found under the blue line. Copied from Hartmann et al. (2019).

It is common to distinguish between primary and secondary sources of microplastics. Primary microplastics are plastic particles designed to be used in that specific size, such as small plastic beads in cosmetic products, and microfibers from clothing or fishing nets. Secondary microplastics are divided into two categories. Category A consists of fragments of bigger products that have broken off into smaller pieces. Category B consists of particles broken off bigger objects like category A, but broken down even more through further abrasion (GESAMP, 2016).

Road associated microplastics

Tire and road wear particles consists of three main components containing polymers. Tire wear particles (TWP), road wear particles (RWP) and particles from road markings (RM). TRWP are usually a mix of these three, as well as minerals and other particles in the road environment. TWP are reported to contain 40-50% rubber. These rubbers are styrene butadiene rubber (SBR), butadiene rubber (BR) and natural rubber (NR). 30-35% are fillers, often carbon black and silica. 2-5% are vulcanizers, such as zinc oxide (ZnO) and sulfur (S). The last 5-10% are different types of additives (Baensch-Baltruschat et al., 2020; Jekel, 2019; Sommer et al., 2018; Wagner et al., 2018). Kreider et al. (2009) analyzed tire particles (TP) and found a content of 54000 ppm Si, 12000 ppm S, and 9000 ppm Zn, and suggested using these as elements to identify TRWP. To use Zn and S as signature elements are supported by Klöckner et al. (2019) who analyzed TP from 21 different tires and found mean values of 16 ± 7.1 mg/g S and 8.7 ± 2.0 mg/g Zn. RWP are fragments of the asphalt. RWP are reported to consist mainly of minerals (~95%), meaning that elements such as silicon, aluminium (Al), calcium (Ca), sodium (Na), potassium (K), manganese (Mn), iron (Fe), and sulfur are abundant. The mineral particles are held together by polymer modified bitumen (PMB) (~5%) (Sommer et al., 2018), which has a polymer content of 3-10% (Saba et al., 2012). Road markings are usually thermoplastic and water based polymer paint, with a respective polymer content of 1-5% (Sundt et al., 2014).

Tire and road wear particles are now recognized as MP, and are known to be a common contaminant even though they do not fit the classic description for MP (Sundt et al., 2014). According to the definitions formed by GESAMP (2016) TWP are secondary microplastics in category A. Through further abrasion between cars and road surface, RWP and RM will get mixed with TWP, minerals and other particles. This process produces TRWP, which can further be defined as secondary category B microplastics. In environmental samples TRWP will often contain different amounts of non-polymers (Figure 2.3) (Kovochich et al., 2021). There can be great variations in mineral content in TRWP. The literature states that TRWP can contain 6–53% of minerals and other particles, potentially making it harder to recognize in environmental samples (Klöckner et al., 2021; Kreider et al., 2009; Sommer et al., 2018).

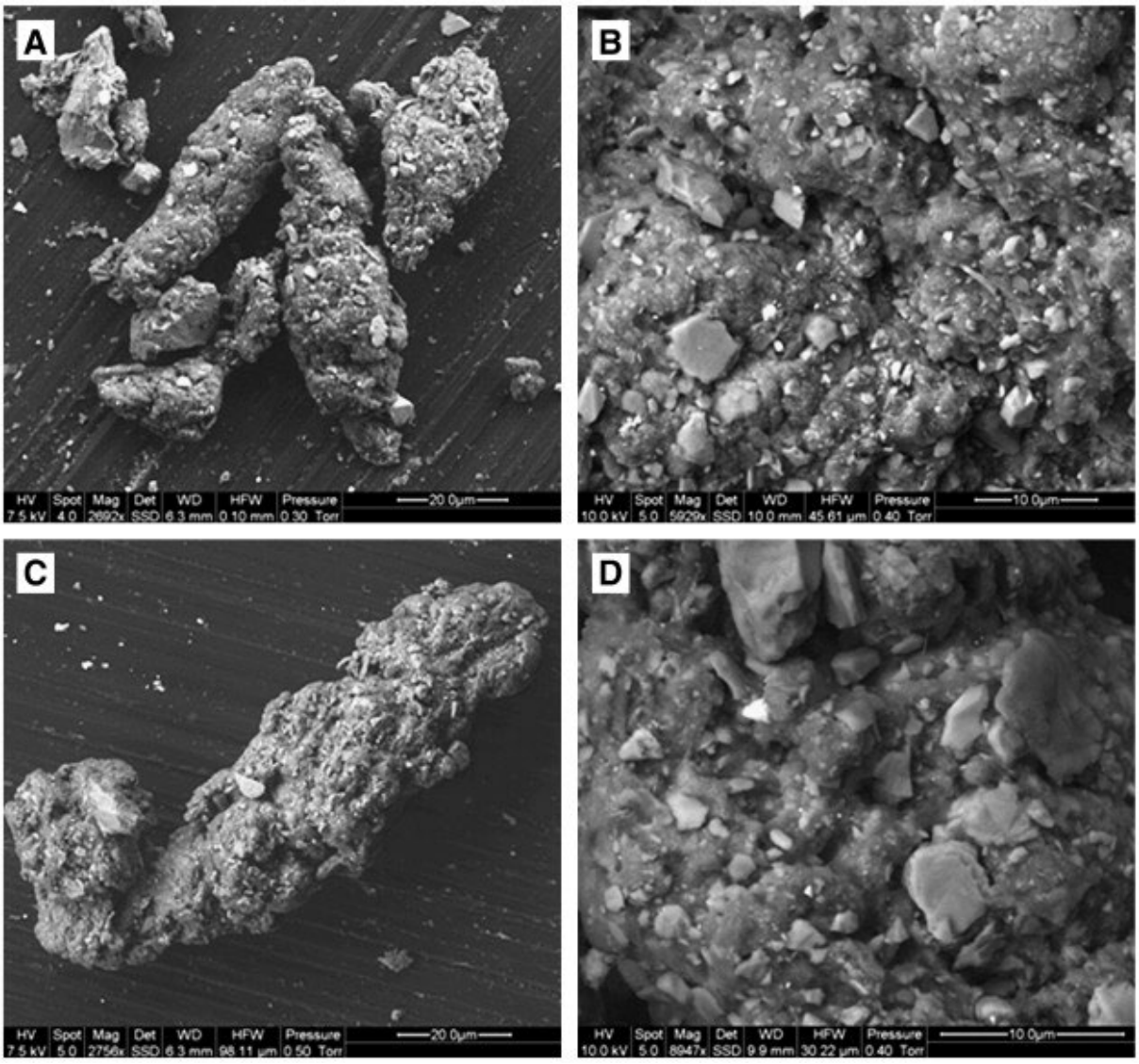

Figure 2.3: Scanning electron microscope images of RWP (A, B) and TWP (C, D). Images B and D show a higher magnification of the same particles, which clearly shows the encrusted minerals on the surface. Copied from Kreider et al. (2009).

Microplastic particles are typically found as thermoplastics in the size range of 1 µm – 5 mm, often colourful with a smooth shiny surface. TRWP are often elongated with rough edges, dark coloured, and encrusted with other materials and minerals. Reportedly, 85% of TWP are in the size fraction of 50-350 µm (Kreider et al., 2009) (Table 2.2). However, a recent study from Klöckner et al. (2021) on tunnel road dust suggests that a large fraction of TWP have a size smaller than 50 µm. Pure TWP have a density of 1.2 g/cm^3 (Degaffe & Turner,

2011). TRWP however, have a density that are dependent on the mineral content of the respective asphalt and other particles that are mixed into the particles. The density of TRWP is reportedly between 1.2 – 2.1 g/cm^3 (Jung & Choi, 2022; Kayhanian et al., 2012; Klöckner et al., 2021).

Table 2.2: Size distribution of tire wear particles. Based on Kreider et al. (2009) and (Klöckner et al., 2019).

SIZE BIN (µM)	VOLUME%
50-350	85
30-50	8
10-30	2
<10	5

2.3 Spreading pathways

Microplastics from roads and traffic may end up in the environment through numerous pathways (Figure 2.4). The pathways of TRWP into the environment are complex, and each pathway are influenced by several factors. These factors may be both spatial and temporal variations depending on local conditions such as weather, speed limit, annual average daily traffic (AADT), and more (Rødland et al., 2022b; Vogelsang et al., 2020).

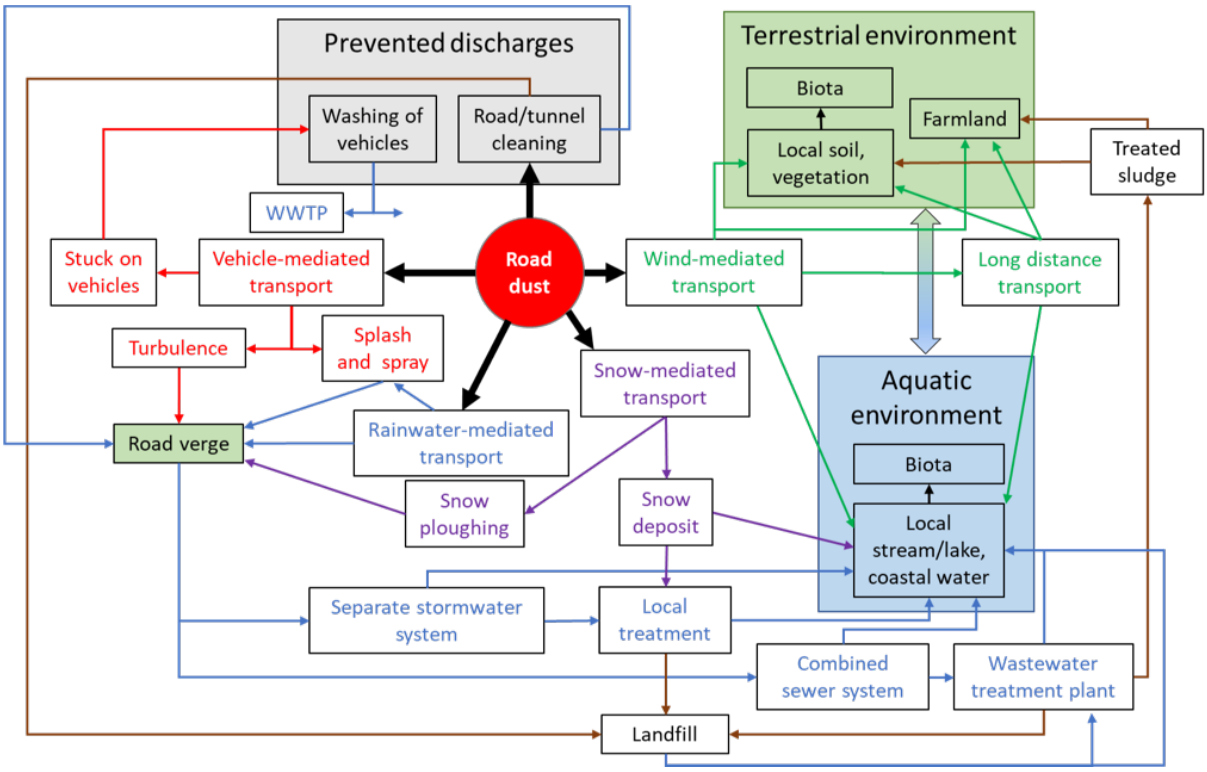

Figure 2.4: Potential pathways for microplastics from roads to aquatic (blue background) and terrestrial (green background) environments. Copied from Vogelsang et al. (2020).

Particles smaller than 2.5 – 10 µm, also called $PM_{2.5}$ and PM_{10}, have a potential to be airborne (Padoan & Amato, 2018). However, particles in the size range smaller than 10 µm only makes up ~5% of the total emissions (Kreider et al., 2009). According to Vogelsang et al. (2020), wind conditions may play a large role in long range spreading of these particles, causing a variation between local conditions (Figure 2.5). Particles in this size range may stay airborne for hours, travelling distances up to 50 km in the right conditions (Kole et al., 2015).

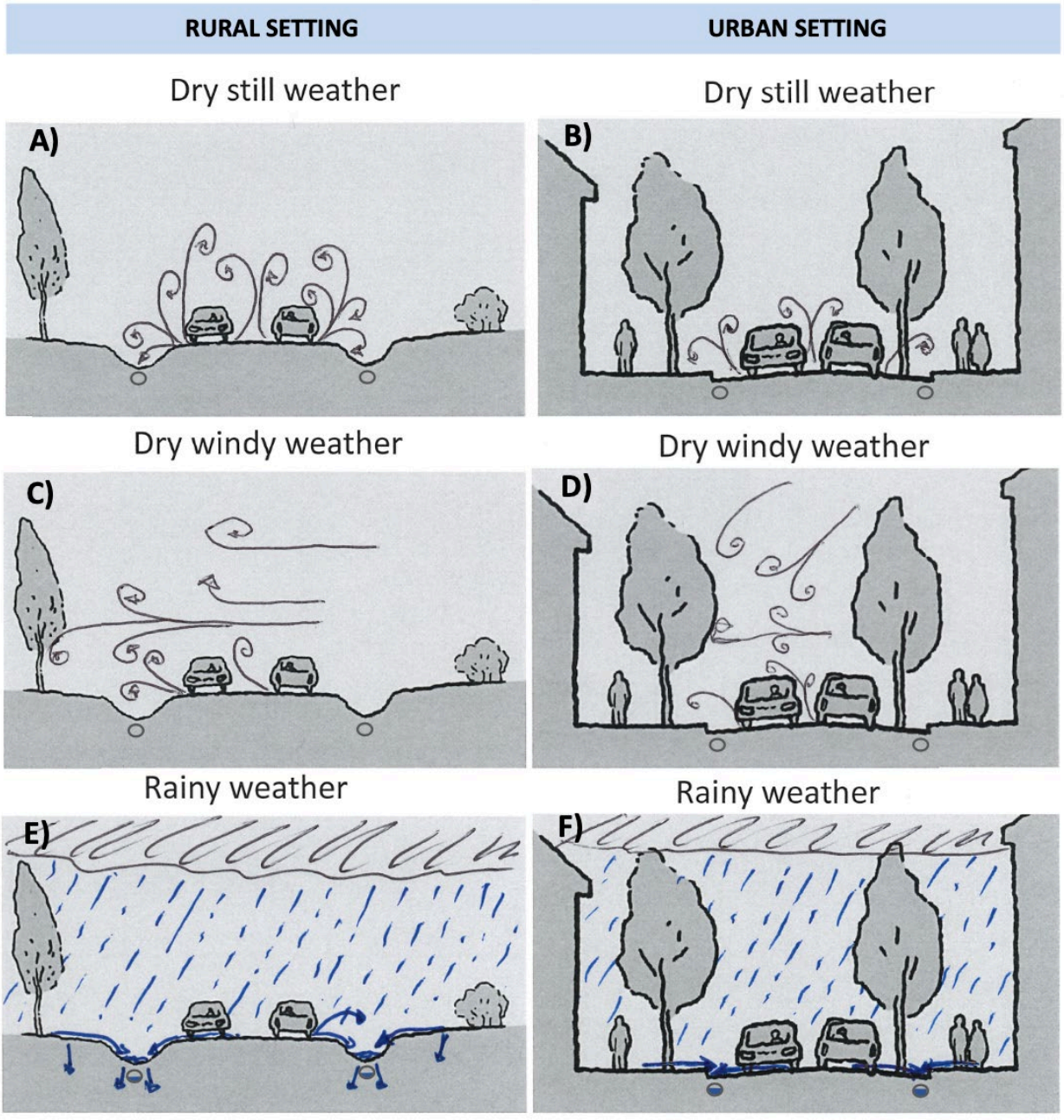

Figure 2.5: Illustrations of how weather conditions can affect particle spreading in rural (left) and urban (right) environments. Copied from Vogelsang et al. (2020), adapted from NPRA (2014b).

Particles may spread far by wind but spreading distance are dependent on weather conditions. This is due to the raindrops ability to catch airborne particles and bring them to the ground (Vogelsang et al., 2020). If the road is wet, particles will be trapped by the water, hindering long transportation of pollutants. According to Vogelsang et al. (2020), snowy weather decreases the spreading distance further because of slower falling speed and bigger size of the snowflakes. This happens even though there are more small sized particles caused by usage of studded tires causing abrasion to the road paving, generating more RWP.

Following a rain event water with high TRWP concentration will be transported through runoff into swales, ditches, or drains. This water is likely to spread the particles to nearby water sources such as lakes and rivers (Vogelsang et al., 2020). Brodie (2007) found that transport of particles increased with rain intensity. However, at low intensities (0.5-2 mm/h) particles accumulated on the road. Further, after 5 hours of intense rain the transported volume of particles levelled out. For long rainfall events there was not found a clear relationship between particle transport and rain intensity. Also, on wet roads there are a chance that particles get spread through water droplets and splashing. These droplets can travel some distance, and make particles stick to cars. Depending on size and wind conditions, the travel distance of the particles increase with smaller droplet sizes (Vogelsang et al., 2020).

During the winter season in Norway the roads are plowed for snow. This can lead to a lot of particles accumulating in the snowbanks. This will depend on the snow melting, and whether the roads are wet or dry, speed limits and AADT (Rødland et al., 2022b). Recently, a study by Rødland et al. (2022b) investigated snowbanks for TRWP and found that the amounts of particles in roadside snow far exceeded the levels of what is allowed to release in tunnel wash water (TWW). It is common procedure in Norway to dump snow that is removed from roads directly into the ocean, or leave the snow to melt on the roadside (Vogelsang et al., 2020). Snow might be left to melt close to water bodies or other environments, which may greatly affect the ecosystems in the immediate area as well as being a risk for further spreading (Tian et al., 2021).

2.3.1 Mitigation measures

Road sweeping is one of the most used methods for cleaning road dust. In Norway it is done on most public roads at least once a year. After sweeping, the collected material is treated as hazardous waste in an authorized landfill, at least in Oslo municipality (Vogelsang et al., 2020). The frequency of tunnel cleaning depends on AADT (NPRA, 2014a). Road and tunnel cleaning are efficient ways to prevent discharge of particles, depending on the applied approach. It is especially effective against particles in the size range bigger than 100-125 µm. However, washing has limited effects on the airborne fraction (Amato et al., 2010). In a newly released article, Rødland et al. (2022a) found that both treated and untreated TWW had lower TWP concentrations (untreated: 14.5-47.7 mg/L, treated: 6.78-29.4 mg/L) than what was found in meltwater of roadside snow banks (76.0-14500 mg/L) (Rødland et al., 2022b).

Gully pots are a common method of preventing suspended solids (SS) from entering the environment. Gully pots are common along highways, in urban areas and in some tunnels, especially highway tunnels (Vogelsang et al., 2020). Studies show that they have a particle removal ratio of approximately 20% with an influent rate of 5 L/s for TRWP with a density of 1.7 g/cm^3 (Figure 2.6). Retention will depend on particle size and influent rate, where bigger particles and lower influent rates are correlated with higher particle retention.

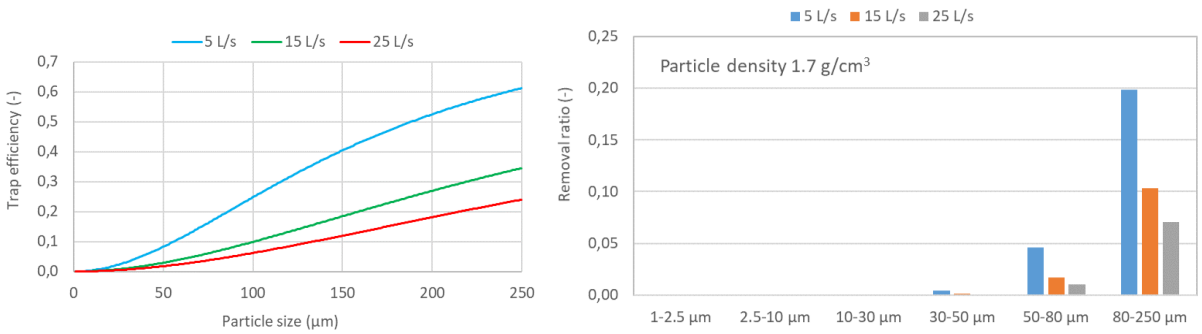

Figure 2.6: Estimated particle trap efficiency (left) and removal ratio (right) of different sized particles with different influents of water in gully pots. Copied from Vogelsang et al. (2020).

2.4 Microplastics in biota

Recently there has been an increase in the number of published articles on MP in biota as reviewed by Lusher et al. (2017). This rapid increase of research has led to new findings suggesting that plastic debris have found its way into the food web in a large scale. Both macro- and microplastics are reported to be the cause of death of many different types of animals. Schuyler et al. (2016) estimated that about 52% of sea turtles worldwide had ingested plastic debris. Another study, also targeting sea turtles, found that once a sea turtle had ingested 14 plastic pieces it was a 50% chance that this would be lethal (Wilcox et al., 2018).

Previous studies have investigated mussels around the world for MP. Most studies focus on marine blue mussels (*Mytilus edulis*) (Browne et al., 2008; Bråte et al., 2018; Bråte et al., 2020), but recently studies are focusing more on freshwater mussels (Atici, 2022; Berglund et al., 2019). Off the coast of the Netherlands, Belgium and France, Van Cauwenberghe et al. (2015) proved that the filter feeding blue mussel had an uptake of microplastics on all investigated locations. The average plastic content in the analyzed mussels were 0.2 ± 0.3 particles g^{-1} tissue. Through modelling they also found a coefficient of MP retention efficiency in mussels of 0.003%, which illustrates that mussels are good at sorting out MP and avoid uptake. This number was based on an estimated average age of 4 years and 14000 filtered plastic particles through their life.

In 2020 Bråte et al. (2020) published a report on microplastics in mussels in the Nordic seas. This presented findings in mussels from all over the Nordic countries, including Greenland and the Faroe Islands and east to the Baltic Sea. The study collected mussels from 100 locations in total. The findings from this investigation found that four out of five collected mussel species contained MP. In three out of the five analyzed species the most common MP found was black rubbery fragments, suggested to originate from road runoff based on particle size and morphology (Figure 2.7).

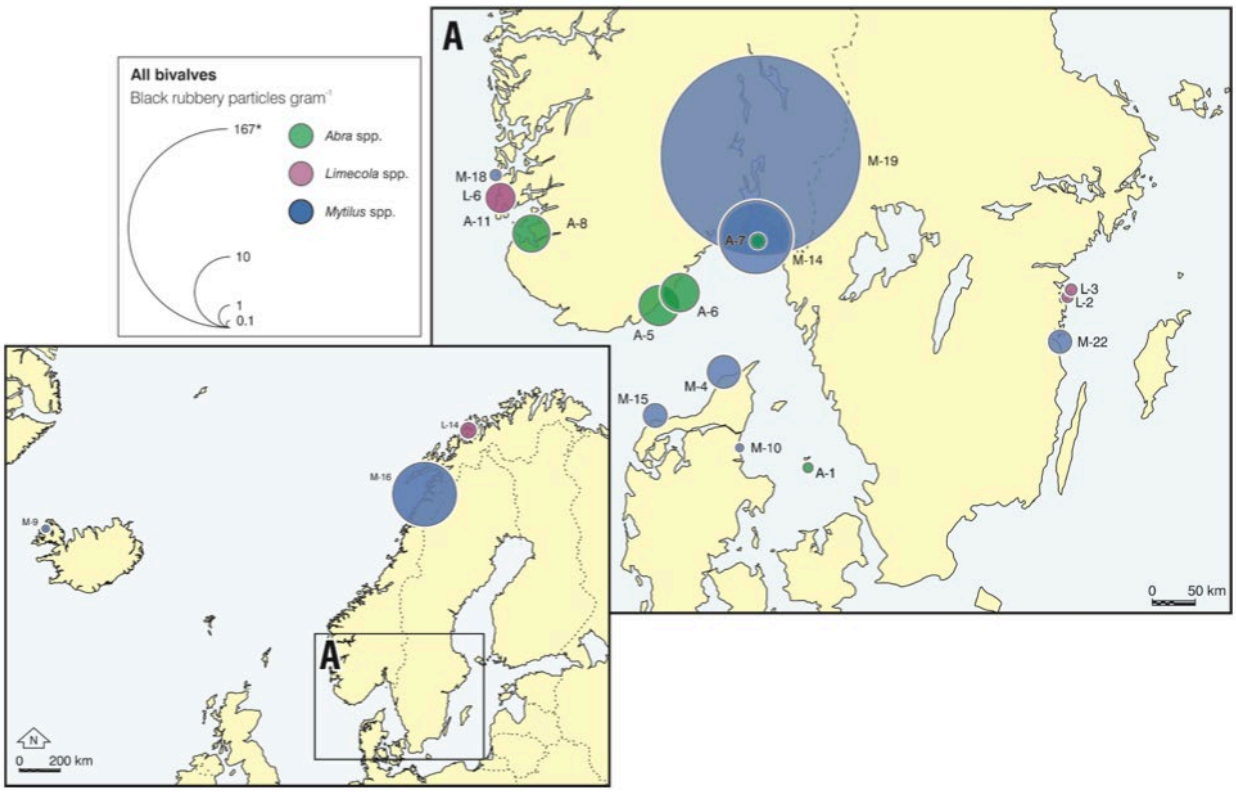

*Figure 2.7: Combined results for the species containing black rubbery fragments from the Nordic environment; Abra nitida (A), Limecola balthica (L) and Mytilus spp. (M). Asterisk * refers to upper quantification limit for particles at site M-19. Copied from Bråte et al. (2020)*

Microplastic particles may cause unknown risks to animals. It is proven that MP tend to accumulate in biota, and there is reason to believe that this accounts for TRWP as well. The potential for bioaccumulation increases with decreasing particle size, which also increases the health risks of affected individuals (Deng et al., 2017; Schirinzi et al., 2017). It has been reported that MP has potential to adsorb organic pollutants, and by doing that cause an increase in uptake of toxic substances in organisms (Rochman et al., 2013a). There is also proven that MP in organisms can cause difficulties for organisms to reproduce and in addition cause problems with nutrition uptake because of accumulation in the digestive tract (Ogonowski et al., 2016). On the other hand, there has been reported that microplastics may attenuate the effects of some organic contaminants such as persistent organic pollutants (POP), polycyclic aromatic hydrocarbons (PAH), polychlorinated biphenyls (PCB), and polybrominated diphenyl ethers (PBDE) in fish (Oliveira et al., 2013; Rochman et al., 2013b).

TRWP are proven to contain compounds that are toxic to water and sediment dwelling organisms (Marwood et al., 2011; Michnowicz & Weaks, 1984; Tian et al., 2021). Earlier, Zn was considered the biggest threat for its toxicity (Michnowicz & Weaks, 1984). Recently N-(1,3-dimethylbutyl)-N´-phenyl-p-phenylenediamine quinone (6-PPDQ) has gained a lot of attention for being proved toxic to coho salmon (*Oncorhynchus kisutch*) causing "urban runoff mortality syndrome" at concentrations that are relevant for roadway runoff (McIntyre et al., 2021; Tian et al., 2021).

2.4.1 Mussels

Mussels are filter feeders, and therefore common organisms to use as bioindicators of MP and other contaminants. The filtering process has proven to cause bioaccumulation of pollutants, including MP (Beyer et al., 2017; Bråte et al., 2018). It is common to use mussels to measure contamination of MP in marine environments. Therefore, this approach should also be viable in freshwater mussels since their way of living is similar in many ways.

Duck mussel (*Anodonta anatina*)

The duck mussel (*Anodonta anatina)* is a freshwater mussel. In Norway it is commonly found in nutrition rich lakes in the south-eastern part of the country (Figure 2.8) (Artsdatabanken, no date)

The duck mussel is a species that lives in the littoral zone or sub littoral zone. It can be found from the surface down to 6-7 meters depth, often in soft bottom substrate. It nurtures itself by filtering organic matter from the water masses, which is usually plankton in calm waters (Økland, 1963).

Figure 2.8: Registered observations of duck mussels in Norway. Map from Artsdatabanken (no date).

3 Materials and methods

3.1 Area description

Lake Padderudvann is a small lake with a surface area of 0.135 km^2. A 2 km stretch of the European highway 18 (E18) runs within the catchment area on the northern side of the lake (Figure 3.1), which has an heavy influence on the lake (Bækken & Færøvig, 2004; Tjomsland et al., 2012). E18 is one of the busiest roads in Norway. With an AADT of 48 210 (NPRA, 2022), it is very likely to be a source of TRWP. The lake is characterized as meromictic, which means it is more or less permanently stratified due to a density gradient. This is caused by high Ca and salt (NaCl) concentrations in the bottom-water of the lake, caused by the lake being beneath the marine limit in the area (Bækken & Færøvig, 2004; Fjeld, 2020).

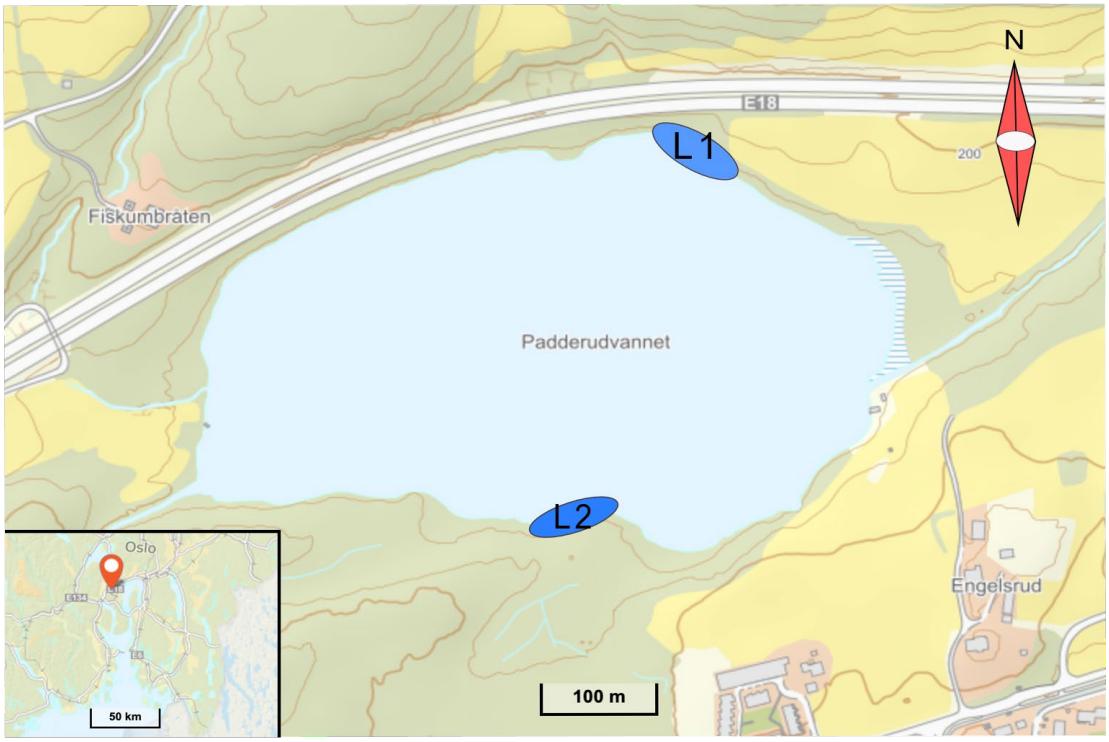

Figure 3.1: Map of Padderudvann and locations where mussels were found (blue ellipses). The location close to the road (L1) contain mussels with assumed high exposure of road related contaminations, and the far side location (L2) marks assumed low exposure. Mussels from the far side are used as reference samples. Map from Norgeskart.no, modified by Ole-Johan Næss Holm.

Padderudvann has been investigated for road related contaminations multiple times before as stated by Bækken and Færøvig (2004), whose results suggested that the lake was affected by road runoff. The locations used in this study are the same locations Bækken and Færøvig (2004) used in their investigations (Figure 3.1). One location is on the roadside of the lake (L1), and one location is on the opposite side of the lake, which is used as a reference site (L2).

The Lake is characterized as a calcic lake because of Ca-rich bedrock in the catchment area (Lutro et al., 2017). This has led to the reported density gradient, which is also being amplified by runoff of road de-icing salt from E18 (Bækken & Færøvig, 2004). Padderudvann has two main inlets, one on the eastern side and one on the western side, and the outlet is in the southwest. Smaller inlets are also found around the lake. Close to L1 there is a small stream, which is running from E18 and into the lake. This stream has a potential to contribute to inputs of road related runoff, including TRWP, especially during spring and snow melting periods (Bækken & Færøvig, 2004).

3.2 Duck mussels from Padderudvann

The mussels used in this study were collected in the summer of 2019. They have been frozen since collection. Collection was performed with permission from the county governor. Mussels were hand-picked from two different locations in Padderudvann and put in plastic bags. To avoid cross-contamination between mussels each bag contained one mussel. The bags were marked and kept cold until freezing. The two locations are found on each side of the lake. L1 is close to the road, having a potentially high exposure from road related contaminations. L2 is at the other side of the lake, presumably with lower exposure of contaminations from the road. It was collected 24 mussels from L1 and 20 from L2 (Figure 3.1).

3.2.1 Dissection and digestion of duck mussels

In total, thirteen mussels were dissected for this study. Four individuals from L1 and three from L2 were digested. Additionally, three individuals from each location were freeze-dried. Prior to dissection, mussels were thawed, measured (shell length) and weighed. Thawed mussels were cut out of their shells and placed on glass petri dishes. The mantle flaps were removed with a scalpel. For each individual mussel, the stomach and mantle, referred to as body, were separated from the gills and put in 50 mL falcon tubes before weighing and marking them. The gills were also put in tubes. Regarding the mussels that were going to be freeze-dried, the inner and outer gills were separated in different tubes, while the ones that were going to be digested were put in the same tubes to get fewer total samples to save time. All mussel samples were marked with organ, individual number, and location. Five empty tubes were weighed, and their average weight were subtracted from the total sample weights after dissection.

The digestion procedure follows an internal protocol for digestion of mussels for MP analysis made at the NIVA laboratory. The protocol uses 10% sodium hypochlorite (NaClO) for digestion which is proven to not harm common polymers found in MP in samples (Lusher et al., 2017).

Prior to digestion, the NaClO were diluted from 12% to 10% solution. NaClO was diluted by adding 833 mL of the original 12% NaClO solution to 167 mL reverse osmosis (RO) water to make one liter of solution. After preparing the solution, the organs of the mussels were put in marked Erlenmeyer flasks. The bodies were put in 250 mL Erlenmeyer flasks, and gills in 100 mL Erlenmeyer flasks, based on their respective sizes and required volume of NaClO, which is a recommended 10:1 relationship between NaClO and biological mass weight. Meaning a stomach and mantle weighing 13 g was digested in 130 mL NaClO. The samples were then put in a pre-heated incubator at 40 °C and set with a continuous rotation frequency at 125 revolutions per minute (RPM) for 16-20 hours. The samples were then placed in room temperature for 16 hours before filtration. If there were observed any shell fragments in the samples this could be dissolved by adding acetic acid in a 1:4 relationship

to the total solution. If saponification of the samples occurs this could be reversed by adding ethanol (EtOH) in a 1:4 relationship to the total sample solution.

The filtration was performed with a vacuum chamber connected to a vacuum pump. Filters were placed on filtration funnels (Figure 3.2)**.** The filters used were Whatman CN-filters with a diameter of 25 mm and 5 µm pore size.

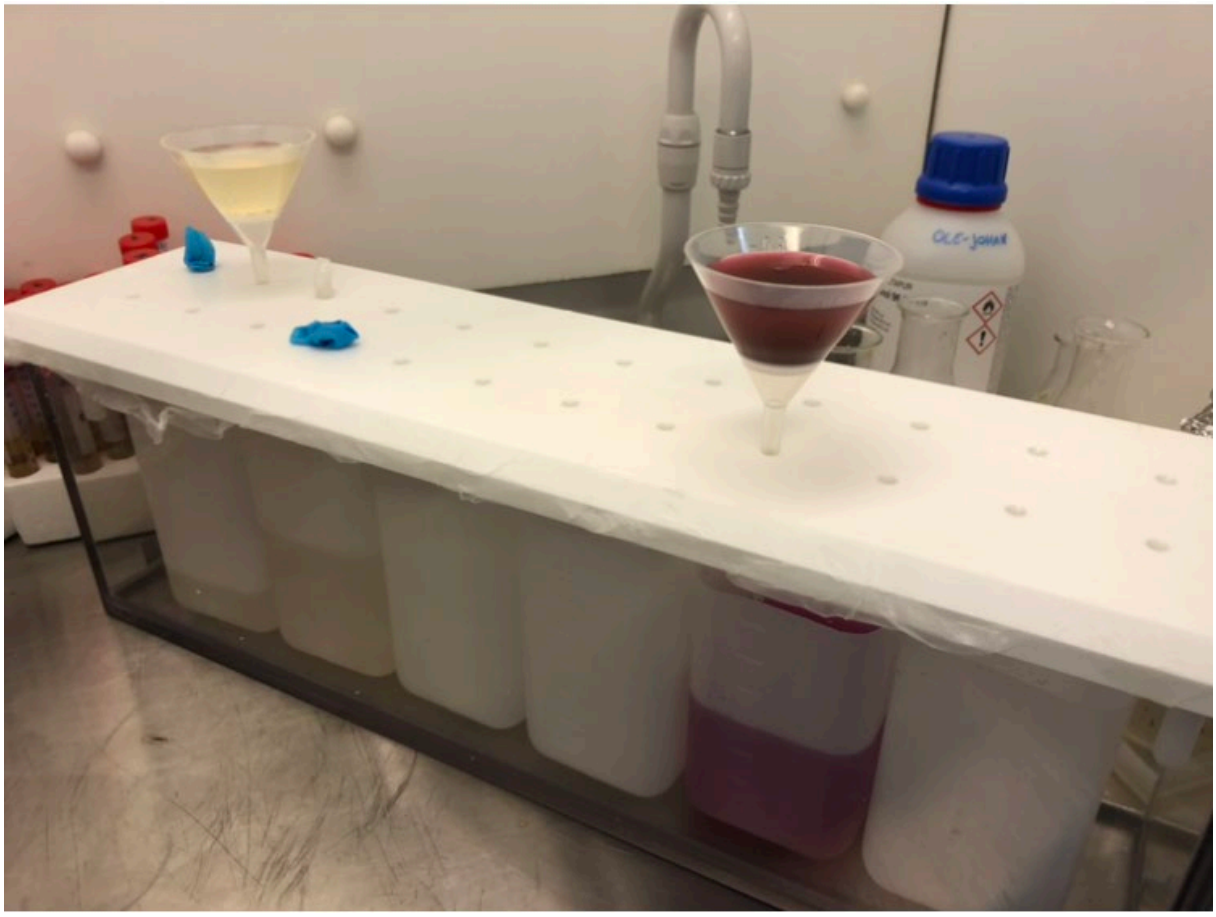

Figure 3.2: Filtration apparatus with samples of body in the left funnel, and gills in the right funnel. Photo: Ole-Johan Næss Holm.

After filtration the filters were placed in petri dishes, covered, and left to dry for ~70 hours (one weekend). When the filters were dry, they were placed on an x-cell (31 mm Double-Open Ended X-Cell) for analysis with µ-XRF (Figure 3.3). To hold the filters in place, mylar was used both over (SPEX sampleprep, 3525 Ultralene, 4µm) and under the filters (FLUXANA, TF-160, 6µm).

Figure 3.3: Examples of filters on µ-XRF sample cups. The photo also illustrates the difference in digestion efficiency between samples. Photo: Ole-Johan Næss Holm

3.3 Tire Particles from reference tires

Reference tire particles (TP_{ref}) were acquired from NIVA for analysis. The particles (n=39) were a mix of cryogenically grinded ten tires for personal vehicles (PV) and three tires for heavy vehicles (HV). Three samples were taken from each tire, which represent the most used tires of PV and HV in Norway (Rødland et al., 2022c). The TP_{ref} were in a size range that matches the size of TWP normally found in the environment (Kreider et al., 2009). Since these particles have not been exposed to road surface environment, they were not encrusted with road material or minerals like TRWP found in the environment.

3.3.1 Analysis of elements in reference tires with ICP-MS

TP_{ref} were analyzed using inductively coupled plasma mass spectrometry (ICP-MS). Acquired data was examined to find out which elements that are commonly found in TRWP, as a support for the results of μ-XRF scans. This analysis was performed in 2019 at the Norwegian university of life sciences (NMBU, Norway). TP_{ref} were transferred to precleaned UltraWAVE Teflon tubes and digestion in 0.6 mL deionized water (DI H_2O) and 0.6 mL Ultrapure nitric acid (HNO_3) in an UltraWAVE (Milestone, Italy). The temperature for the digestion were set to rise from ambient temperature to 110° C in 10 minutes, followed by a rise from 110° C to 260° C in ten minutes and then to stay at 260° C for 20 minutes. The samples were transferred to precleaned 15 mL Saarstedt tubes and filled with 10% HNO_3 overnight before dilution with DI H_2O to a 6 mL solution. The instrument was set to high sensitivity and calibrated using standards made from Inorganic Ventures (USA), which was checked for errors using a house standard.

Digestion of reference tire particles

Reference tire particles were tested in the digestion approach using NaClO. The digestion follows the same procedure as the digestion of mussels found in chapter 3.2.1. Three samples containing TP_{ref} were prepared. Each sample had a different amount of TP_{ref}, low, medium and high number of particles. This test was done to examine visual effects of particles that had been treated with NaClO, by comparing them to particles that had not been treated, as well as analyzing the treated TP_{ref} with μ-XRF.

Another purpose of this experiment was to examine particle loss during the filtration process. This was done by examining filter funnels after removal of filters and look for different amounts of particles that had escaped the filter, thus being stuck on the funnel.

3.4 Micro-XRF and development of analysis approach

Micro-X-ray fluorescence is a non-destructive semi-quantitative method used to examine elemental composition of samples (Haschke, 2015). Micro-X-ray fluorescence use X-rays to directly excite elements in the sample, thus inducing characteristic fluorescence emissions for elemental analysis (XOS, no date). The instrument is a M4 Tornado (Bruker Nano Analytics, Germany). The X-rays are generated with a rhodium (Rh) tube, running at 50 kV and 600 µA. The incident beam is focused by a polycapillary optic to focus the incident X-rays to a diameter of 25 µm. Fluorescence is counted by two XFlash silicon drift detectors. The detectors are set at a 45° angle to the beam, each with an active area of 30 mm^2. This process outputs detailed two-dimensional mapping images of where different elements are located in samples, as well as quantification of element composition in each pixel. Acquired XRF-data was analyzed with the ESPRIT software (Bruker Nano Analytics, Germany).

3.4.1 Optimizing scan parameters through systematic experimentation

There are three main parameters for analysis. Dwell time determines how long each pixel is scanned. Pixel (px) size, which is the distance the stage moves between each measurement, and the areas covered by each pixel in mappings. Cycles determines the number of full area scans. These parameters can be adjusted, which affects precision as well as stage speed and total scan time.

Testing of the parameters were performed to observe the differences in scan quality to optimize the µ-XRF results. Testing was performed in four steps. One analysis to focus on one parameter at a time, and one scan with a combination of high/medium settings. This means that for each test, one parameter was set to be more precise, while the other two were set to be less precise (Table 3.1). Higher parameter settings mean more precise measurements, but often at the cost of time consumption.

Table 3.1: Parameters used in the different parameter tests, and the resulting stage speed caused by the parameters. The tests are named after the parameter in focus.

PARAMETER IN FOCUS	DWELL TIME (MS/PX)	PIXEL SIZE (µM)	CYCLES	STAGE SPEED (MM/S)
DWELL TIME	25	25	1	1
PIXEL SIZE	2	10	1	5
CYCLES	2	25	5	12.5
COMBINATION	20	20	2	1

Following the systematic experimentation with the different parameters, an experiment focusing on time consumption were performed. Tests were performed with five different combinations of settings (Table 3.2). Since this experiment was focused on time usage, the parameters were adjusted with regards to time usage only. One control test was performed with high settings on all the parameters, making it a more thorough, as well as a more time-consuming analysis. This was followed by four tests performed with lower settings.

Table 3.2: Parameters used for the different time tests, and the resulting stage speed.

TEST NUMBER	DWELL TIME (MS/PX)	PIXEL SIZE (µM)	CYCLES (MIN)	STAGE SPEED (MM/S)
TEST A	5	30	1	6
TEST B	3	25	2	8.3
TEST C	3	40	1	13.3
TEST D	3	40	4	13.3
CONTROL	40	17	3	0.425

The scans were performed on a part of a filtered mussel gill containing placed TP_{ref} of different sizes (Figure 3.4). The sample was approximately 1 cm wide and 2 cm long, making the scan area approximately 2 cm^2 in total. The performed scans took the results of the parameter tests in account, although time consumption was the main focus.

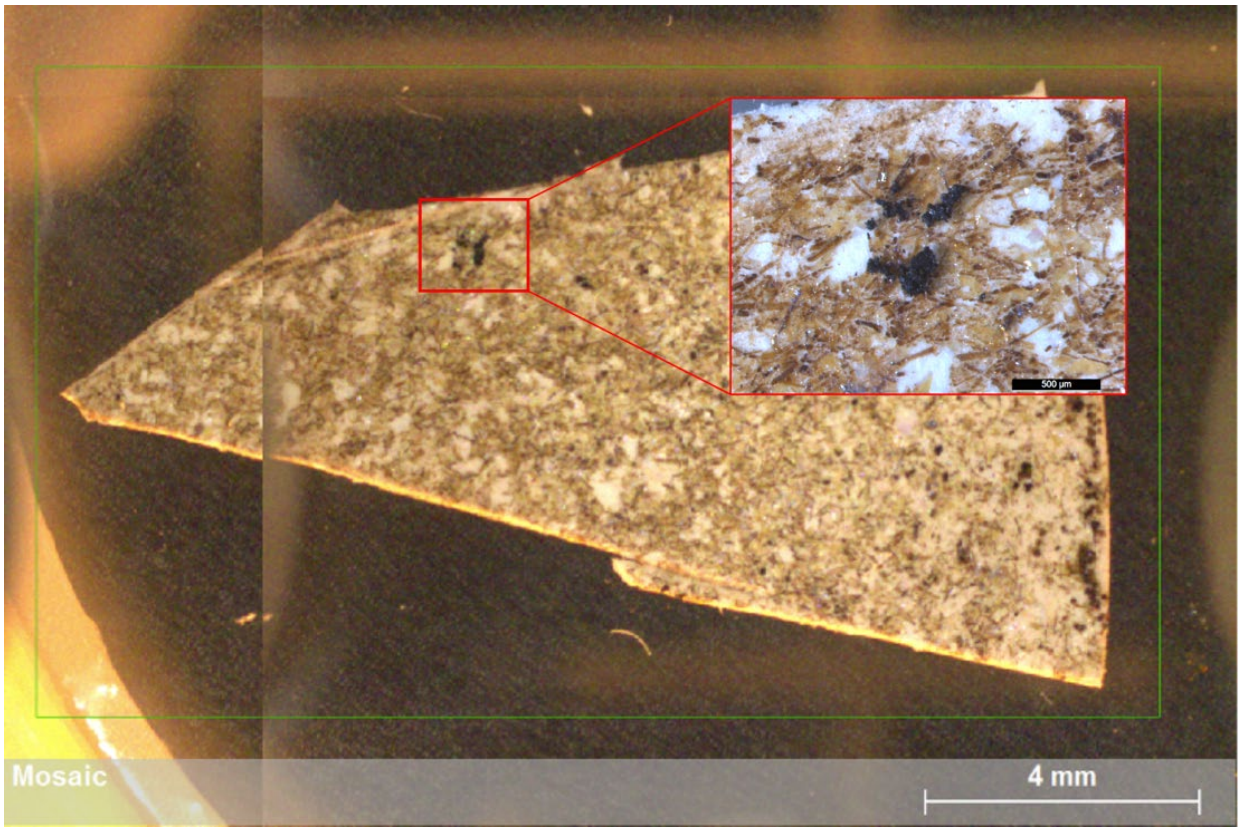

Figure 3.4: Mosaic image of the spiked filter with gill material. The green square marks the area of the µ-XRF mappings. The red square shows the area where TP_{ref} are placed. The particles moved in between capturing the different images.

While scanning the filters the method and time consumption for each filter part were adjusted as more data and experience of the instrumental performances and capabilities were gained. In the early stages of this study there was no standard parameter settings, hence the scans varied in resolution, dwell time and cycles. Vacuum was used in all scans to get better detection of elements with lower atomic number than 16 (BRUKER, 2015).

3.5 Reference tire particles on different sample media

To explore the capabilities of the μ-XRF to detect TRWP, spiked samples were made. These samples were prepared by placing TP_{ref} onto six different samples. Samples prepared for this purpose include two samples on a clean cellulose nitrate (CN) filter, one potassium hydroxide (KOH) digested and filtered mussel gill and one sample of freeze-dried gill. Lastly, NaClO-digested body and gill on CN-filters. These samples were analyzed with point scans, line scans and area scans. Point scans were performed with a dwell time of 30 seconds per point. Acquired data from point scans were shown as normalized mass percentages, meaning the detected elements were summed to 100 percent. Elemental content were ZAF-corrected (JEOL, no date). Line scans were performed with 150 ms dwell time, 6 μm pixel size, and 5-10 cycles (depending on the sample). These parameters are within the recommended settings from the user manual of the M4 Tornado (BRUKER, 2015). To make the figures from the line scans, an averaging was used to make the line smoother. Number of points used for the averaging varied with the size of the scanned TP_{ref}, usually 3-9 points.

Samples of TP_{ref} on clean filters were prepared (Figure 3.5). These filters were 5 μm Whatman CN-filters, which is used at NIVA for their pyr-GC-MS tests of MP in biota. TP_{ref} were placed on the filters using a tungsten probe (W-probe) with a 10 μm tip from Electron Microscopy Sciences (All Tungsten Probe Tip, Cat.75960-02) under a microscope (Leica m205c). Placing only a few particles in the desired positions proved to be a challenge. The particles, filter, W-probe and mylar were all affected by electrostatic forces. This made the particles attract to various locations on the filter. This was most evident on the smallest particles. Hence, they became hard to line up straight (Figure 3.5A).

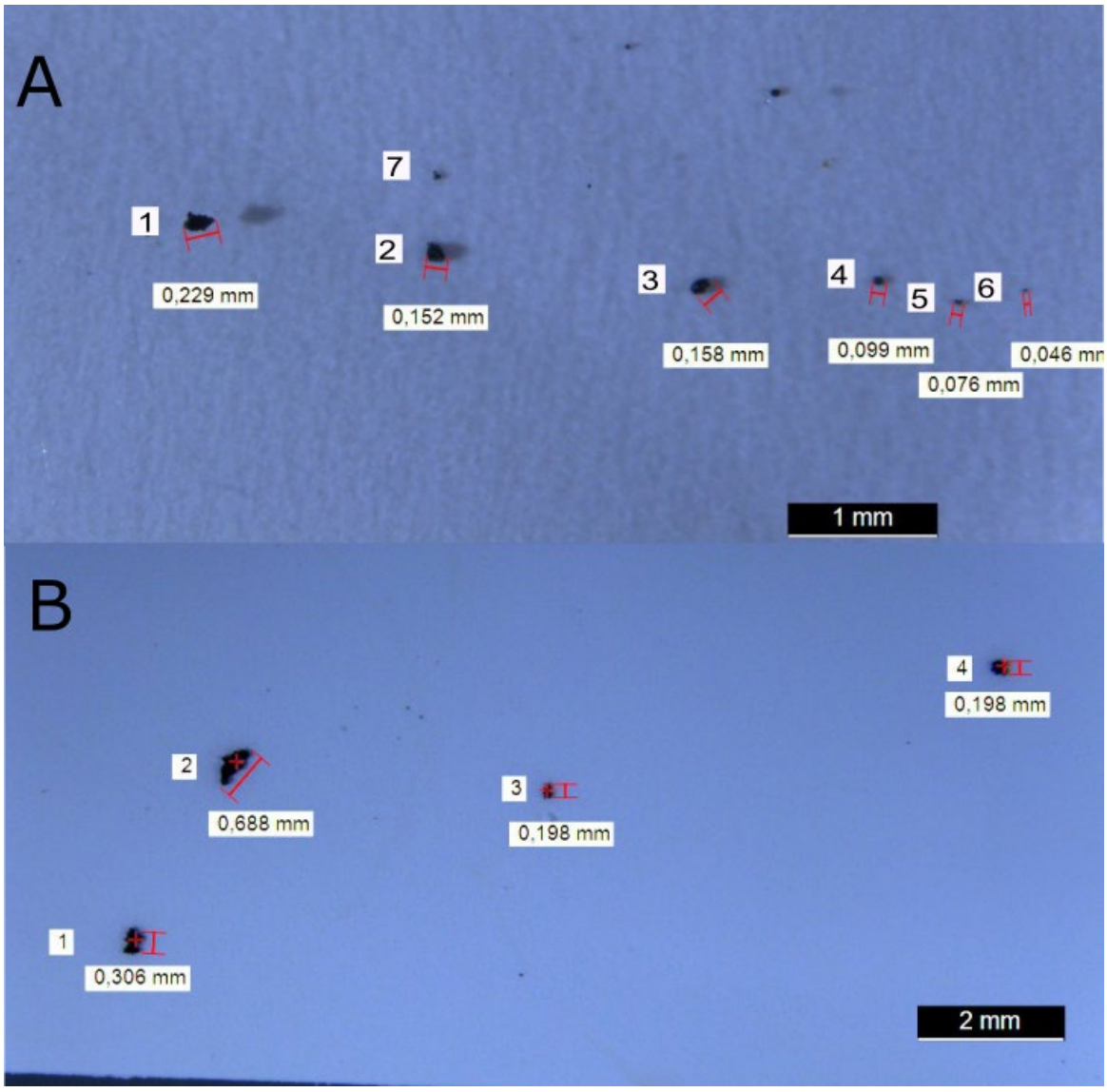

Figure 3.5: Microscopy images of the particle line filter (A) and the TP_{ref} placed on a filter under laminar air flow (B).

To avoid dust settling on the sample, and enhancing the control of particle deployment, another sample was prepared of a clean filter with TP_{ref} using an alternative approach (Figure 3.5B). This time the sample was prepared in a laminar air flow bench to avoid contamination. TP_{ref} were suspended in distilled water, and a glass pipette was used to move and deploy the particles. This was also done under a microscope. With this approach, four particles were deployed on the filter, without dust or other particles settling.

A sample on a KOH-digested mussel gill was prepared to examine how well the signal from the TP_{ref} showed in mappings on biological samples. This sample was also used for the parameter tests and scanning time tests (Figure 3.6). The particles were moved to the filtered media using narrow metal forceps. The particles may have moved after the microscopy images were taken and when the scans were performed. This can be seen in the µ-XRF scans (Figure 4.9), where the particles marked as 1 and 3 were closer together.

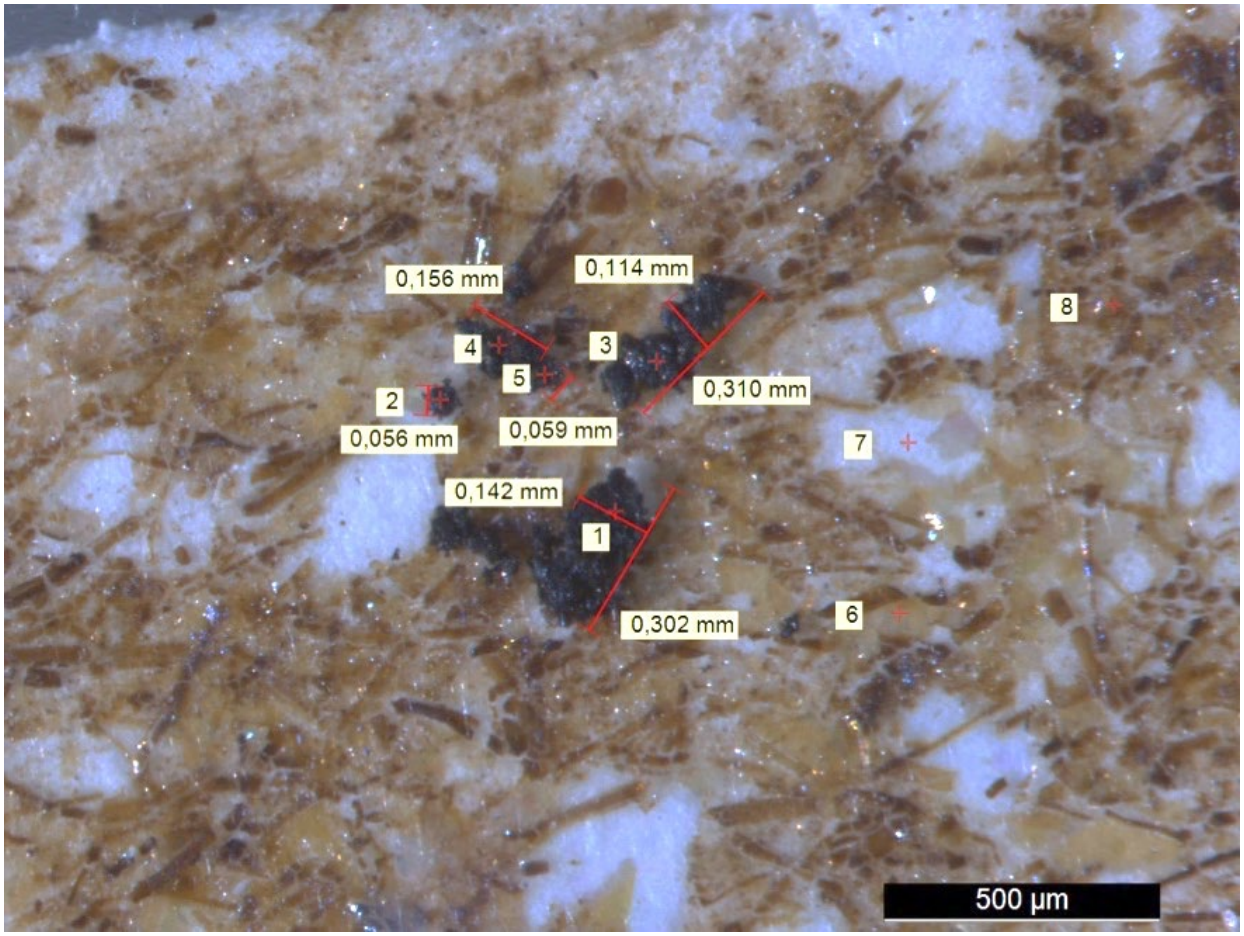

Figure 3.6: Microscopy image of TP_{ref} on a filter with dissolved gill material. Points 1-8 are approximately where the point scans were performed. Points 1-5 are point scans of TP_{ref} and 6-8 are point scans of the background. Photo: Ole-Johan Næss Holm.

Reference tire particles were also placed on a part of a freeze-dried gill to examine the signal strength. The gill was scanned before and after placing the particles. The particles were placed using a W-probe, and the particles were attracted to the sample by static charges. Particles 1-3 (Figure 3.7A) are the smallest, and particle 4 (Figure 3.7B) is the largest. The size variation was intentional to make a comparison of the signal variations between particles in various sizes. Before the images of the samples were captured, particle 1 got stuck under a part of the gill, and is half covered by the gill material (Figure 3.7A).

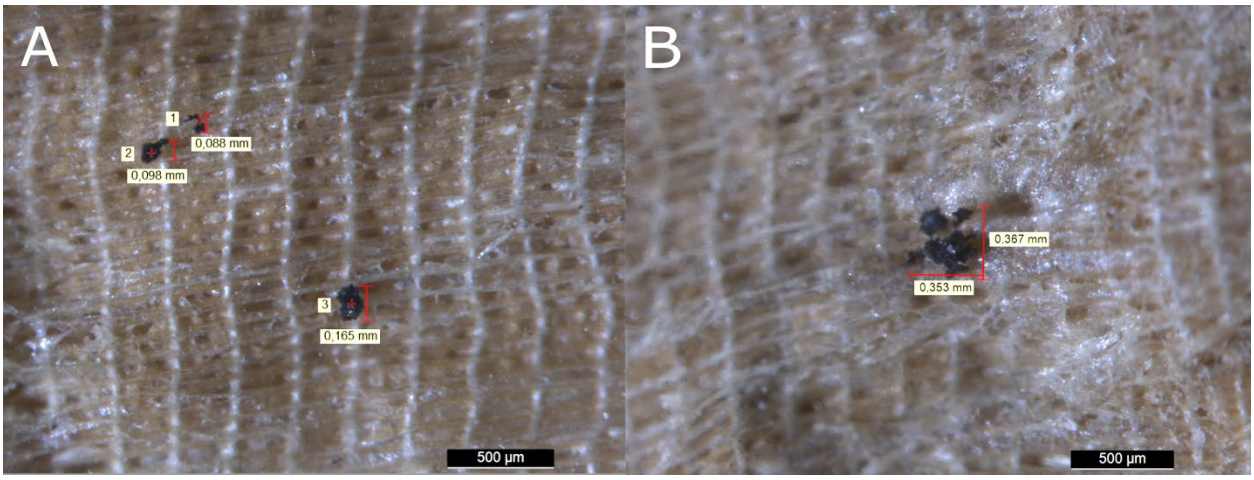

Figure 3.7: Microscopy images of TP_{ref} on a freeze- dried gill. A and B Both show particles from different locations on the freeze-dried gill. Particles 1-3 are placed on the right side of the sample and particle 4 is placed on the left side of the sample. See Figure 4.16 for locations on the full sample. Photo: Ole-Johan Næss Holm.

3.6 µ-XRF analysis of duck mussels from Padderudvann

The digested and filtered mussels were scanned with µ-XRF. It was a total of 18 filters. Seven of the filters were gills, one per individual. The bodies yielded one to three filters per individual. The parameters that were used for the area scans were 3.5 ms dwell time, 25 µm pixel size and 3 cycles. These parameters gave the best results in the systematic experimentation, with one extra cycle. Each sample took approximately five hours to scan, making it possible to scan two filters per day.

When examining the results from each filter it was used a function from the Esprit software called “spectrum elements 300”. This function runs collected data through 300 cycles to calculate a background signal intensity to make identification of peaks from elements in the spectra easier. All spectra were examined using this function. Once all elements in the samples were identified, element maps were examined for hotspots, and images were saved for further analysis.

Since the digestion method and sample matrix of the experiment were different than the method used in the systematic experiment, two new positive controls were made. These were made after initial scanning to be able to look for differences in detected elements. Reference tire particles treated with NaClO were placed on the samples to make the signals from the particles as equal to potential TRWP as possible. Due to the difficulty of placing particles inside of the material of the body samples, one out of two particles (~150 µm) was placed close to the biological matter on the sample (Figure 3.8A). In the middle of the filter multiple smaller (60-30 µm) particles were placed.

Regarding the gill sample, six particles were put on top of the sample, and two particles (~200 µm) were put inside the sample material. One particle was completely covered, and the other partially covered. This was done to examine the signal difference between a free, partially covered and a completely covered particle (Figure 3.8B). It was also observed multiple crystals in the sample material, which was analyzed further.

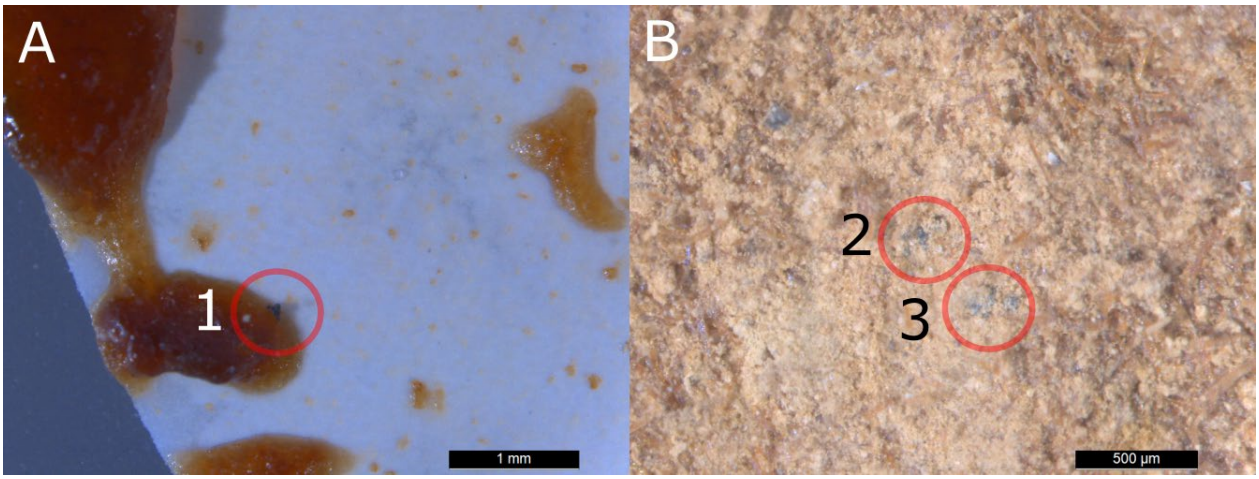

Figure 3.8: Microscopy images of TP_{ref} on samples. A = body sample, B = gill. Particles are marked with red circles. 1 = TP_{ref} close to biological matter, 2 = fully covered TP_{ref} and 3 = partially covered particle. Photo: Ole-Johan Næss Holm

Microscopy of filtered samples

Filtered samples were investigated with a microscope to examine the samples for differences in particle content. To analyze the samples, images were captured with a microscope (Leica m205c). Two areas were captured from each filter in both high and low magnification. The magnification level was not changed between taking the images, only the focus. This was done to make the images cover approximately the same area sizes, thus making them comparable. Particles were counted manually using the multi point tool in ImageJ. When counting the particles, only particles matching the reported characteristics of TRWP from the literature were counted.

3.7 Image analysis using ImageJ

Images from µ-XRF were analyzed using ImageJ (version 1.53k). By using built in functions in the software it is possible to filter out signals from the maps. Firstly, images must be converted to greyscale 8-bit format. Then, they may be inverted. This step is not necessary, but it makes identification of high intensity pixels easier due to the change of colours. Further, unwanted signal intensities can be sorted out, and desired intensities can be highlighted through the threshold function.

In these analyses it was used single element mappings and composite images of multiple elements. The signature elements were mostly used, and potential particles were identified by colocalizing high intensity pixels between the signature elements. When analyzing samples with known particle locations (especially positive controls) images were inverted to make contrasts more visible.

3.8 Statistical analysis

To investigate significant differences and important factors in the data RStudio version 1.4.1717 (April 2022) was used (Rstudio, 2021). It was performed a Welch's t-test and principal component analysis (PCA). The t-test and PCA were performed using the built in Stats package in R to find significance in the difference between the counted possible particles in the mussels and PCA were used to investigate patterns within compositional data (R, 2021). Compositional data were logarithmically transformed, and zeroes were replaced using the zCompositions function lrEM (Palarea-Albaladejo & Martin-Fernandez, 2015).

Figures and plots of statistical data were made in Microsoft excel (version 16.60) and in Rstudio using ggplot2 (Wickham, 2016) and ggforce (Pedersen, 2021). Outputs that did not fit the ggplot2 format were transformed using ggfortify (Horikoshi & Tang, 2016; Tang et al., 2016). Inkscape (version 1.0.2) was used to modify figures (Inkscape, 2020).

4 Results and discussion

The first chapter covers the digestion of the mussels and the potential effects of the digestion on TRWP. The next chapter is an ICP-MS-analysis of TP_{ref} to verify the values found in the literature and investigate if there were any variations in elemental composition of the TP_{ref}. Optimization of the µ-XRF approach follows.

The last two chapters covers the validation and usage of the approach on duck mussels from Padderudvann. The digested mussels were scanned, using the optimized scanning approach. With data from these scans, regions of interest (ROI) were identified for more thorough investigations with µ-XRF (Figure 4.1).

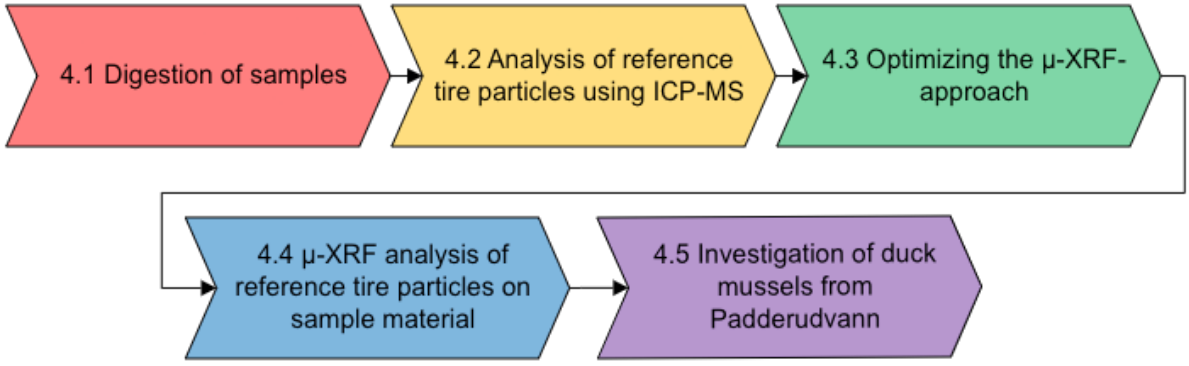

Figure 4.1: Flowchart of the chapter order and the developiment the approach. The top three boxes show method development, and the bottom two show validation and usage of the method.

4.1 Digestion of samples

4.1.1 Dissection and digestion of mussels

Thawing the mussels took approximately 2-3 hours, depending on the respective size of the individual. Shell lengths and weights of the mussels can be seen in Table 4.1.

Table 4.1: Length and weight of dissected mussels, including averages and standard deviations.

SAMPLE	SHELL LENGTH	WEIGHT (BODY)	WEIGHT (GILLS)
	(mm)	(g)	(g)
L1-1	111	13.1	3.65
L1-2	104	9.91	3.36
L1-3	114	13.8	4.36
L1-4	97.0	9.31	3.44
MEAN (L1)	**107**	**11.5**	**3.70**
SD (L1)	**7.59**	**2.24**	**0.455**
L2-1	103	8.70	5.01
L2-2	97.0	11.9	4.70
L2-3	99.0	10.1	4.02
MEAN (L2)	**99.7**	**10.2**	**4.59**
SD (L2)	**3.06**	**1.59**	**0.06**

The mussels from L1 were digested first and were therefore also weighed first. Some mussels were still not completely thawed during weighing, which might have caused the weight of the mussels from L1 to be heavier due to ice in the samples. It was observed more water in the sample tubes of the mussels from L1 compared to L2 before digestion. To avoid the risk of losing particles, water was kept in the sample.

Analyzed samples in this thesis were digested using two different approaches. The filtered gill used for systematic experimentation (Chapter 3.4) was digested using KOH at NIVA. The mussels that were digested for testing hypothesis 2 regarding TRWP-content in mussels from Padderudvann were digested using NaClO. KOH-digestion is a more common and optimized approach (Fraissinet et al., 2021; Hurley et al., 2018), but problems with saponification of samples are reported to cause clogging of filters due to high lipid content

(Bessa et al., 2019; Dawson et al., 2020). Digestion with KOH may also leave residues such as humic substances among other alkali-insoluble substances undigested (Bläsing & Amelung, 2018). When analyzing mussels from freshwater lakes, humic substances might be abundant (Driscoll et al., 2003; Hongve et al., 2004), causing a risk of high debris content in samples. This debris might affect the results when analyzing for TRWP.

Digestion with NaClO dissolved the mussels within the first hours. When the mussels were moved from the incubator to room temperature, some of the samples were already completely dissolved. After being in room temperature overnight, there were little change in the amount of digested material. The incompletely digested samples were given more NaClO in an attempt to make them fully digested. Higher volumes than what was initially used might have dissolved the mussels completely, leaving more free particles on the filters after filtration, as well as minimizing the experienced clogging of filters. Further experimentation with this approach is needed. A potential solution could be to increase the amount of NaClO from the 10:1 relationship or use the undiluted 12% solution. It was also discussed to increase the temperature in the incubator to 50 °C, which could be a way of making the process go faster. If the problem resides in depletion of digesting properties in the NaClO, adding more of the chemical would be an applicable solution.

Body samples that were not completely digested were handled by filtering the liquid part of the sample before adding more NaClO to the digested mussels. The samples were then put back in the incubator with the same conditions as stated in the protocol. The liquid was filtered to avoid dilution of NaClO when refilling the sample beakers, without potentially losing particles in the process. The re-digested samples were filtered after the second digestion. After re-digestion there were still undigested material in the samples. Clogging of filters was experienced for some samples. Both those containing a lot of residues as well as in better digested samples and re-digested samples (Figure 4.2A).

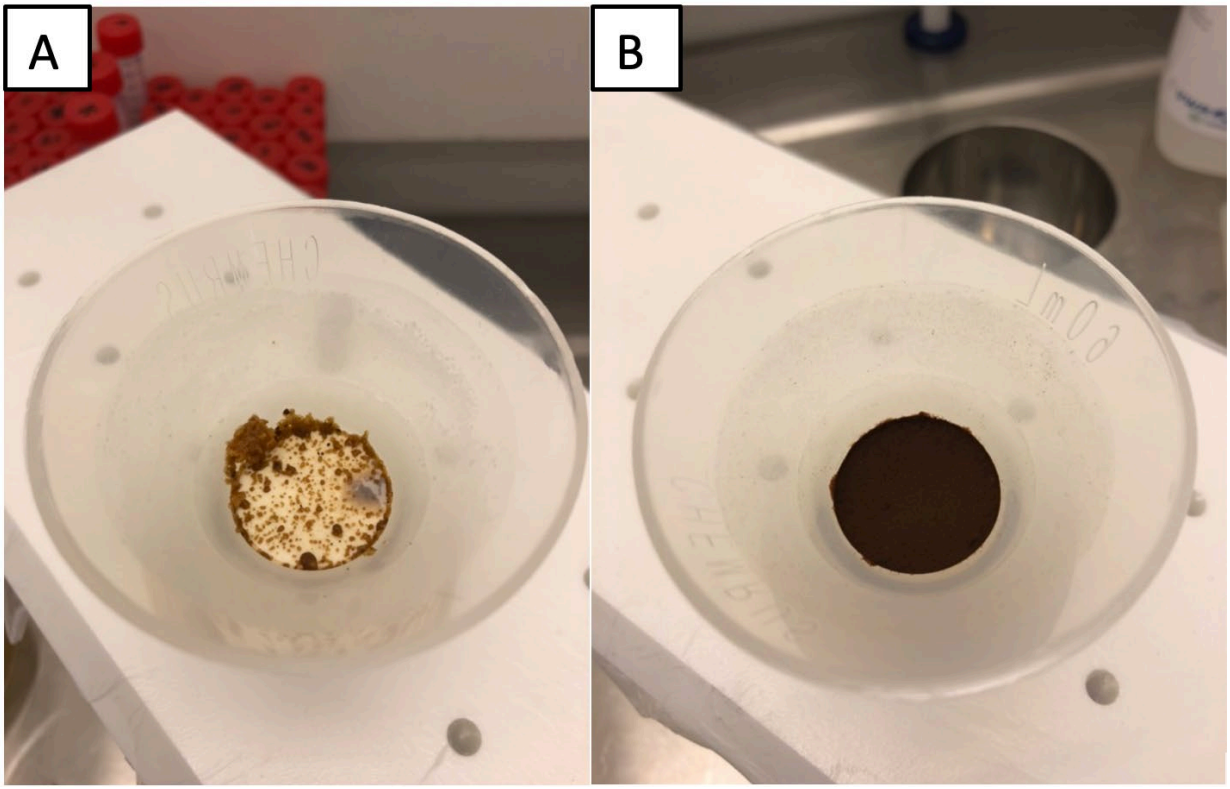

Figure 4.2: Filters with residues of a body (A) and gills (B) of a digested duck mussel. Photo: Ole-Johan Næss Holm.

The material of the digested gills came out as a dark-brown powdery mass (Figure 4.2B). This material was sedimented in a purple solution (Figure 3.2). What caused the purple colour is not known, but some sort of complexation in the sample is likely. Purple colour was also seen at NIVA during their experiments (Internal protocol at NIVA). The powder made a layer approximately one millimeter thick on the filters, making visual inspection with a microscope challenging. White crystals were found in the sample matrix. It is not known whether these were formed during the digestion process or if they were present in the samples from the beginning, but it was not seen any crystals in the freeze-dried samples, nor in the samples digested with KOH.

4.1.2 Digestion of reference tire particles

Particles that were tested in the digestion approach with NaClO got an elevated content of chlorine (Cl) after the treatment. The signals from the signature elements were still strong. Average mass percentages in the particles were measured with µ-XRF point scans. Content of signature elements were measured to 4 ± 4% Si, 6 ± 4% S, and 1 ± 2% Zn. The content of Cl increased from an average of 3 ± 4% (untreated particles) to 76 ± 6% (treated particles) (appendix B, table 1 and 2).

Filtration of samples with treated TP_{ref} indicated highest loss of particles in the samples with the highest particle content (Figure 4.3). Particles were observed to have avoided the filter on all samples after filtration. The number of particles that avoided the filter seemed to be corresponding to the number of particles in the sample. To filter samples with a closed filtering solution would possibly eliminate this problem. The usage of filters with pore size of 5 µm might also cause some loss. The pore size was however chosen with care. In the literature it is stated that only a small portion (5%) of TWP are smaller than 10 µm (Kreider et al., 2009). Further, the incident beam on the µ-XRF have a minimal diameter of 25 µm. This makes detection of particles smaller than 25 µm, very time consuming on big scans (whole filters) as the pixel size would have to be lower than what is used in this study. However, many of the particles lost in this filtration are larger than 5 µm and must therefore have escaped the filters on the edges.

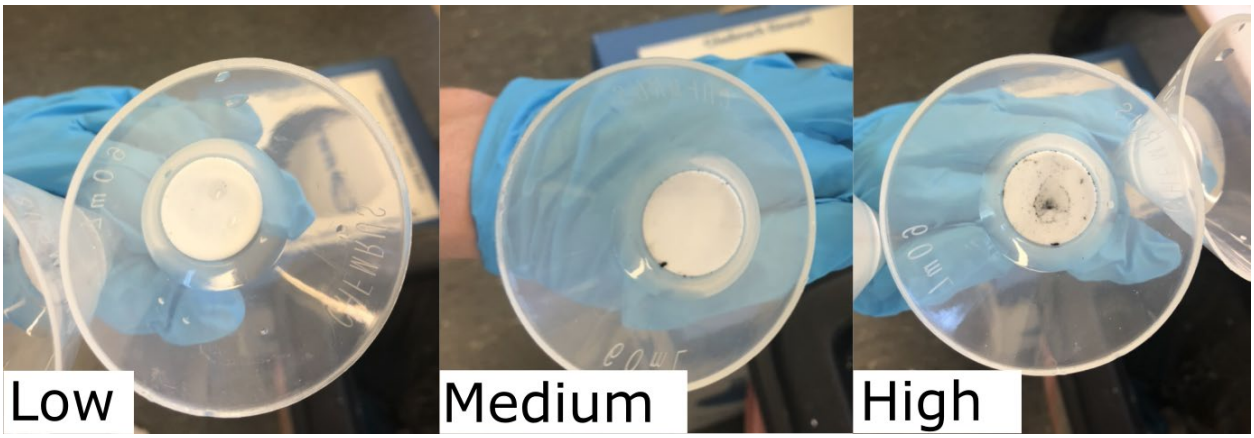

Figure 4.3: Images of filter funnels after filtration of samples and removal of filters. On the filter funnels it can be seen particles that escaped the filters. The filter funnels are sorted by particle amount in the sample before filtration. The lowest amount on the left, increasing to the right. Photo: Ole-Johan Næss Holm

Treated and untreated particles were studied under a microscope. The results suggest that particles may be affected by the digestion process. This can be seen on the edges of the particles. The untreated particles tend to have rougher edges than the treated particles (Figure 4.4). Some of the particles were seen to have a shiny surface. This was observed in more of the treated particles than the untreated. Dark circles can be seen around some of the treated particles. However, rugged edges were observed in both groups, but appeared to be more abundant among the untreated particles. A possible explanation for this could be that the rough edges observed on the untreated particles consisted of small particles attached to larger particles by electrostatic forces. Particles that have been suspended in a fluid and filtered would naturally have a lower number of smaller particles attached, as the charges would be neutralized by the fluid and smaller particles would be washed off. Another possibility is that the chemical affects the particles in a low degree which cannot be concluded with the present investigations. However, a report from Collard et al. (2015) examined this on common polymers found in MP and found no significant effect on any tested polymer. To examine the direct effects of NaClO on TRWP, it is recommended to analyze the same particles before and after treatment. This was not done in this experiment.

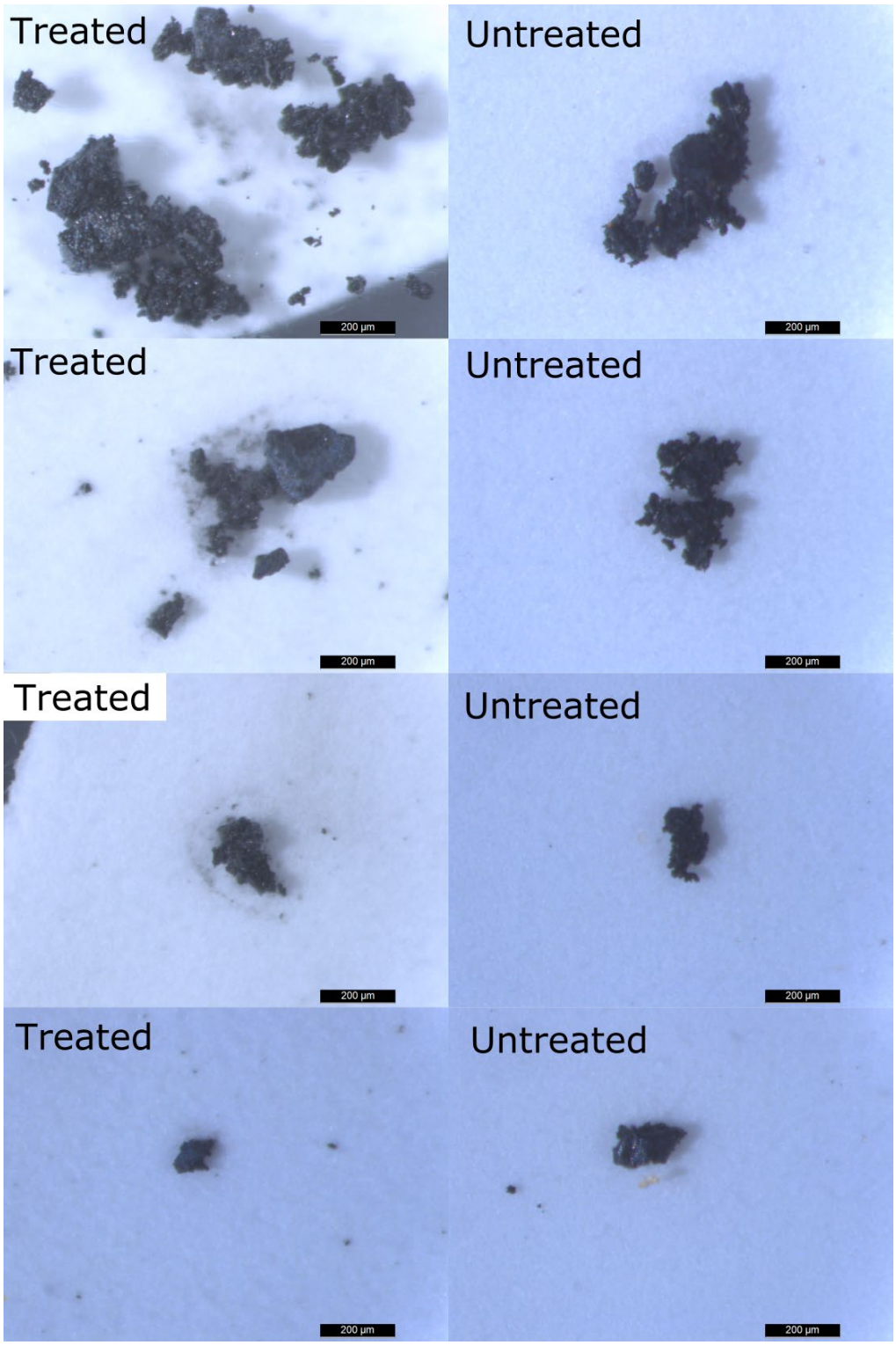

Figure 4.4: Comparison of particles that have and have not been treated with NaClO. It can be seen in the images that the untreated particles have rougher edges than the treated particles, and that the treated particles have a shinier surface in some of the particles.

4.2 Analysis of reference tire particles using ICP-MS

The results of the ICP-MS analysis show that S and Zn have the highest concentrations of the detected elements. Average content of S in all tires were 15410 ± 2248 mg/kg, and 11777 ± 3022 mg/kg for Zn (Appendix A, table 1). These measured concentrations are in line with the content reported in the literature (Klöckner et al., 2019; Kreider et al., 2009). It was also found high levels of P in some samples, however there was also many undetected values. If the zero-values are excluded, the average content of P was 3156 ± 1925 mg/kg. It was not found a correlation between P-content with tire type or producer (Appendix A, figure 2).

The dataset contained a lot of elements with low values and zeroes. Elements with values below 0.1 mg/kg or more than 60% zeroes were removed to make the data less noisy before doing statistical analyses. The remaining elements were then converted to normalized mass percentages and logarithmically transformed (Figure 4.5) (all elements detected elements in appendix A, figure 1).

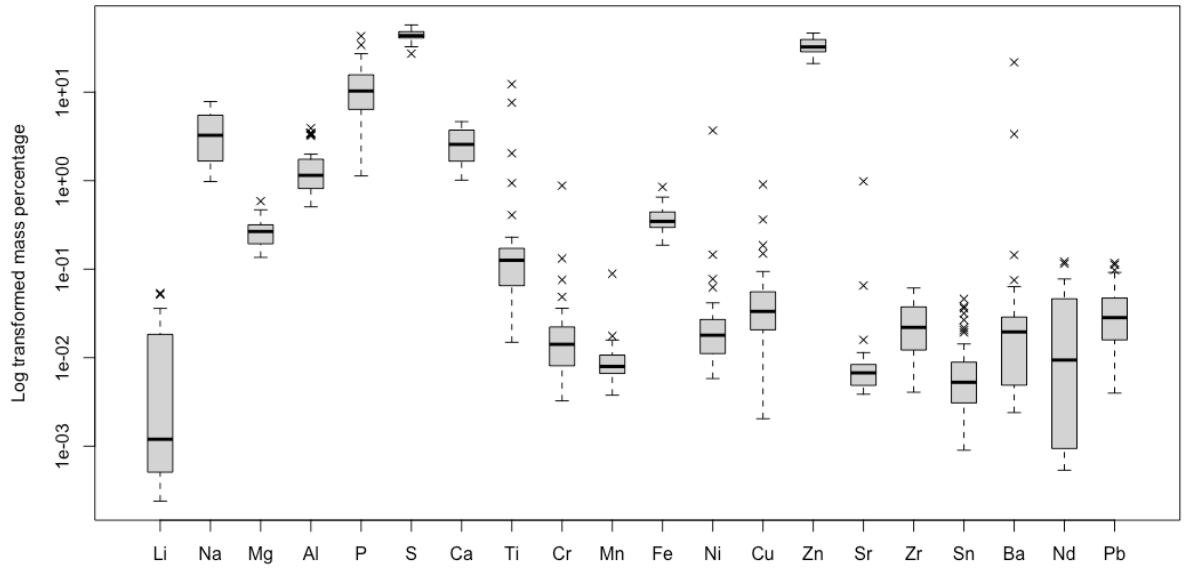

Figure 4.5: Box plot of the most abundant elements found in TP_{ref} (n=39). Data is shown as logarithmically transformed mass percentages.

There is little variation between average values of S between summer (156667 ± 2534 mg/kg), winter (14888 ± 1779 mg/kg), and truck (16111 ± 1764 mg/kg) tires. Differences between Zn are larger (summer = 11933 ± 2885 mg/kg, winter = 9672 ± 1279 mg/kg, truck = 15777 ± 667 mg/kg), thus making Zn a more important variable in regards of explaining the composition. Through PCA it was found differences between types of tires on the log-transformed data (Figure 4.6). Truck tires (both winter and all-year tires) were more correlated towards Zn than summer and winter tires of personal vehicles. Summer tires are often negatively correlated and sometimes not correlated towards Zn. This means that Zn is a less important variable for explaining the variations between summer tires (see appendix A, figure 2A for all types).

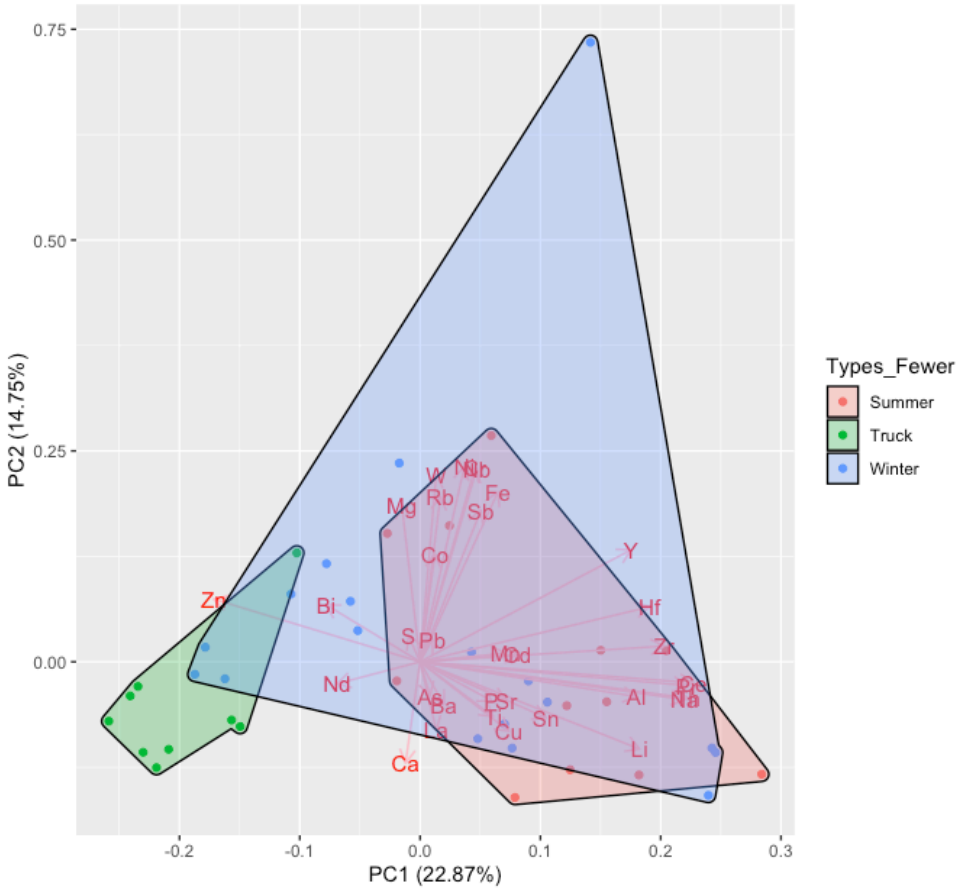

Figure 4.6: PCA-plot of elemental compositions in TP_{ref}. Differences between summer (red), truck (green) and winter (blue) are shown. The truck tire category consists of both winter tires and all year tires. Summer and winter tires are from personal vehicles.

Winter tires had values spread all over the plot, suggesting that there are big variations in composition between the different samples. Because of the spread, a PCA focused on winter tires were performed. In the analysis it was investigated whether the variations came from differences between studded and non-studded tires (Figure 4.7). The analysis did not show a large difference between the types of tires, other than a bigger spread.

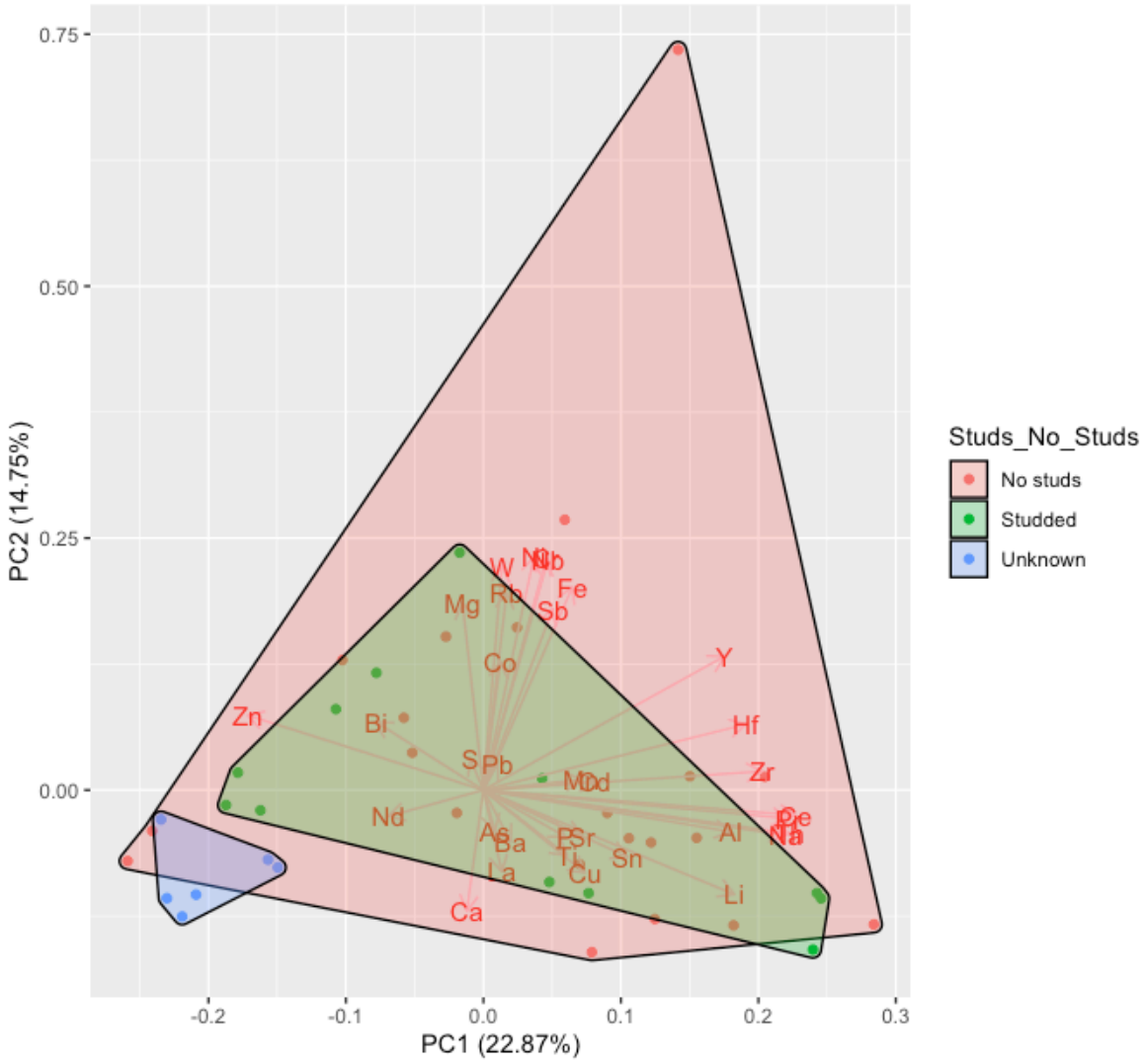

Figure 4.7: PCA-plot of studded (green) and non-studded (red) tires. Unknown (blue) are truck tires.

4.3 Optimizing the µ-XRF-approach

4.3.1 Testing the parameters

The best intersection between a fast scan and good results were investigated through systematic experimentation. Testing of parameters illustrates how the different parameters affect a mapping in practice. Pixel size can be seen to have smaller pixels and stronger background signals than the other tests. Dwell time and number of cycles sorted out background signals. However, bigger pixel size (25 µm) in these scans makes them less precise. The results of the combination test have sorted out even more background signals, as well as barely detecting the smallest particle (Figure 4.8).

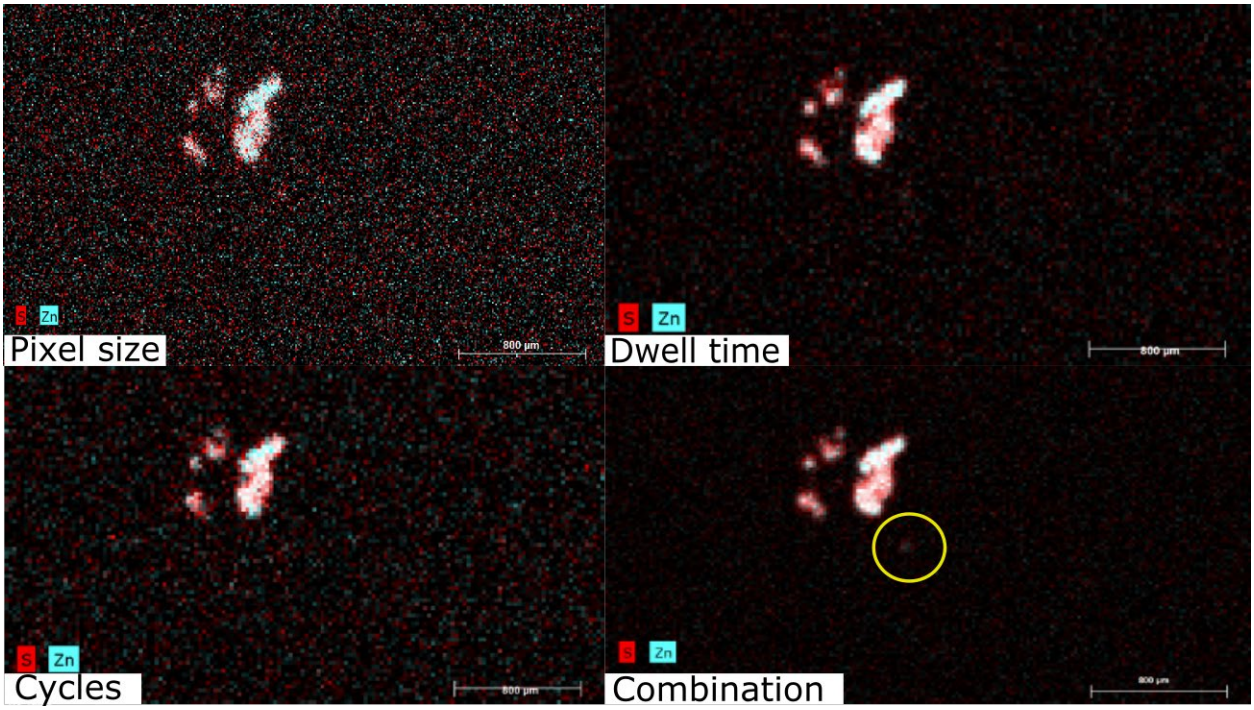

Figure 4.8: µ-XRF mappings from the parameter testing, illustrating visual differences of the different parameters. The test labelled combination was performed with medium precision parameters and had the best result. It was also the only of the four scans that detected the smallest particle (inside yellow circle).

4.3.2 Scanning time

In the control scan there were a background signal of S from the filter. The mylar that the filter is packed in emitted a signal of Zn (Figure 4.9). Nevertheless, the higher concentration of zinc and sulfur from the particles have a strong contrast to the background. This mapping took approximately 23 hours. The smallest particle on this sample is about 30 µm wide and 60 µm long.

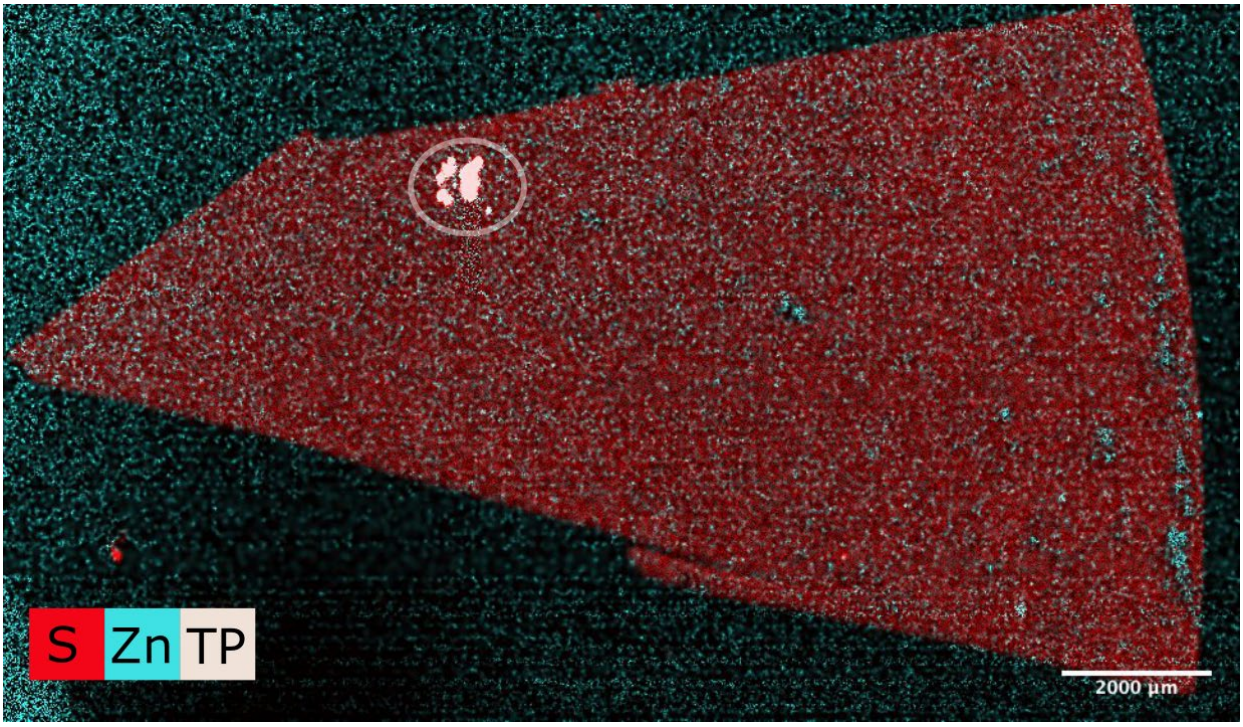

Figure 4.9: µ-XRF mapping of the control test of the filter sample. Red = sulfur, cyan = zinc. The circle marks area of $TP_{ref.}$ The smallest particle can be seen on the right side and below the bigger particles in the circle.

To optimize the µ-XRF approach, it was important that the scans were as quick as possible, without hampering the quality of the results. The tests were based on the information that was gained from the parameter tests. Particles were found in all tests, but only test B detected the smallest particle (Figure 4.10). Total time spent per test are listed in Table 4.2.

Table 4.2: Time usage of the different time tests. Measure time lists the active measure time of the detector. Overall time is the total time from start of scan until it is finished, including movement of the stage, amongst other factors.

TEST NUMBER	MEASURE TIME (MIN)	OVERALL TIME (MIN)
TEST A	13	21
TEST B	24	41
TEST C	4.6	10
TEST D	18	39

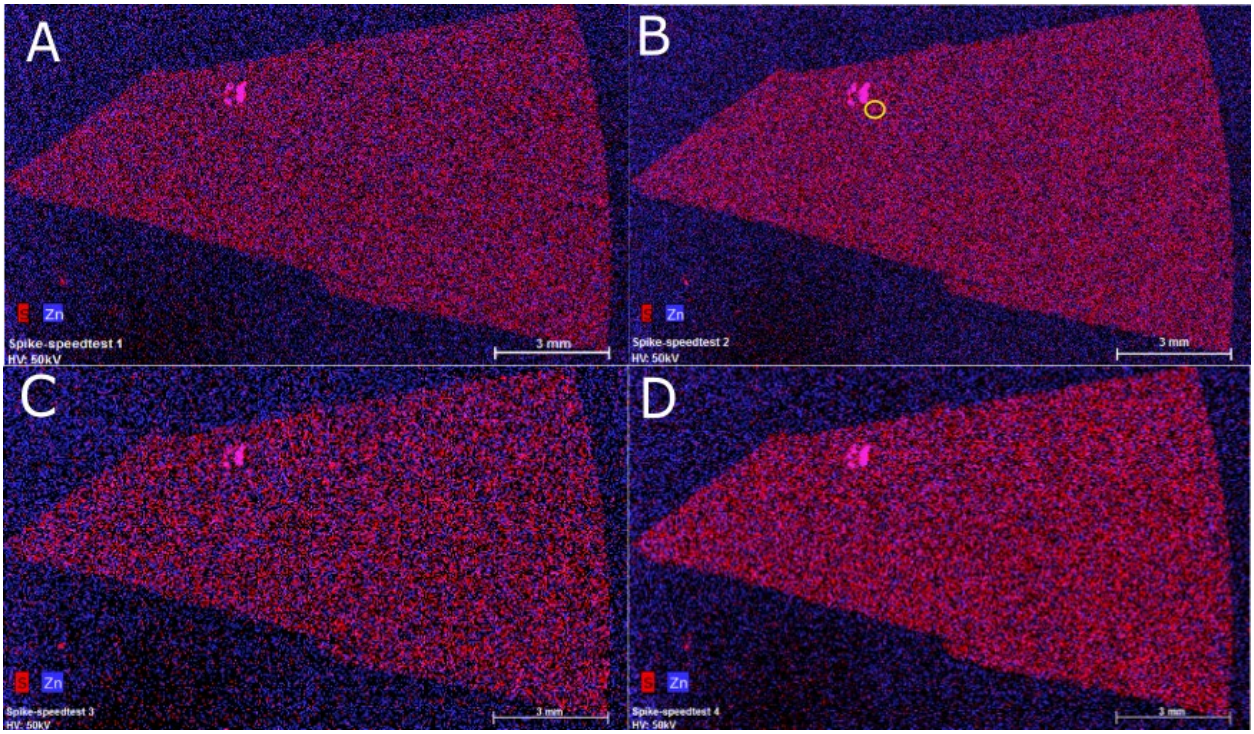

Figure 4.10: µ-XRF mappings of the scanning time tests illustrating the differences of time used in a scan does. Test B is the only scan the smallest particle was detected, marked with yellow circle.

4.4 µ-XRF analysis of reference tire particles on different sample media

Positive controls were made with TP_{ref} to test the abilities of µ-XRF to detect TRWP. When preparing the positive controls and method testing, three different approaches were attempted to place TP_{ref} on the samples. The first method was to pick out particles with narrow metal forceps. This led to too many particles being picked up and placed on the sample, along with little control of where the particles were placed. Additionally, the TP_{ref} that fell on the filter were challenging to move with the forceps. In the second approach a W-probe was used. This efficiently moved particles in a controllable amount. Electrostatic charges of the particles proved to be a challenge, making it hard to precisely place the particles. The third approach was to suspend particles in water and use a narrow glass pipette to move the particles. This was done to minimize potential problems with electrostatic charges. The challenge with this approach was getting the particle into the pipette and keep it in the tip for extraction. If too much water was taken in with the particle, the particle would float and get stuck on the pipette wall. Overall, the approach using the W-probe gave the best results. Even though the TP_{ref} were hard to place in an exact position, it was better to have control of the number of TP_{ref} that were deployed. To suspend TP_{ref} in water before moving them with the W-probe would possibly be a better approach. This was not tested. With this approach, the water would possibly neutralize the surface charges and make the particles settle after placing. A possible challenge with this is that the particles will be hard to move with the W-probe, due to the loss of surface charge.

4.4.1 µ-XRF analysis of reference tire particles on a clean filter

Seven TP_{ref} were analyzed using the point scan function (Figure 4.11). All particles (except 5 and 6) have a similar mass percentage. The mass percentage of signature elements in all scanned TP_{ref} varied between 60-75% Si, 18-26% S and 1.3-3.6% Zn (Figure 4.11). These variations indicate that the particles have strong signals from the signature elements, and that there are variations between the different particles.

Reference tire particle 6 was the smallest particle in the sample and does not match the profile of the other particles scanned. This is likely because of the small size of the particle (~45 µm) resulting in higher contribution of S and Ca from the filter caused by the beam penetrating the particle and hitting the filter. It may also be caused by variations in elemental content of the particle.

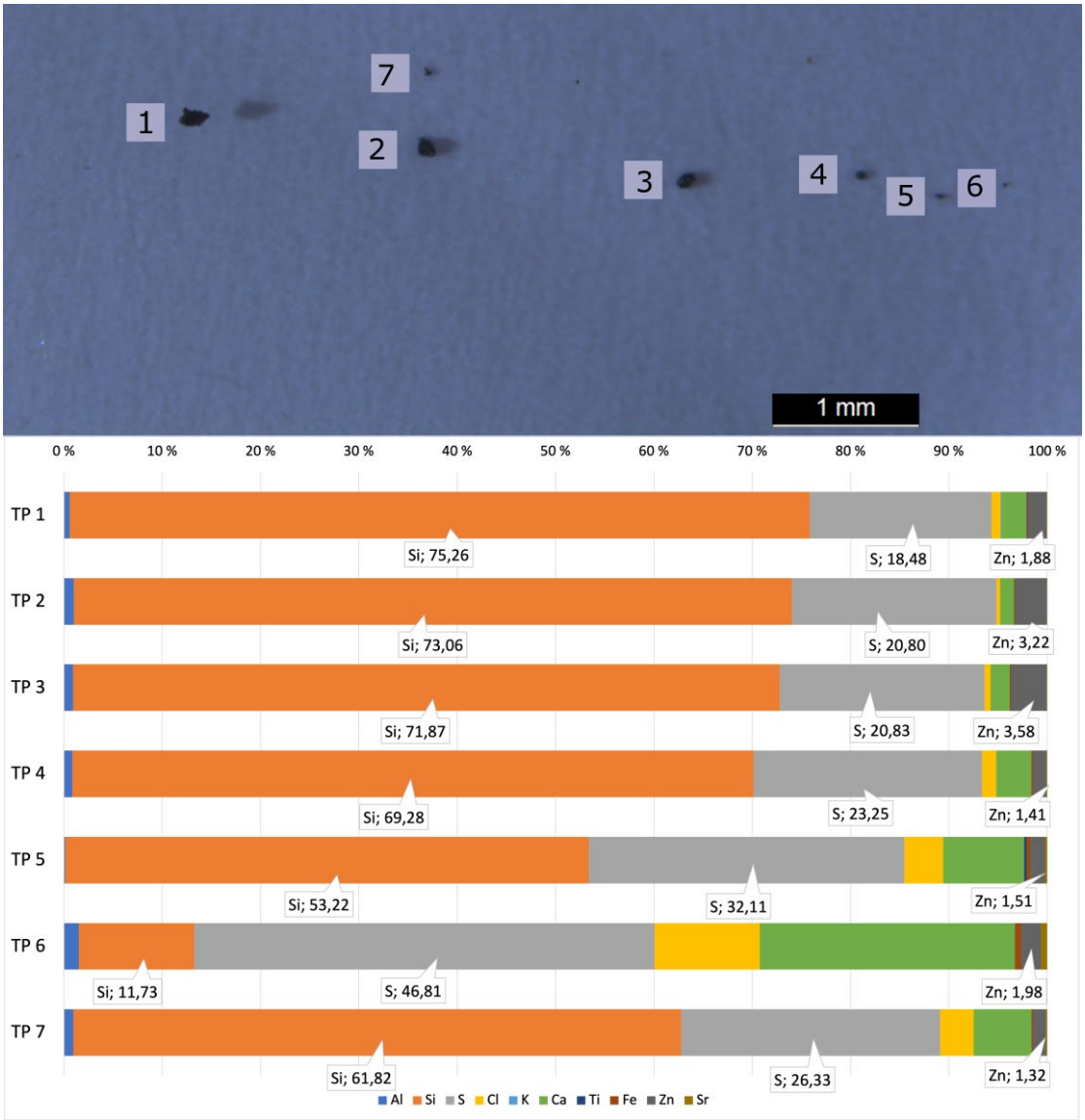

Figure 4.11: TP_{ref} on a filter (top), and normalized mass percentages of elements found in the particles (bottom).

To further investigate the elemental content and signals from the particles, a line scan over two particles (TP 4 and 5) were performed (Figure 4.12). The y-axis shows the signal strength in relation to the highest measured signal. This yielded a maximum peak of Si from the particle on the left (TP 4), as well as elevated levels of the signature elements from both particles. One thing to note from this scan is that the signals from of Si and Zn may be dependant on the size of the particles, while the signal from S does not change as much with decreasing particle size. The signal from Si varied from 100% to 35%, Zn from 85% to approximately 50% and S from 35% to 20% between the two particles. Since the particles are from a mix of different tires, this may also reflect variations in elemental composition between the different tires.

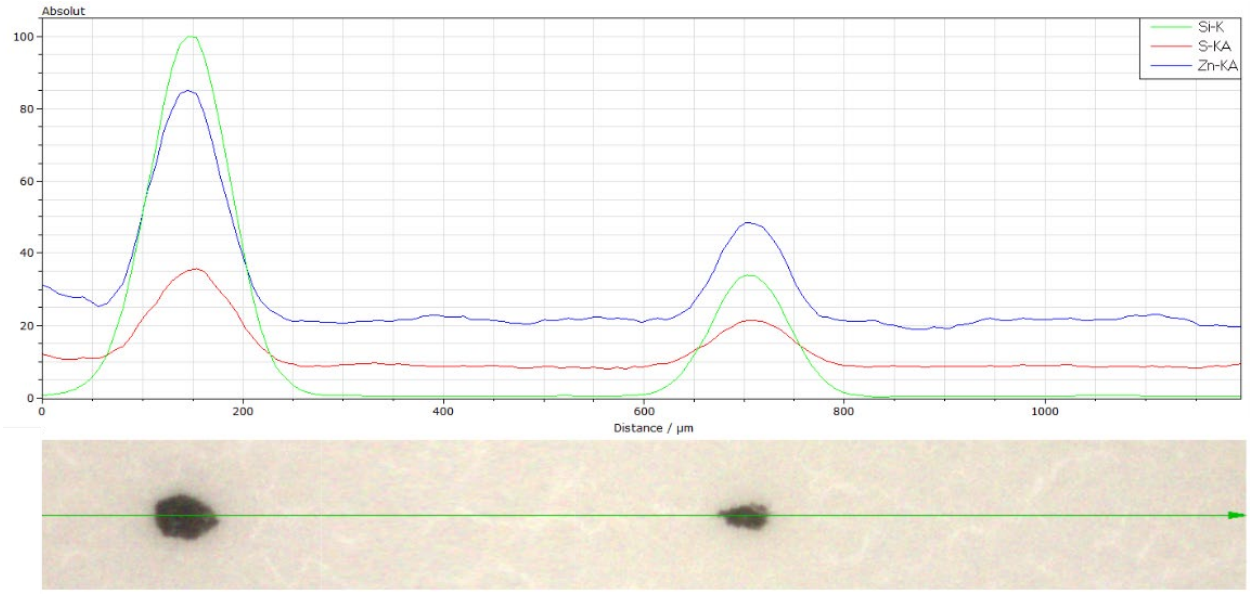

Figure 4.12: µ-XRF line scan of elemental signal strength over two TP_{ref} (TP4 and 5) on a clean CN-filter. Increase in signature element signal can be seen over the locations of the particles. The scale of the y-axis is absolute, meaning the maximum signal received sets the level at 100%. Below the line scan data there is an image of the scanned particles. The green arrow shows the scanned line over the particles.

The results of the performed area scan shows that the TP_{ref} stands out from the background signals from the filter (Figure 4.13). The filter exhibits a background signal of S, but the particles have a stronger signal, making a good contrast to the background. Some background can also be seen in the mapping of Zn, but not to the same extent as S. Although there are some background signals in the maps showing signals of S and Zn, all seven TP_{ref} are detected. In the map showing Si-signals, the smallest (TP 6) is not detected. Particle 6 also has a weak signal from the other elements but is possible to see.

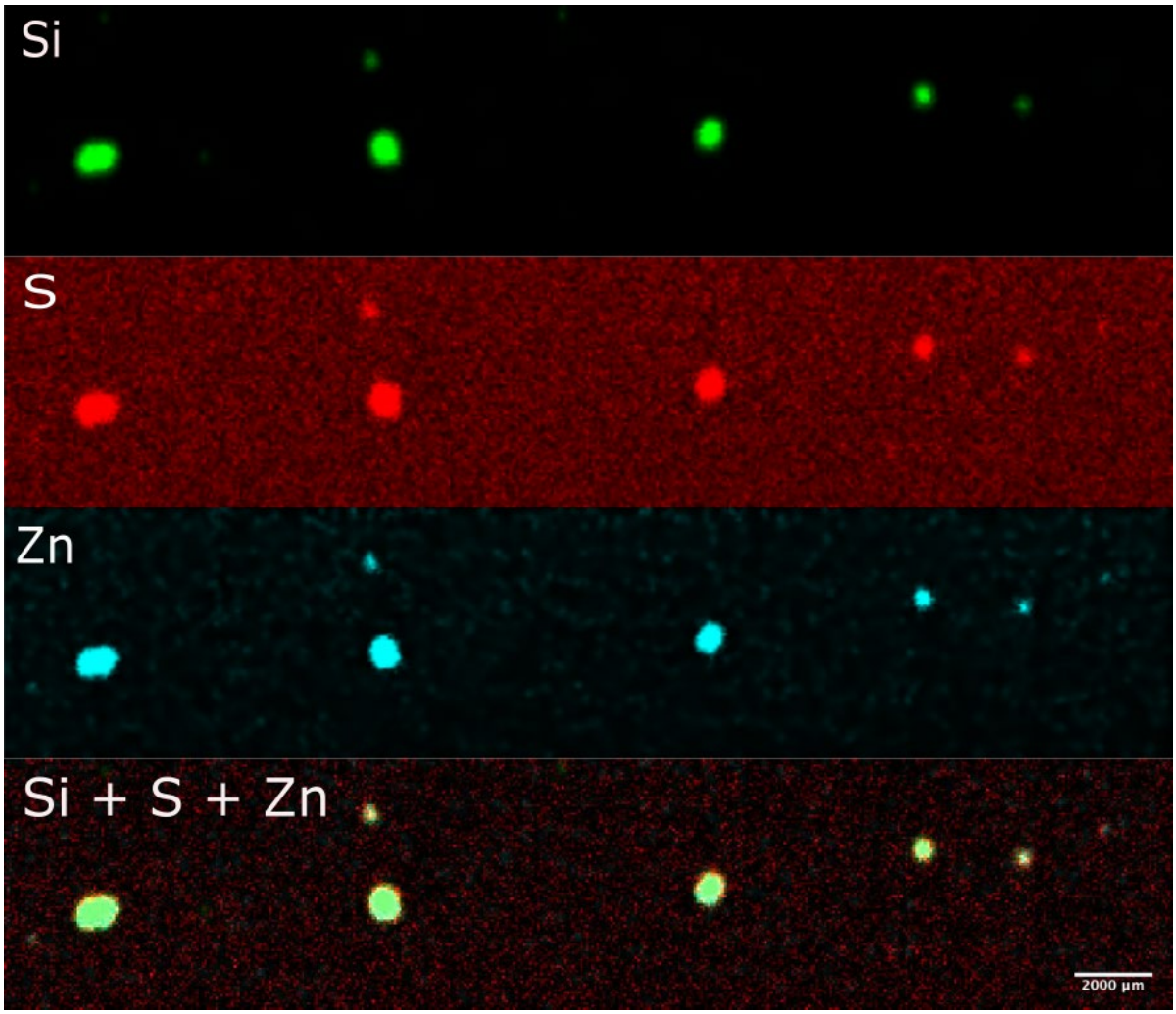

Figure 4.13: µ-XRF mappings showing signature elements found in TP_{ref} on a clean filter. All TP_{ref} are detected in the scans, except the smallest particle (particle 6) on the Si-mapping. Background from the filter can be seen in the S-mapping, but the particles still have a contrast to the background signals.

4.4.2 μ-XRF analysis of TP_{ref} on a freeze-dried gill

Point scans of TP_{ref} placed on a freeze-dried gill show that the signals were affected by the sample media. The results show that particles 1 and 2 have a similar elemental composition, which is quite different in comparison to the two larger particles (3 and 4) (Figure 4.14). The content of Ca is high in all scans, likely caused by parts of the incident x-ray beam penetrating the particles, hitting the gill material which contains high levels of Ca.

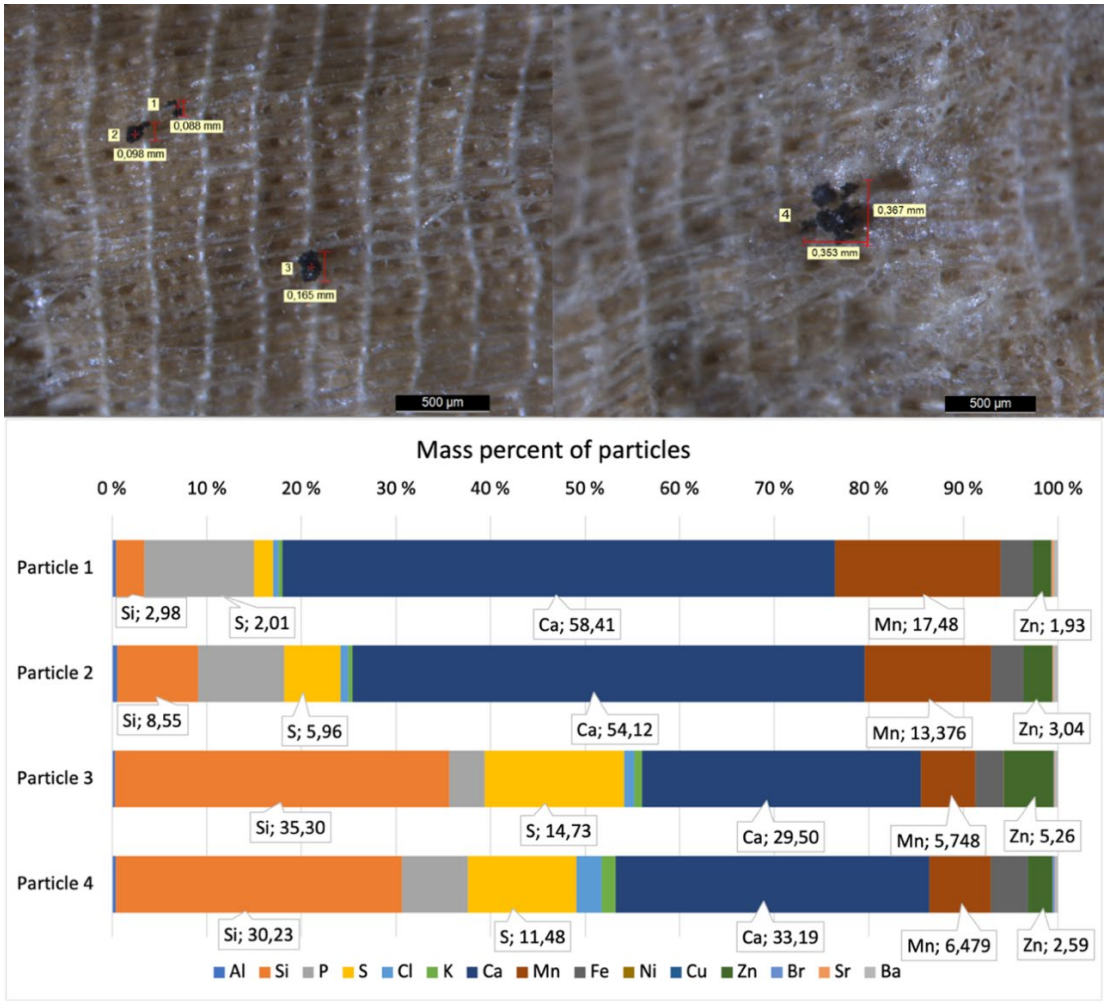

Figure 4.14: μ-XRF point scans of TP_{ref} on a freeze-dried gill, and the normalized mass percentages of each particle. High Ca-contribution imply that the gill material is contributing to the measurement. The two smallest particles (particle 1 and 2) and the biggest particles (particle 3 and 4), have similar elemental compositions.

The line scan of particle 3 from the freeze-dried gill exhibits the strongest signal from Ca, as expected from previous scan results. Elevations of the signature element signals are correlating with the scanning position of the x-ray beam at the particle location (Figure 4.15). This indicated that there was a significant level of these elements, and that the particle is possible to detect on the sample. However, this illustrates the incident beams penetration through the particle, as the signature elements of the TP_{ref} does not have a stronger signal than Ca over the location of the particle.

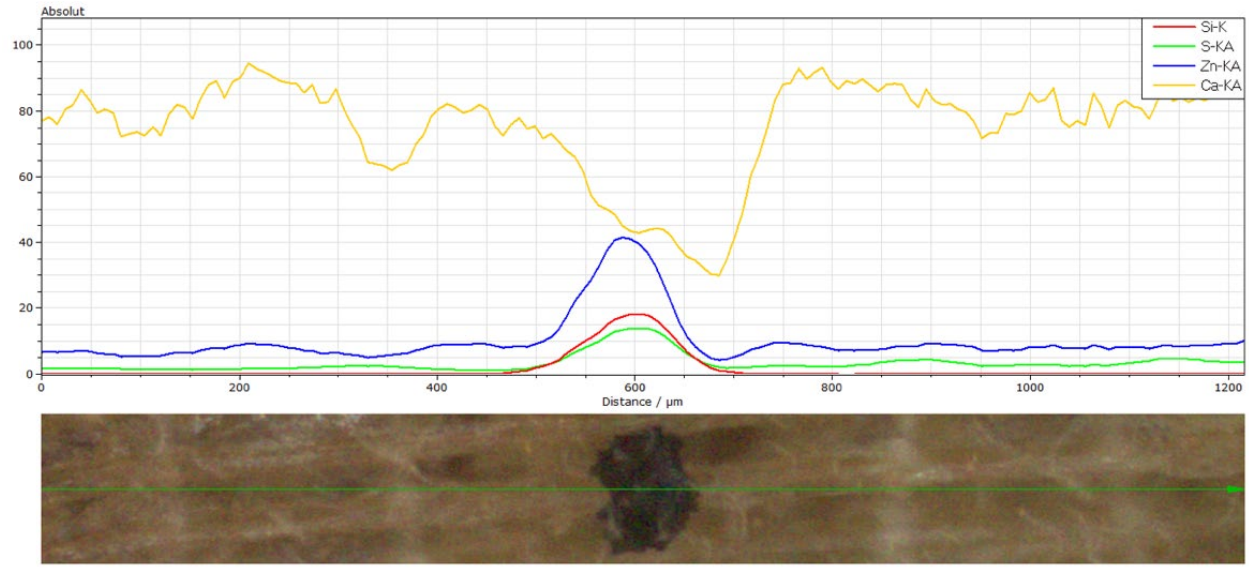

Figure 4.15: µ-XRF line scan of a TP_{ref} on a freeze-dried gill showing the total signal from different elements scaled after the highest signal received. Signals from signature elements are elevated at the particle location. This figure illustrates the beams penetration through the particle, as the signature elements in the TP_{ref} does not have a stronger signal than Ca over the location of the particle.

An area scan of the freeze-dried sample was performed. After acquisition of the scan results, the image was analyzed with ImageJ. The image was inverted to get better contrasts of the TP_{ref} and the background. All four particles were detected in the scan, although the smallest ones (particle 1 and 2) were difficult to see due to their small size (Figure 4.16).

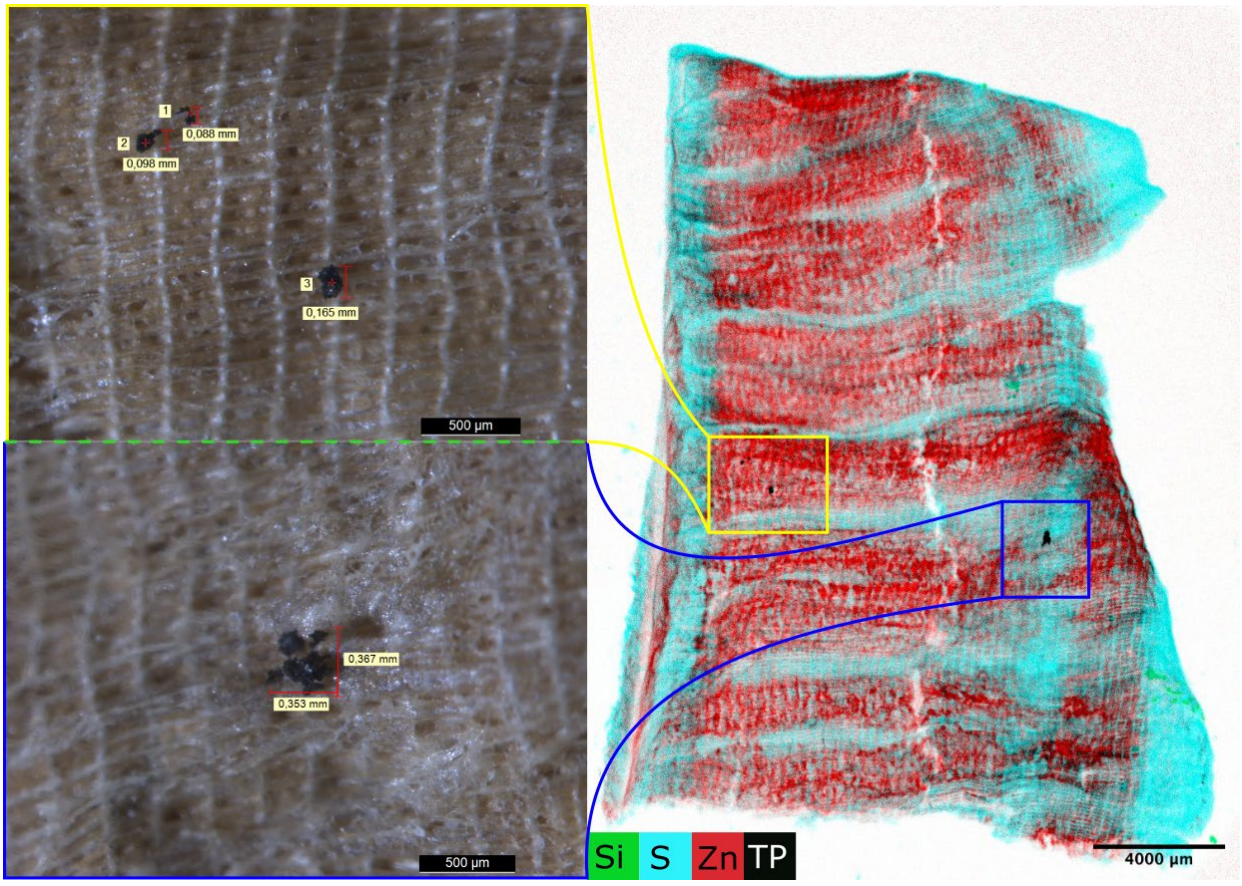

Figure 4.16: µ-XRF mapping of particles on a freeze-dried gill. Image has been inverted in ImageJ for better contrast. Yellow and blue marks the location of the particles on the sample. Black pixels mark strong signal intensity of all signature elements. Four TP_{ref} were identified in this mapping, although particle 1 is hard to see.

4.4.3 µ-XRF analysis of tire particles on a filtered mussel gill

Reference tire particles were placed on a filtered sample from NIVA, which was digested using KOH (Figure 4.17). Point scans of TP_{ref} on a filtered gill show strong signals of the signature elements. However, strong signals of phosphorous, calcium and iron were also detected (Figure 4.18). The signals are likely emitted from elements in the gill material, which could contain minerals as well. Based on the mass percentages of Fe, Mn, Ca and P, particle 5 is likely to be a mineral and not a TP_{ref}. There is a chance that it is a TRWP with mineral encrustations but based on the low content of signature elements, especially Zn, as well as lack of morphology found in the literature, this seems unlikely.

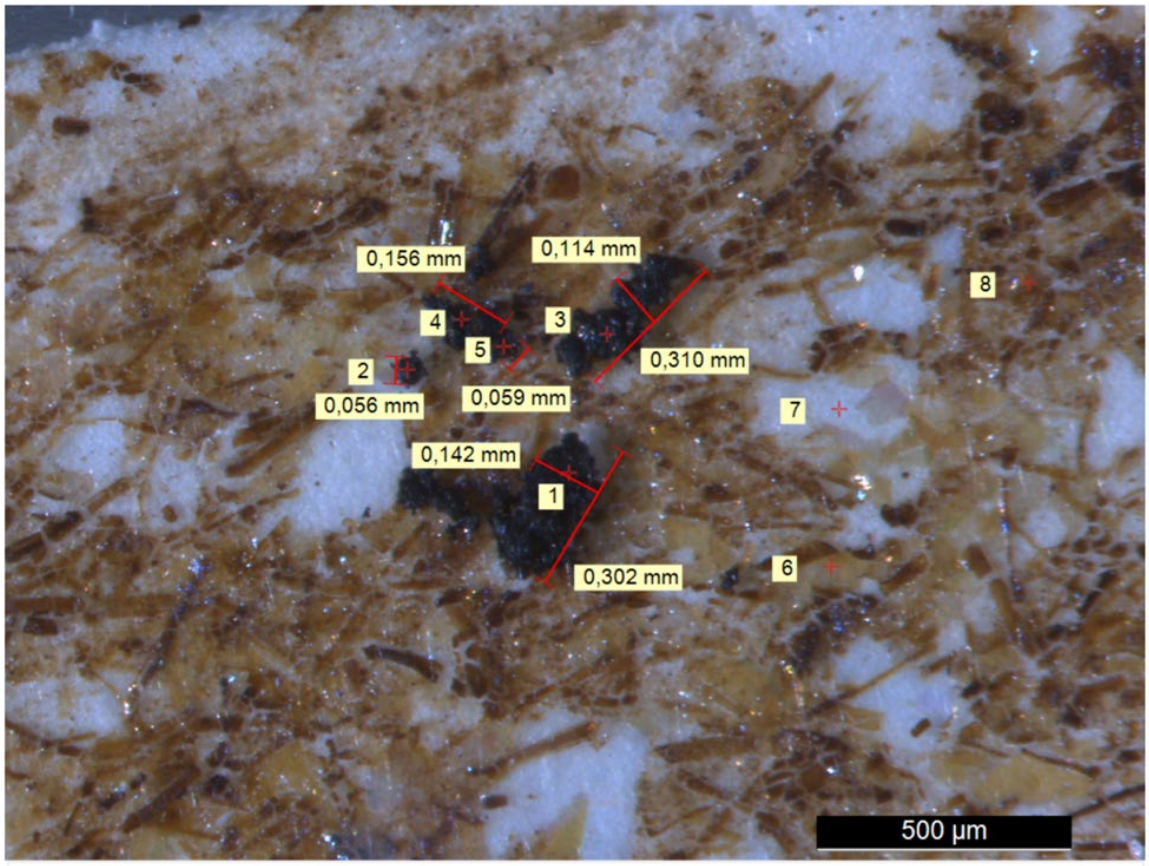

Figure 4.17: Microscopy image of particles placed on a filtered gill that were digested with KOH at NIVA. The numbers mark where point scans were performed.

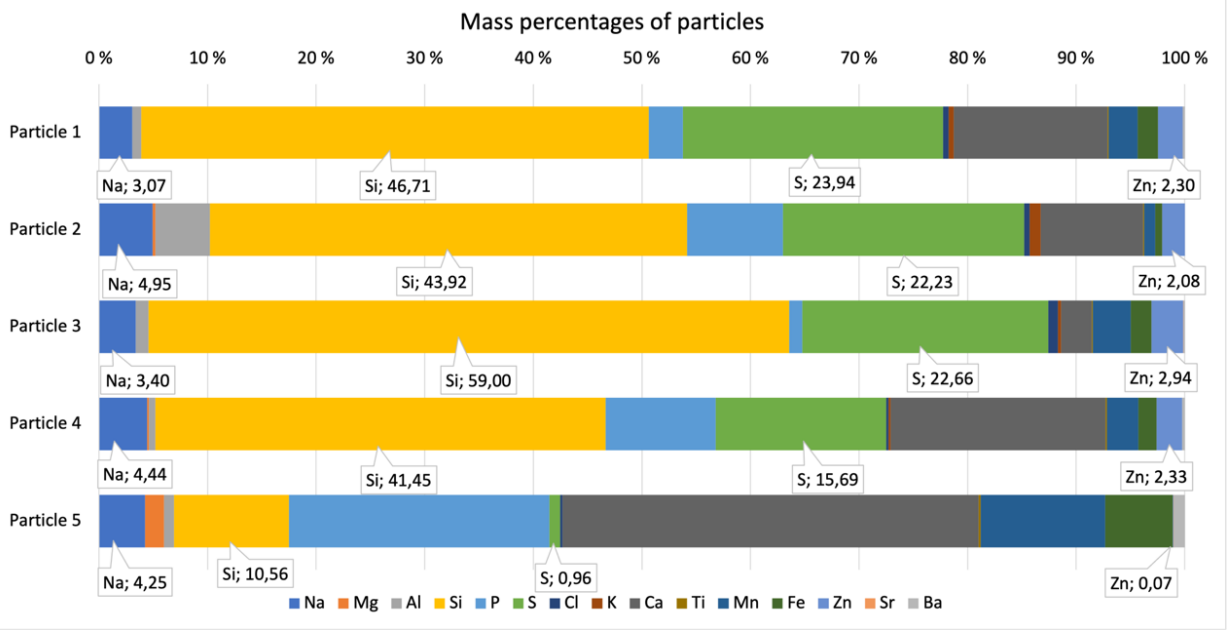

Figure 4.18: µ-XRF point scans of particles on a filtered gill digested with KOH at NIVA. Particles 1-4 can be seen to have approximately the same content of the signature elements. Particle 5 do not match the contents of the other particles and is most likely a mineral.

The results from the line scan of the digested gill show that there are strong signals of the signature elements in two out of the three TP_{ref} placed on the sample (Figure 4.19). The particle 5 emits strong signals from Ca and Fe in this scan as well. No change was observed in signal strength from the signature elements. This is further indicating that particle 5 is of mineral origin and not a TRWP, as the signature elements do not change over the particle location. If this particle were a TRWP, at least one of the signature elements should show an increase in detected signal. This was not observed in this scan; thus, the particle is unlikely to be a TRWP.

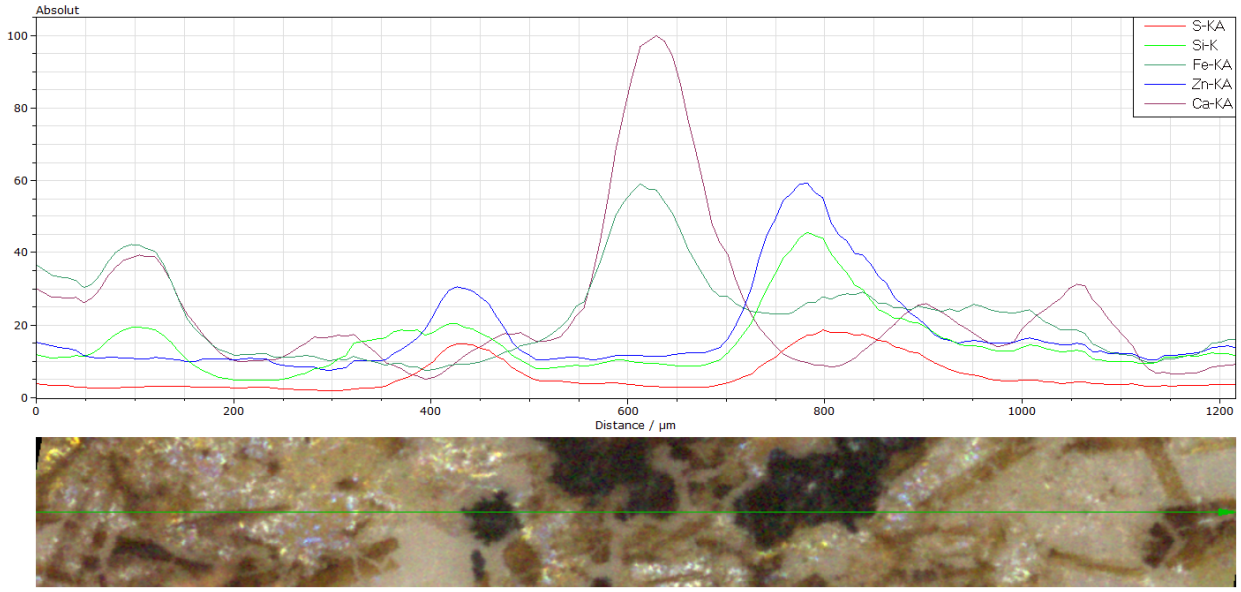

Figure 4.19: µ-XRF line scan of TP_{ref} placed on a filtered mussel gill. The particles at 500 µm and 800 µm have elevated signals of the signature elements. The particle (5) at 600 µm have high levels of Ca and Fe, indicating it is of mineral origin.

4.5 Investigation of duck mussels from Padderudvann

4.5.1 Microscopy analysis and counting of possible particles

All samples were investigated with a microscope. The organic matter that was left on the filter was easier to investigate in mussels digested with NaClO compared to KOH. The material has properties like harpix/resin, and most of the observed particles were embedded inside this material. The colour of the material was yellow/brown and was transparent on most samples (Figure 4.20). This made it easy to see particles trapped in the material. Although particles were easy to see, they were challenging to remove from the material for further analysis without breaking the samples. Where the biological material was thicker, it was more difficult to see potential TRWP.

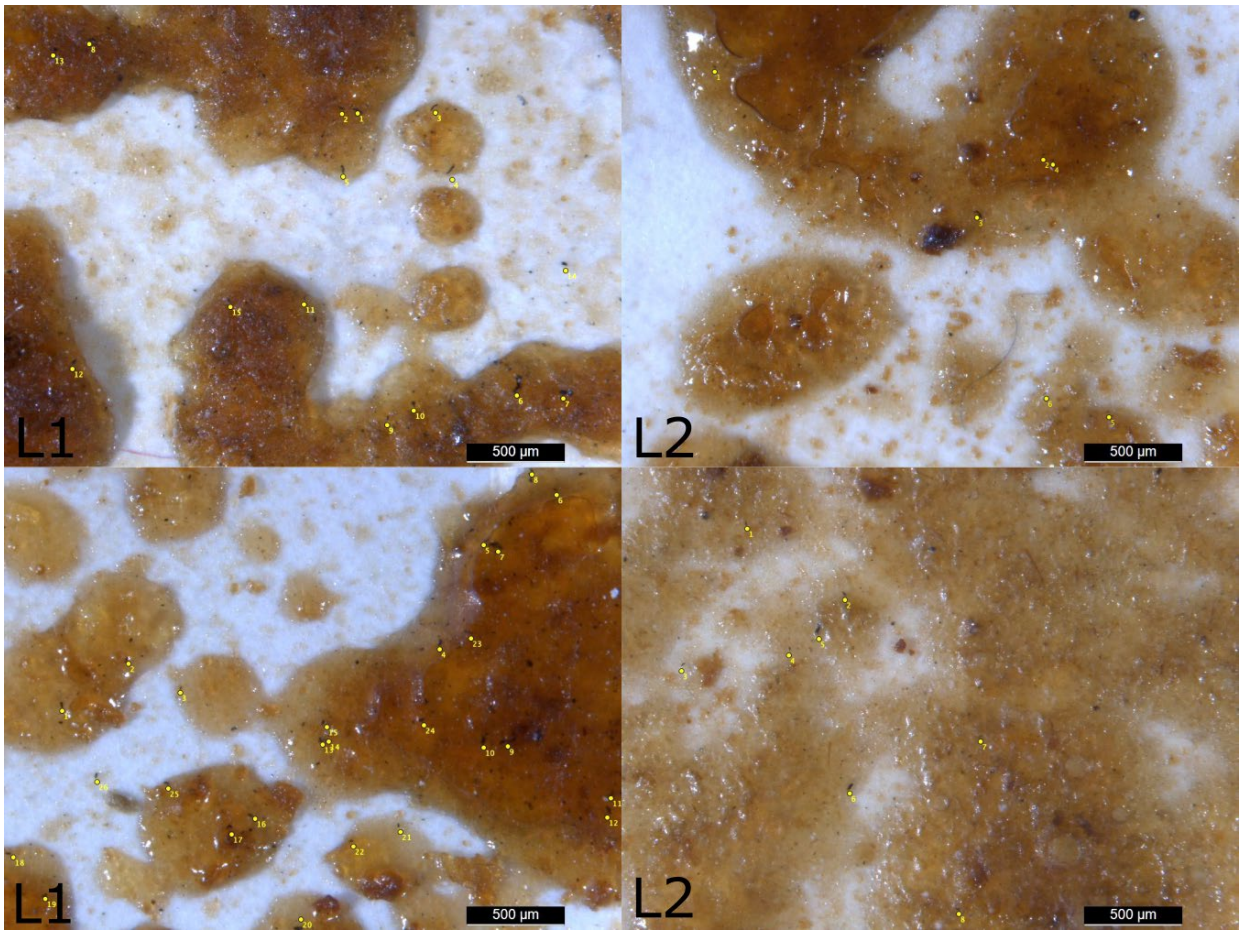

Figure 4.20: Examples of mussels from the different locations. Yellow dots mark the counted particles that are suspected TRWP. The images from L1 contains 15 (upper image) and 26 (lower image) potential TRWP. The mussels from L2 contains 4 (upper image) and 8 (lower image) potential TRWP. Photo: Ole-Johan Næss Holm.

The visual inspection showed an apparent higher content of black particles in mussels from L1 compared to L2 (Figure 4.20). Many particles also matched the described morphology of TRWP, being elongated and black. To verify that there were more potential TRWP in mussels from L1, particles matching the description of TRWP in the samples were counted. The counts indicated that a majority of samples from L1 had a higher content of particles matching the described attributes of TRWP than samples from L2 (Figure 4.21). Out of eleven counted areas from mussels from L1, eight of the counts were higher than the highest number of particles counted in a mussel from L2 (8 particles) (Appendix C, table 1). Mussels from L1 had an average of 13 ± 7 potential TRWP image^{-1}, while mussels from L2 had an

average of 4 ± 2 potential TRWP image^{-1} from the high magnification image. The difference in observed potential particles was greater between the images with lower magnification. In the images with lower magnifications mussels from L1 contained an average of 21 ± 11 potential TRWP image^{-1}, and L2 an average of 4 ± 2 potential TRWP image $^{-1}$. The area sizes of the images were 7.4 mm^2 (high magnification) and 26.3 mm^2 (low magnification). If the areas are added together a total of 44.4 mm^2 (low magnification) and 157.6 mm^2 (high magnification) were investigated from each location. Mussels from L1 had a total of 80 (high magnification) and 104 (low magnification) potential TRWP. Meaning each filter contained 1.8 particles/mm^2 (high magnification) and 0.66 particles/mm^2 (Low magnification). Mussels from L2 had a total of 24 (high magnification) and 23 (low magnification) particles contain 0.15 particles/mm^2 (High magnification) and 0.54 particles/mm^2 (low magnification). These numbers are calculated assuming an even distribution of potential TRWP across the filters. This might cause large deviations to each sample. However, given that one filter from each location had very few particles the total number are lowered, to give a better representation of the results.

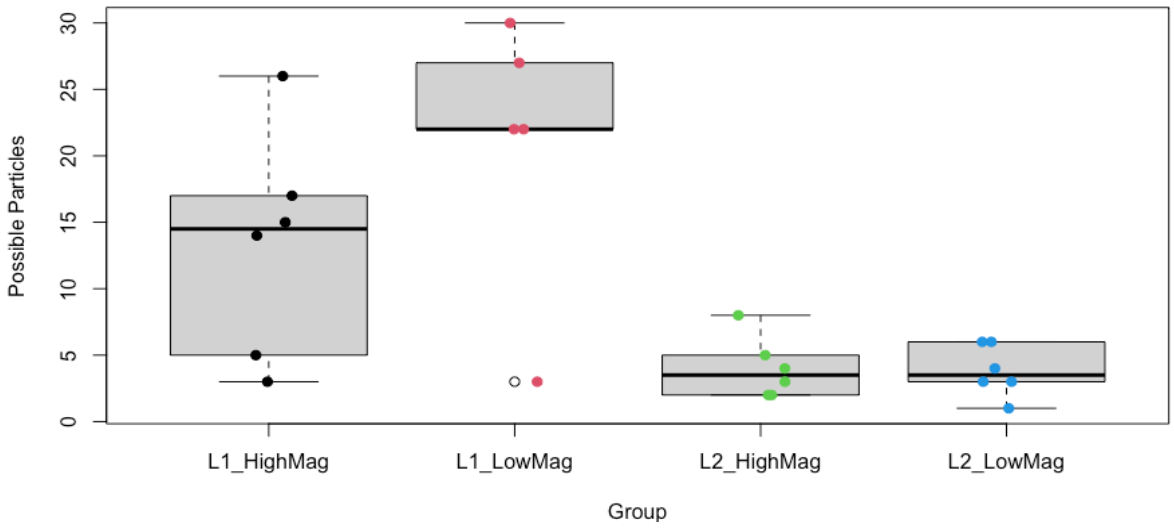

Figure 4.21: Boxplot of counted potential TRWP found in images of digested mussels. The boxes are grouped after location and magnification used in the microscopy. The coloured dots mark the individual sample values, and the black circle marks an outlier.

Counting of potential TRWP could not be done by built in functions in ImageJ. This was likely caused by the mylar that the filters were packed in, as well as dark spots in the sample material giving false positives. It was also observed that particles that would not be counted in a manual count were counted, while particles that matched the description of TRWP were not counted. Since the counting had to be done manually, there were a risk of the counting being biased towards finding more particles in the mussels from L1. To counter this problem, strict parameters of choosing which particle to count were set to make it as unbiased as possible. This meant that only particles that matched the reported morphology from the literature were counted, meaning colour, shape, and size had to be right. Another way to make an unbiased counting would be to count particles in the samples without knowing which location the mussels were from.

To investigate whether there was a significant difference between the two locations or not, t-tests were performed. These tests were performed with a null hypothesis assuming no difference between the two locations. The test of high magnification images of L1 suggests that there was a statistically significant difference in number of particles in mussels inhabiting L1 compared to L2 (13 ± 8 (L1) vs. 4 ± 2 (L2), $p = 0.041$). Difference is also suggested in low magnification images (21 ± 11 (L1) vs. 4 ± 2 (L2), $p = 0.022$), as well as in all images (16 ± 10 (L1) vs. 4 ± 2 (L2), $p = 0.0014$. With all tests showing a significant difference it can be assumed that there is a difference in particle content between the two locations.

4.5.2 Positive controls of NaClO-digested mussels

The mappings of positive controls were inverted in ImageJ after μ-XRF analysis. This was done because the signals of all elements together had better contrast to the background when the colours were inverted, making them darker instead of lighter.

The body sample used as positive control had issues with the electrostatic charges of the TP_{ref}. The particle in area 4 was detected and found where it was placed through microscopy (Figure 4.22). In area 2, signals of all three tracer elements were detected. However, it was not found any particle in area 2 through visual inspection. The detected particle had likely

moved to area 1 in between the scanning and microscopy. This is likely due to the topography of the sample not being flat enough for the mylar to hold the TP_{ref} in place, giving the particle room to move. The small TP_{ref} in area 3 were not detected. The largest of these undetected particles were measured to approximately 60 µm in the longest axis, and the others were 10-30 µm in the longest axis. This was surprising, as there were no residues covering them that could hamper the emissions of element characteristic X-rays. For the particles smaller than the incident beam size (25 µm), the lack of emissions can be explained by elevated background emissions causing self-absorbance of the emitted X-rays from the sample. The particles that have a size >25 µm should be detected as in other scans in this thesis. This problem might be caused by high Cl-levels caused by the NaClO, thus shadowing the S-signals. Another possible explanation is that the mylar were scattering the beam, thus weakening the effect of the X-rays in both directions, hampering the focusing effect.

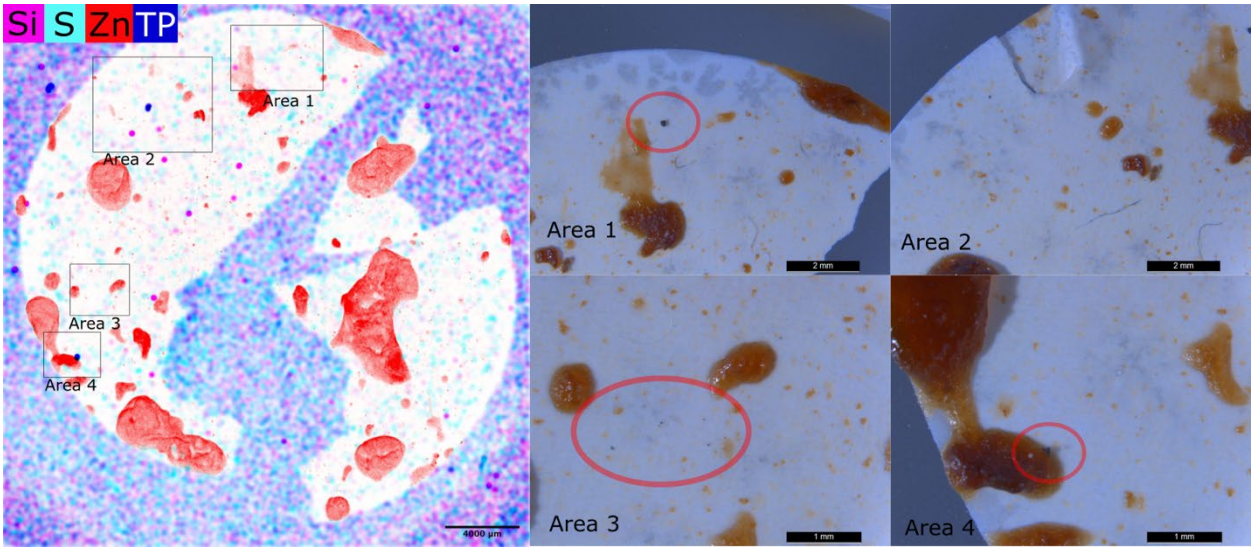

Figure 4.22: µ-XRF mapping that has been inverted in ImageJ for better contrasts of a positive control of a body sample with ROI (black squares, left image). Microscopy images of the ROI (right) show where the particles are or should be. The detected TP_{ref} in area 2 from the µ-XRF map has likely moved to area 1. In area 3 small TP_{ref} were placed, and no signals are detected. The TP_{ref} in area 4 is detected well.

The particles that were added to the samples were added on top of the samples, rather than inside the material because of the characteristics of the sample material. However, knowing the location of the particles proved to be challenging because of the particles ability to move around on the samples.

Gills

The positive control of the gill sample did not have issues with particles moving as seen in the sample of the body. The particles that were covered and partially covered in the sample material emitted signals of all the signature elements. Although particle 1, which was put deepest into the sample, gave a weaker signal, it was still detectable for all three elements (Figure 4.23). The weaker signal that was observed from the particle covered in biological material might suggest that the same is happening in the samples of the bodies, where many potential TRWP were observed but not detected with μ-XRF.

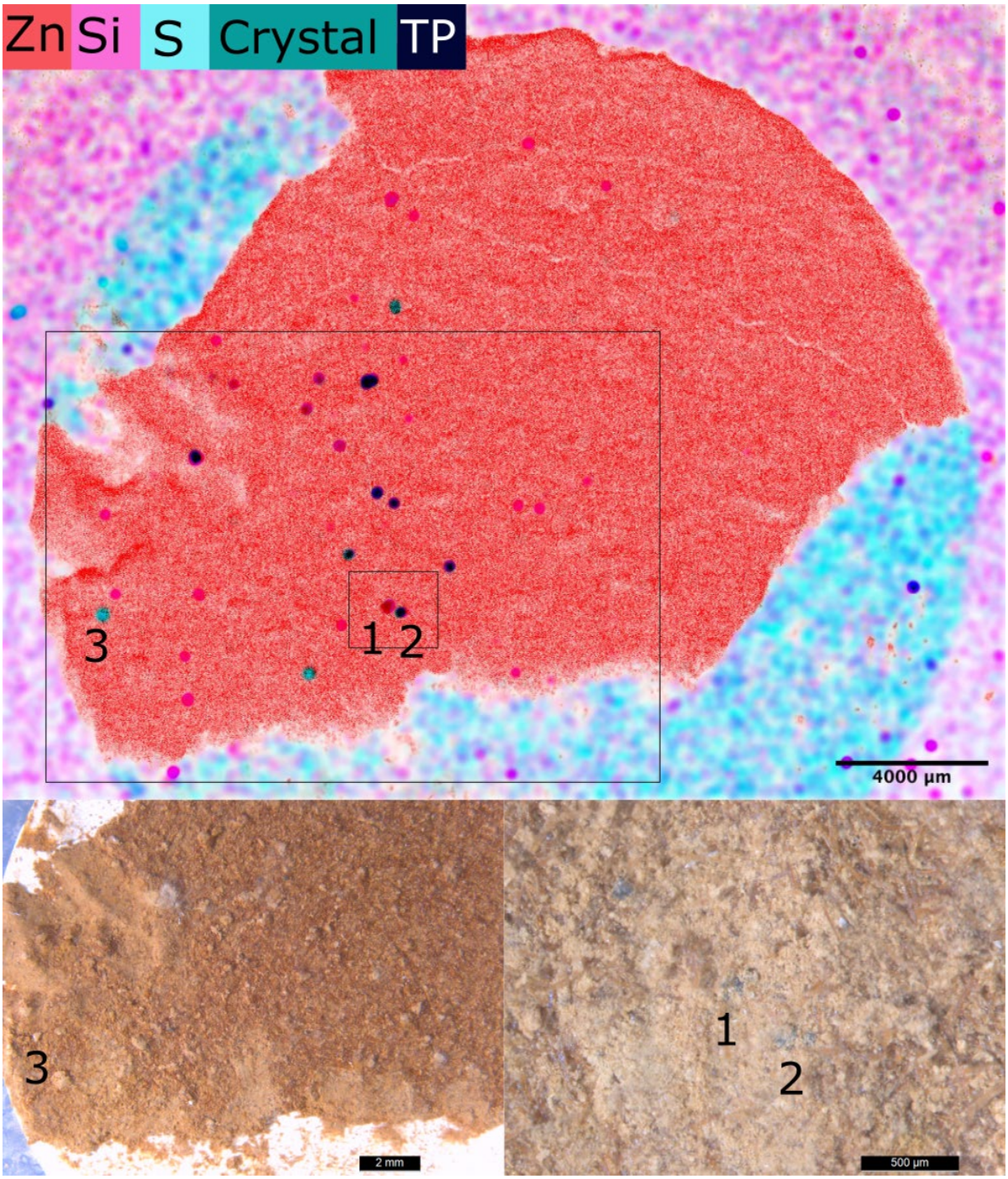

Figure 4.23: µ-XRF mapping of positive control of a gill sample with ROI (black squares). At the top colour codes for the different signature elements are shown, in addition to the colorus of crystals and TP_{ref}. The biggest ROI is shown in the image on the bottom left and the smallest on the bottom right. The numbers 1 and 2 marks the TP_{ref} that are covered by the sample material, and 3 marks a crystal.

4.5.3 Scanning of samples

Point scans of different samples were performed to find differences in elemental composition in mussels between the locations. It was found that mussels from L1 have a higher level of all the signature elements (Figure 4.24). Results of point scans of treated particles were also included to see the difference between the samples and sample media. Note that some detected elements are removed from the data because of very low content, or because of strong interference with the composition (see appendix B, table 1, 4 and 5 for total normalized mass percentages, and figure 1 for XRF-spectrum).

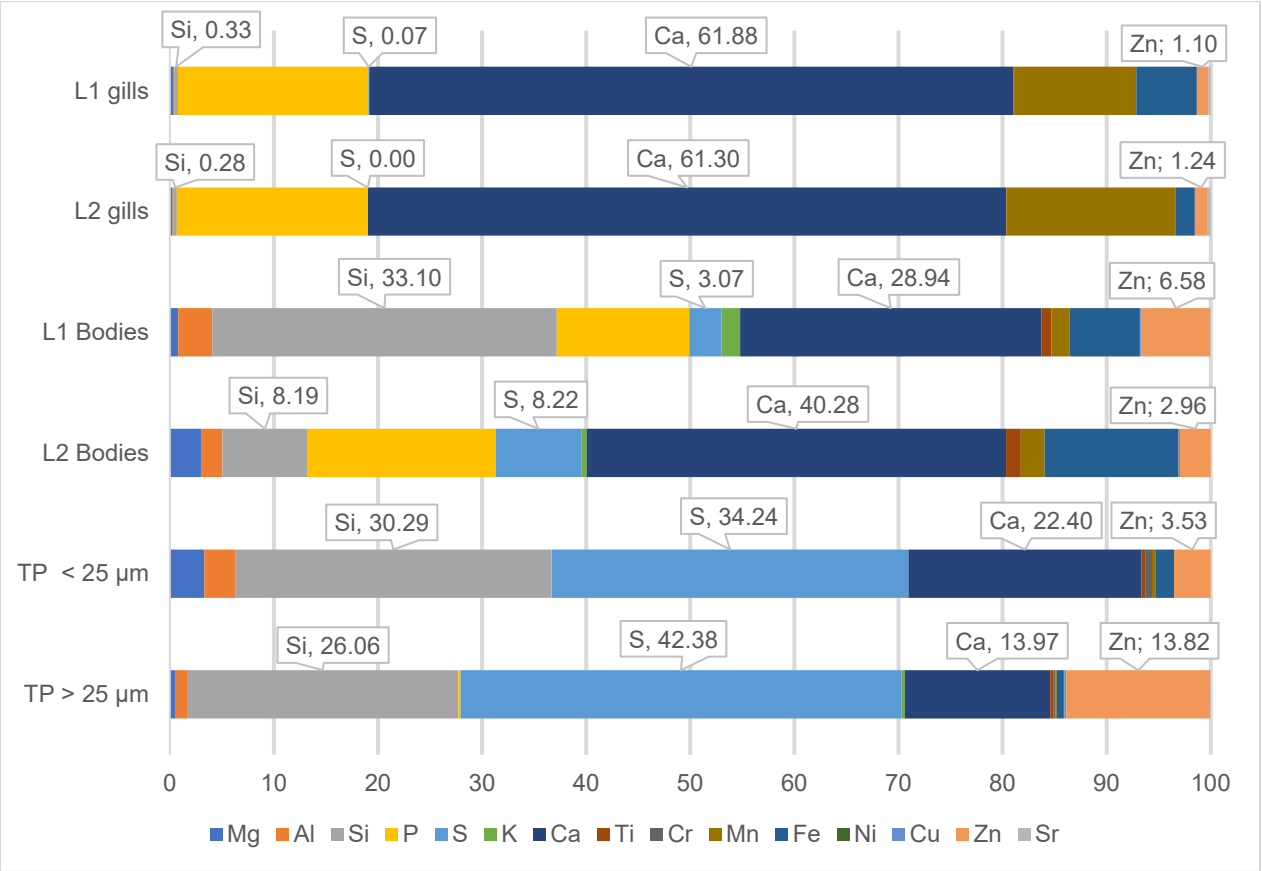

Figure 4.24: Average normalized mass percentages of TP_{ref} of different sizes (< 25 µm, > 25 µm), and mussels from the different locations. Na and Cl are removed from the data because of high levels caused by the digestion process, as well as elements containing very low levels and many zero-values. The data have been converted to 100% after removal of these elements. Values are shown in percent.

The elevated Cl-content of the treated particles made µ-XRF detect the particles through area scans. It was thought that this digestion protocol had a potential of spiking TRWP with Cl to make detection easier with µ-XRF in biological samples. Area scans done of the treated particles illustrates the effects of NaClO-digestion on particles. Many particles that were not detected by the signature elements were detected by their Cl-content (Figure 4.25). However, when scanning treated particles in positive controls, the Cl-signals of particles were not detected. This is likely caused by high levels of Cl in the biological residues on the filters.

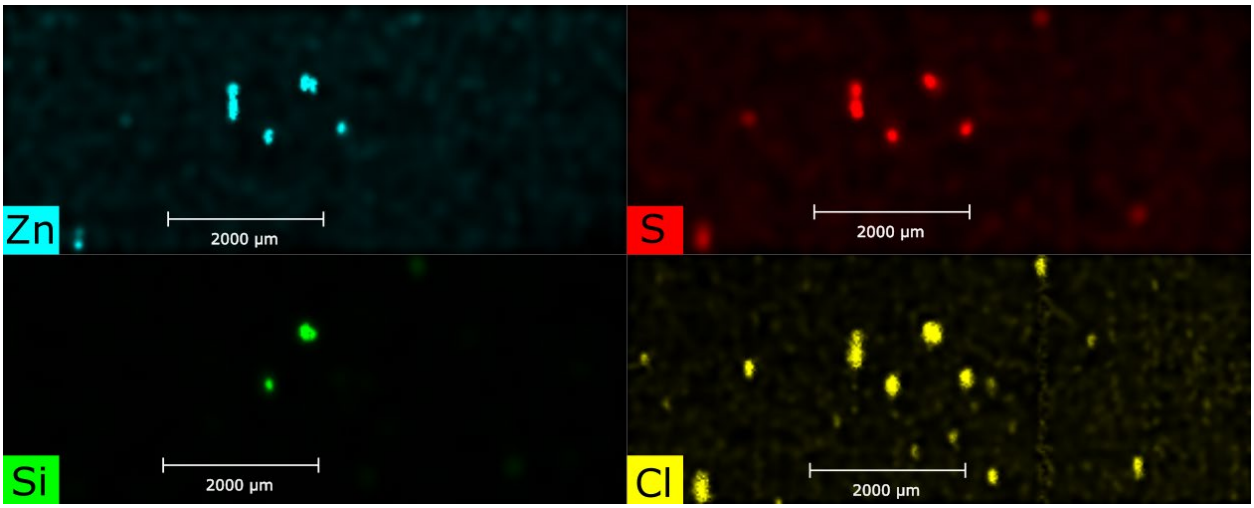

Figure 4.25: µ-XRF mapping of treated and filtered TP_{ref}. More particles are detected with Cl than the signature elements.

4.5.4 Compositional analysis

To further investigate the difference between the two types of samples PCA was applied. Because of the digestion approach, Na and Cl were removed from the data to avoid residues from the chemical to affect the results. Elements with low values were also removed from the dataset. The PCA show a difference between gills and bodies (Figure 4.26). Since the gills were known to have a high content of Ca, this element was removed from the analysis. The bodies had a bigger spread than the gills. However, the bodies from L1 had a stronger correlation towards Zn and copper (Cu), indicating that these mussels were affected by the road.

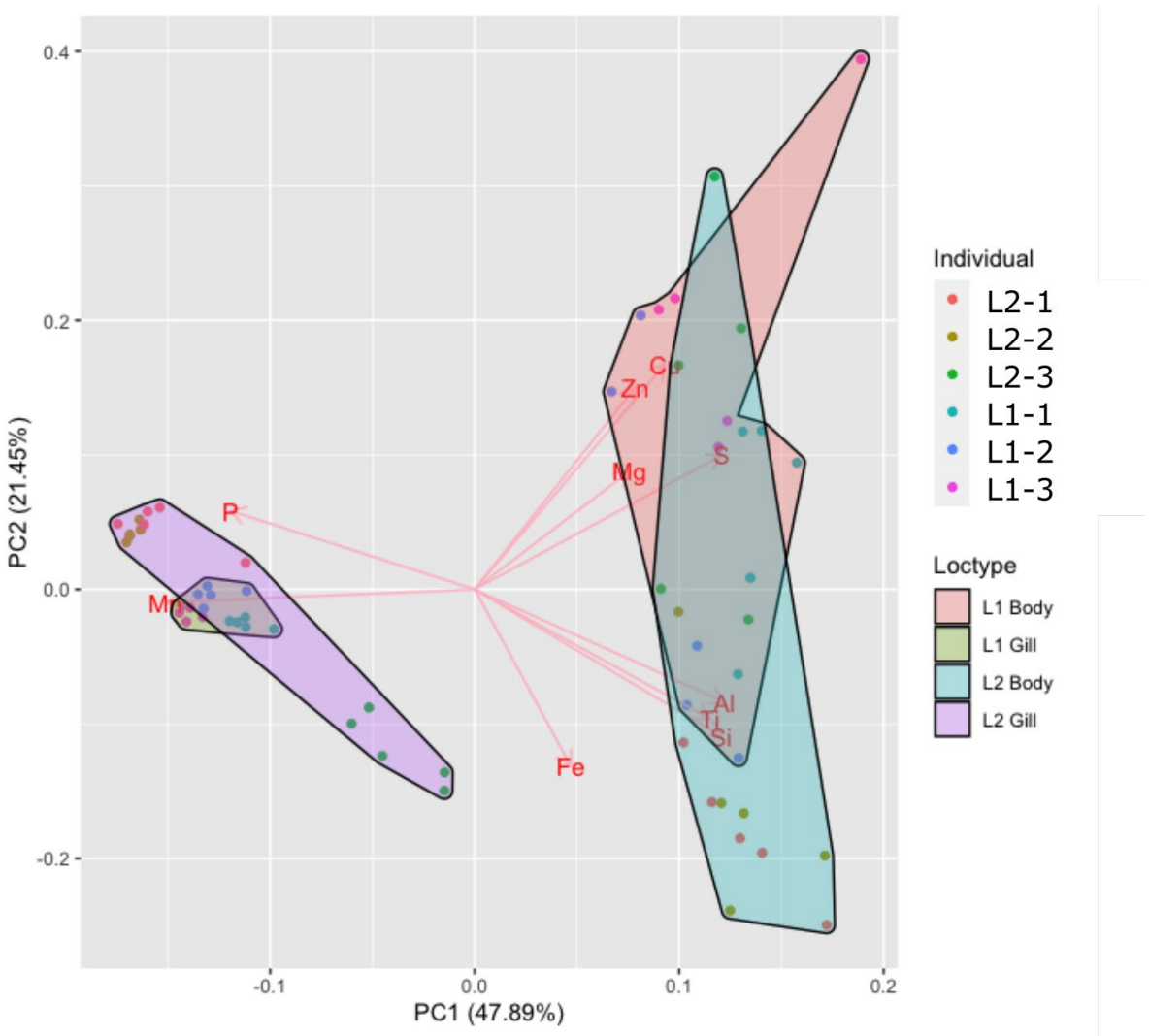

Figure 4.26: PCA-plot of gill and body samples from six different mussels. The PCA is based on mass percentage of elements measured in different samples. Control 1, 2, and 3 mean mussels from L2 and exposed mean mussels from L1. The gills have a larger spread among individuals from L2 than those from L1. The bodies are more equally distributed, although a larger fraction of the mussels from L1 are correlated towards S, Zn and Cu than from L2.

The bodies and gills were analyzed separately to look for differences in elemental composition between the locations in more detail (Figure 4.27). Bodies and gills were seen to be separated in the plots, with the mussels from L1 being correlated in the direction of Cu and Zn (among others) in both results.

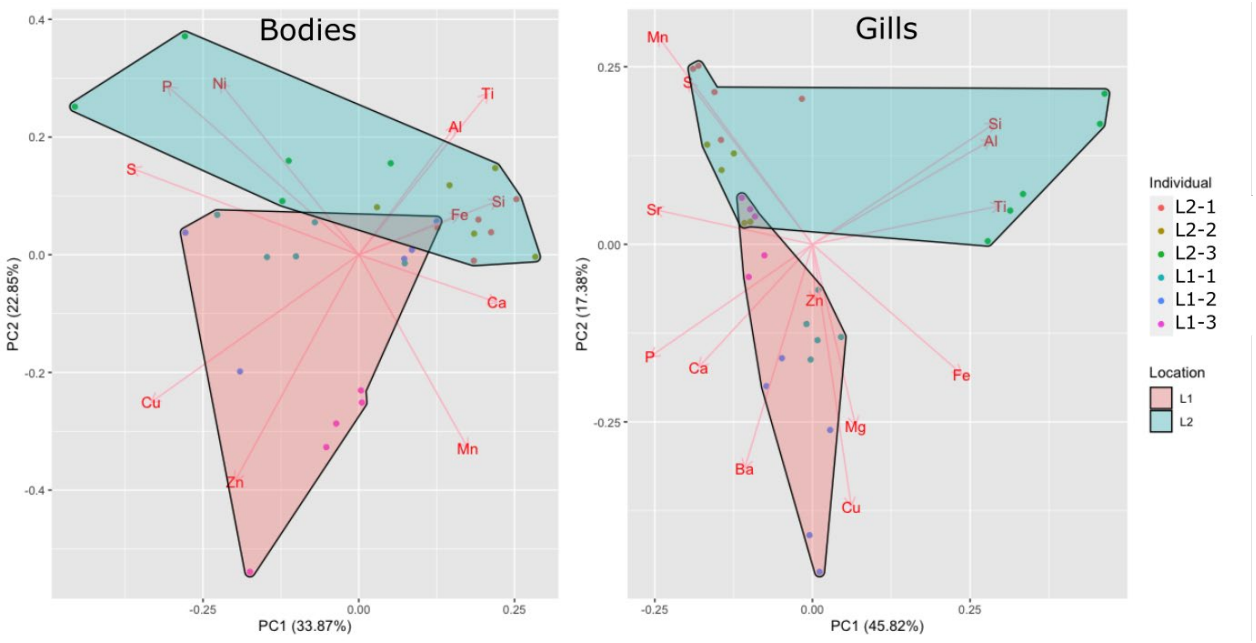

Figure 4.27: PCA-plots of bodies (left) and gills (right). The mussels are grouped after location. PCA is based on mass percentages of elemental composition in the samples. Mussels from L1 (both gills and bodies) are more correlated towards Cu and Zn than mussels from L2.

These results suggest that mussels from L1 contains a higher content of Cu and Zn, which are related to road runoff. Individual L2-3 differ from the other individuals from L2 in the plots. The body is correlated towards Nickel (Ni) and the gills towards aluminium and titanium (Ti). These are metals related to road runoff as well (Westerlund & Viklander, 2006).

4.5.5 Detailed μ-XRF investigations for potential TRWP on filtered samples

The performed area scans of the filters show hotspots of different elements. Point scans done of the samples show that the stomach and mantle had high average mass percentages of Si (2 ± 2%) and Zn (1 ± 1%) in the organic matter. This were a challenge for identifying potential TRWP, which has an average mass percentage content in line with these values. The measured average level of S (0.5 ± 0.1%) differs more from the expected S-content in particles, leading to ROI for further investigations were made using only mappings of S-signal (Figure 4.28).

Only mappings of S were used to define ROI, therefore high levels of Cl in the samples may have caused the results to be underrepresented. Since Cl and S are neighboring on the energy spectrum of μ-XRF, high levels of Cl might have had a shadowing effect of lower levels of S. Levels of Cl in the samples were measured up to 80-90%, while small clean TP_{ref} treated with the digestion method contain an average of approximately 3% S. The red marks in figure 4.28 that have not been marked as an ROI were not scanned because there were no particles matching TRWP in those areas, or the detected signals were caused by damage or topography issues in the filters.

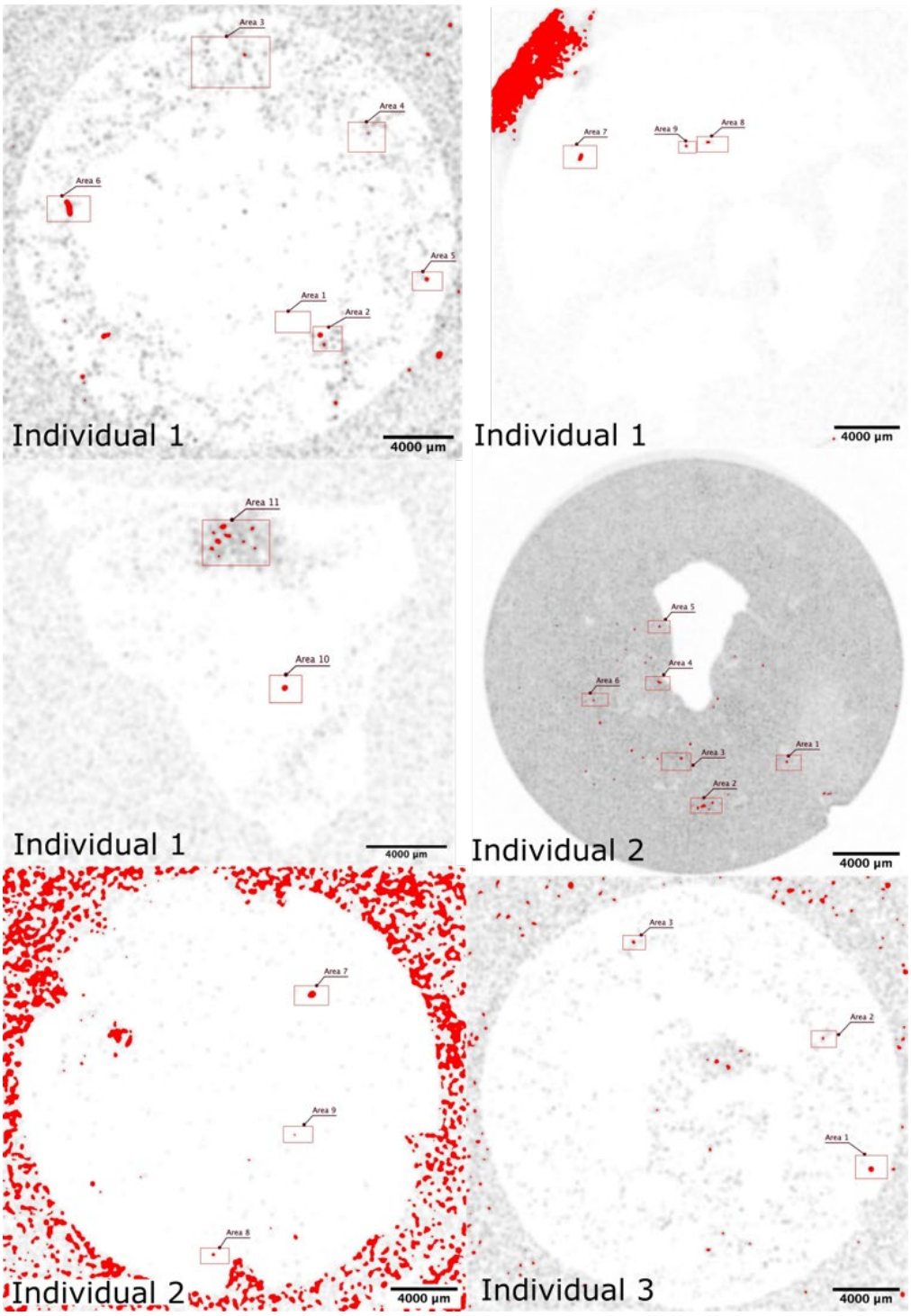

Figure 4.28: µ-XRF mappings of body filters treated in ImageJ showing high intensity S-signals from filters containing digested mussels from L1. Red objects are areas with a high intensity of S-signal. Red squares mark areas that contained particles that were suspected TRWP. Numbering of areas starts at 1 for each Individual.

Individual 1

Individual 1 (Figure 4.28) was the only individual showing signals of potential TRWP in the detailed scans. Areas 1-5 had no significant signals of the tracer elements. The areas were scanned because particles that matched the morphology of TRWP were observed near the high intensity S-signals.

In area 10 (Figure 4.28) there was found one particle matching the reported morphology of TRWP, and that matches the mass percentages of the small particles (Figure 4.29). The particle is 150 µm long and 25 µm wide. The strongest signals from the detailed area scan were S, Fe and Zn which was found on the left side of the particle where the organic matter layer is thicker (Figure 4.30). The line scan exhibits a higher level of Zn on the left of the particle, which also can be seen in the area scan.

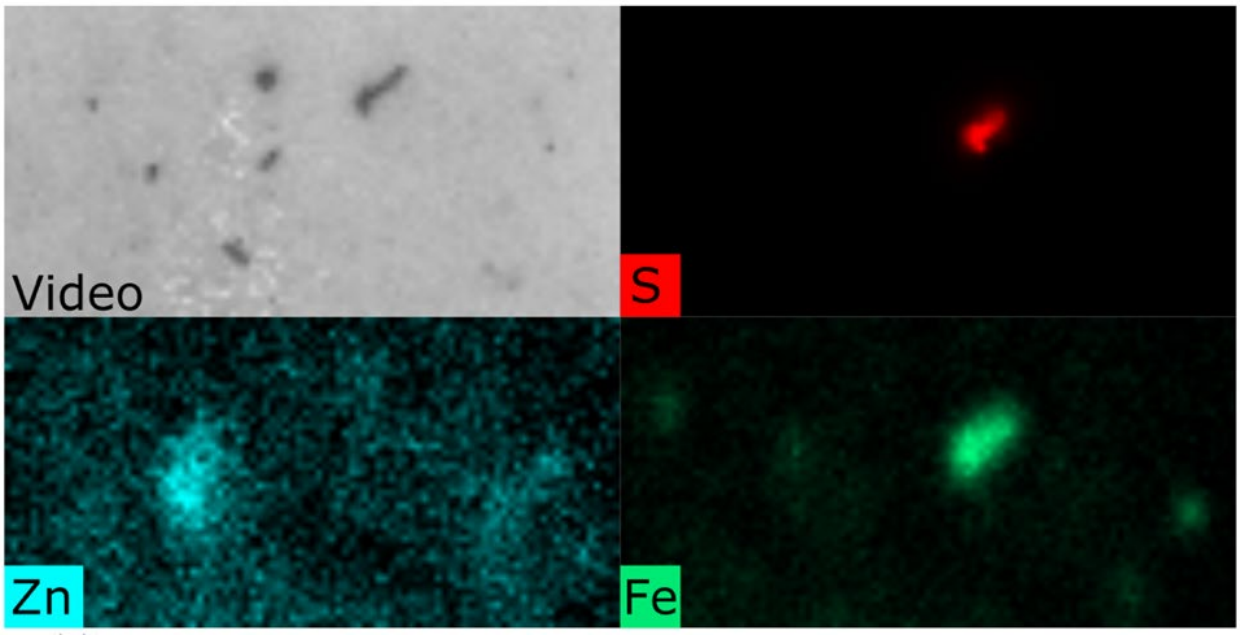

Figure 4.29: µ-XRF area scan of a potential TRWP. Strong emissions of S and Fe is exhibited from the potential particle. Zn-signals is not from the potential TRWP, but an area with a thicker layer of organic matter from the mussel.

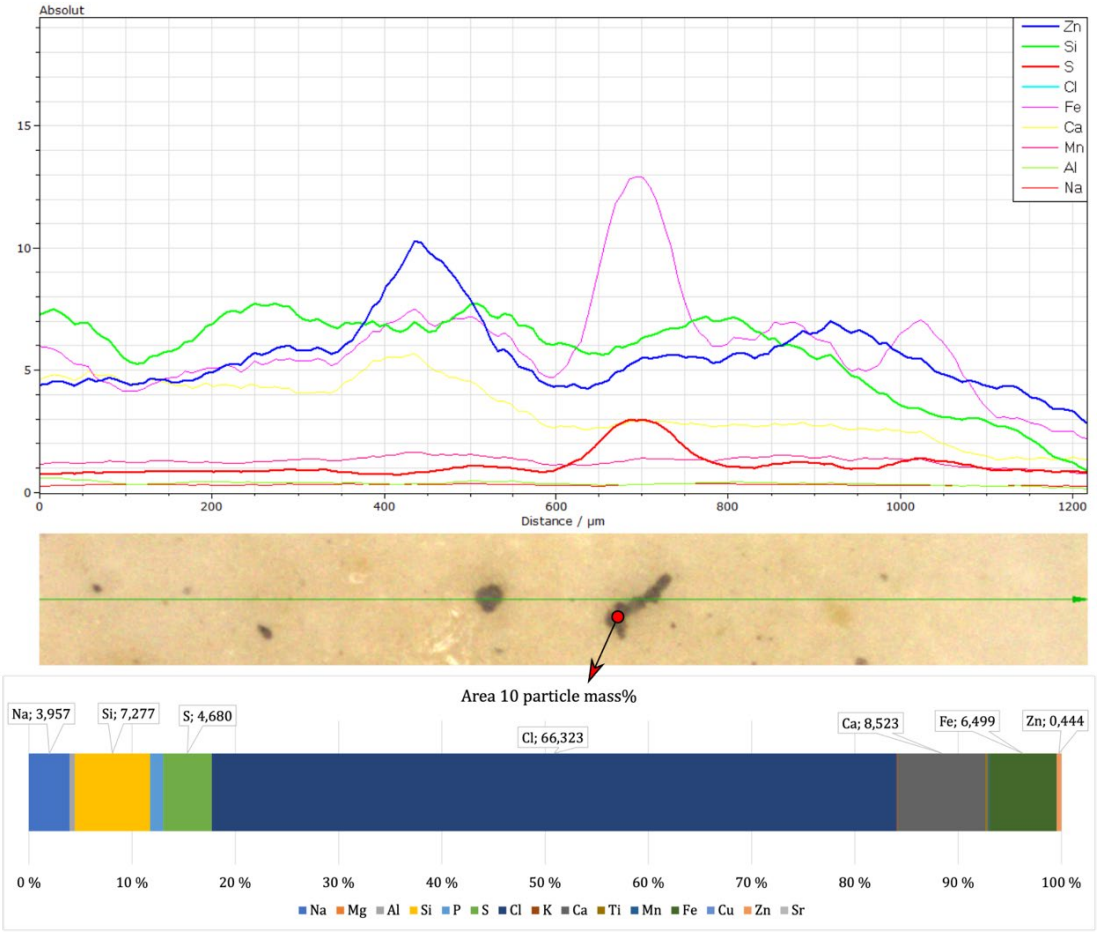

Figure 4.30: µ-XRF line scan and point scan results showing mass percentage of a potential TRWP found in a digested mussel (individual 1 area 10). The arrow marks the point that the point-scan was performed. The content of Si, S and Zn are in line with scanned TP_{ref} in the same size.

The potential TRWP fits the description of a TRWP in both shape, size and colour, along with elevated signals from S and Fe indicating it was encrusted with minerals. It is very likely that this is a TRWP from the mussel. The levels of Si and Zn did not elevate very much from the background, although some increase, especially for Zn, can be seen. This is likely due to the similarity of the content of these elements in the sample material and the TRWP. A point scan with µ-XRF showed that the particle had approximately the same levels of all signature elements as treated TP_{ref} in the same size. The particle was found in a mussel from L1. The particle was embedded in a thin layer of residues from the digestion, indicating that if the digestion method can be optimized, µ-XRF may be able to detect TRWP in samples.

Individual 2 and 3

In the samples from individual 2 and 3 (Figure 4.28) it was not found any signals of the signature elements in the ROI when analyzing them with more detailed scans performed with μ-XRF. However, when investigating the samples under a microscope there were particles that fit the description of TRWP and other MP in the sample media. However, these were not detected through μ-XRF. This may be caused by the amount of organic matter on these samples. These individuals had more residues from the mussels compared the filter where the potential TRWP were found.

Analysis of gills

The filters containing gill material had a lower content of Si and S than the samples of the bodies. One sample stood out with a cluster of signals from S (Figure 4.31). The material with the strong S-signals were scraped off and spread out in a petri dish and examined under a microscope. In this process no particles matching the description of TRWP were identified. However, it was found multiple crystals in the material that originated from the same locations on the filter as the strong S-signals. These were picked out and analyzed with μ-XRF, which showed a high content of Ca (87 ± 3%) and Mn (4 ± 1%). The mass percentage of S in the crystals were low (0.3 ± 0.1%) (Appendix B, table 3). However, the signals of S were exhibited well in the scans. This is likely because of the low content of S in the gill material (0.07 ± 0.02%). Sulfur was however only detected in eight out of thirty points scans performed on the gill material, suggesting it is barely detectable (appendix B, table 5).

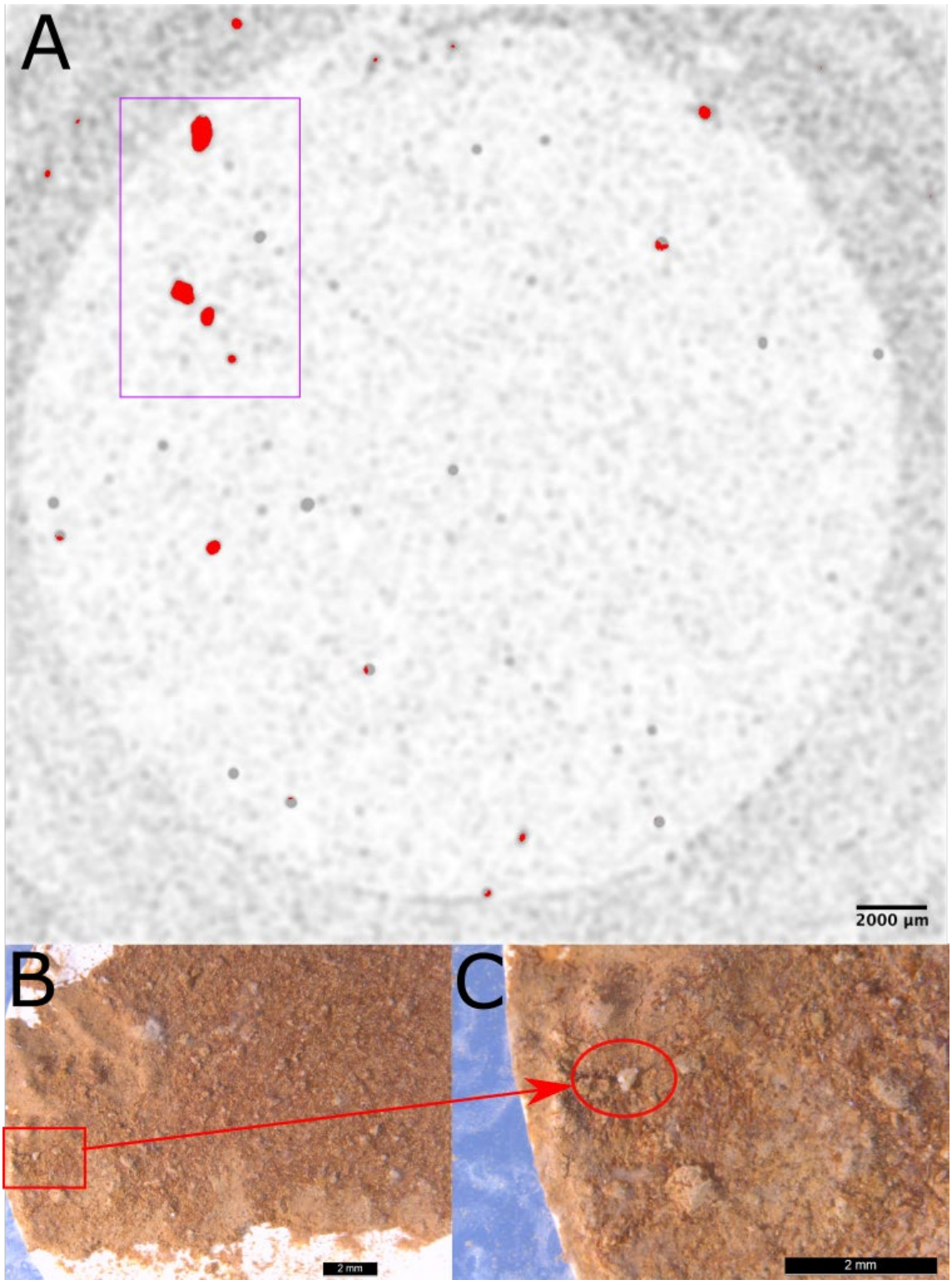

Figure 4.31: µ-XRF area scan results of a scanned gill treated with ImageJ (A). The purple square marks high intensity S-Signals from crystals the were scraped off and analyzed. B and C show a crystal in the sample material.

5 Conclusions

The developed μ-XRF approach has a potential to be a robust method to identify TRWP in biota. Reference tire particles that were not covered by residues from the digestion were detected and identified with the proposed μ-XRF approach. Therefore, hypothesis 1 is supported. However, there is a need for further research to understand the full potential of this approach. Tire and road wear particles that were embedded in residues from the digestion were not detected. Thus, to fully utilize the potential of μ-XRF to identify TRWP in mussels, a more complete digestion is needed. If the digestion approach of mussels is optimized, μ-XRF may be a novel state-of-the-art approach to identify TRWP on filtered biota in the future.

Challenges with biological residues might be overcome by deploying higher intensity X-ray beams, such as those at synchrotron facilities, which provide better information depths. With increased sensitivity, detection of TRWP through biological residues might be possible.

There are strong indications towards there being more TRWP in mussels from the roadside (L1) compared to the reference site (L2). The mussels from L1 had a higher content of metals related to road runoff, indicating influence of highway runoff. Potential TRWP were counted in mussels from L1 and L2 using a microscope, and there was a statistically significant difference in potential TRWP content between the two sites, with mussels from L1 having most potential TRWP. Hypothesis 2 is therefore supported as well.

One potential TRWP were identified in a mussel which was from L1 using μ-XRF. The particle was in line with all criteria that were not hampered by the biological material on the sample. However, the lack of detection of all signature elements from the particle means it cannot be confirmed as a TRWP.

6 References

Amato, F., Querol, X., Johansson, C., Nagl, C. & Alastuey, A. (2010). A review on the effectiveness of street sweeping, washing and dust suppressants as urban PM control methods. *Sci Total Environ*, 408 (16): 3070-3084. doi: 10.1016/j.scitotenv.2010.04.025.

Arthur, C., Baker, J. & Bamford, H. (2009). *Proceedings of the International Research Workshop on the Occurrence, Effects, and Fate of Microplastic Marine Debris*: NOAA.

Artsdatabanken. (no date). *Andemusling Anodonta anatina*. Available at: https://artsdatabanken.no/taxon/Anodonta%20anatina/121313 (accessed: 11.10.2021).

Atici, A. A. (2022). The first evidence of microplastic uptake in natural freshwater mussel, Unio stevenianus from Karasu River, Turkey. *Biomarkers*, 27 (2): 118-126. doi: 10.1080/1354750X.2021.2020335.

Baensch-Baltruschat, B., Kocher, B., Stock, F. & Reifferscheid, G. (2020). Tyre and road wear particles (TRWP) - A review of generation, properties, emissions, human health risk, ecotoxicity, and fate in the environment. *Sci Total Environ*, 733: 137823-137823. doi: 10.1016/j.scitotenv.2020.137823.

Berglund, E., Fogelberg, V., Nilsson, P. A. & Hollander, J. (2019). Microplastics in a freshwater mussel (Anodonta anatina) in Northern Europe. *Sci Total Environ*, 697: 134192-134192. doi: 10.1016/j.scitotenv.2019.134192.

Bessa, F., Frias, J., Kögel, T., Lusher, A., Andrade, J., Antunes, J., Sobral, P., Pagter, E., Nash, R., O'Connor, I., et al. (2019). *Harmonized protocol for monitoring microplastics in biota*.

Beyer, J., Green, N. W., Brooks, S., Allan, I. J., Ruus, A., Gomes, T., Bråte, I. L. N. & Schøyen, M. (2017). Blue mussels (Mytilus edulis spp.) as sentinel organisms in coastal pollution monitoring: A review. *Marine Environmental Research*, 130: 338-365. doi: https://doi.org/10.1016/j.marenvres.2017.07.024.

Bläsing, M. & Amelung, W. (2018). Plastics in soil: Analytical methods and possible sources. *Sci Total Environ*, 612: 422-435. doi: 10.1016/j.scitotenv.2017.08.086.

Brodie, I. M. (2007). *Investigation of stormwater particles generated from common urban surfaces*: University of Southern Queensland.

Browne, M. A., Dissanayake, A., Galloway, T. S., Lowe, D. M. & Thompson, R. C. (2008). Ingested Microscopic Plastic Translocates to the Circulatory System of the Mussel, Mytilus edulis (L.). *Environ. Sci. Technol*, 42 (13): 5026-5031. doi: 10.1021/es800249a.

BRUKER. (2015). *M4 Tornado user manual*.

Bråte, I. L. N., Hurley, R., Iversen, K., Beyer, J., Thomas, K. V., Steindal, C. C., Green, N. W., Olsen, M. & Lusher, A. (2018). Mytilus spp. as sentinels for monitoring microplastic pollution in Norwegian coastal waters: A qualitative and quantitative study. *Environ Pollut*, 243 (Pt A): 383-393. doi: 10.1016/j.envpol.2018.08.077.

Bråte, I. L. N., Hurley, R., Lusher, A., Buenaventura, N., Halsband, C. & Green, N. (2020). *Microplastics in marine bivalves from the Nordic environment*. In Agency, N. E. (ed.). M-1629|2020.

Bækken, T. & Færøvig, P. J. (2004). *Effekter av vegforurensninger på vannkvalitet og biologi i Padderudvann*. Publikasjon (Vegdirektoratet. Teknologiavdelingen : trykt utg.), vol. nr 106. Oslo: Vegdirektoratet, Teknologiavdelingen.

Carpenter, E. J., Anderson, S. J., Harvey, G. R., Miklas, H. P. & Peck, B. B. (1972). Polystyrene Spherules in Coastal Waters. *Science*, 178 (4062): 749-750. doi: 10.1126/science.178.4062.749.

Collard, F., Gilbert, B., Eppe, G., Parmentier, E. & Das, K. (2015). Detection of Anthropogenic Particles in Fish Stomachs: An Isolation Method Adapted to Identification by Raman Spectroscopy. *Arch Environ Contam Toxicol*, 69 (3): 331-339. doi: 10.1007/s00244-015-0221-0.

Cózar, A., Sanz-Martín, M., Martí, E., González-Gordillo, J. I., Ubeda, B., Gálvez, J. Á., Irigoien, X. & Duarte, C. M. (2015). Plastic accumulation in the Mediterranean sea. *PLoS One*, 10 (4): e0121762-e0121762. doi: 10.1371/journal.pone.0121762.

Dawson, A. L., Motti, C. A. & Kroon, F. J. (2020). Solving a Sticky Situation: Microplastic Analysis of Lipid-Rich Tissue. *Frontiers in environmental science*, 8. doi: 10.3389/fenvs.2020.563565.

Degaffe, F. S. & Turner, A. (2011). Leaching of zinc from tire wear particles under simulated estuarine conditions. *Chemosphere*, 85 (5): 738-743. doi: 10.1016/j.chemosphere.2011.06.047.

Deng, Y., Zhang, Y., Lemos, B. & Ren, H. (2017). Tissue accumulation of microplastics in mice and biomarker responses suggest widespread health risks of exposure. *Sci Rep*, 7 (1): 46687. doi: 10.1038/srep46687.

Driscoll, C. T., Driscoll, K. M., Roy, K. M. & Mitchell, M. J. (2003). Chemical Response of Lakes in the Adirondack Region of New York to Declines in Acidic Deposition. *Environ. Sci. Technol*, 37 (10): 2036-2042. doi: 10.1021/es020924h.

Fischer, M., Goßmann, I. & Scholz-Böttcher, B. M. (2019). Fleur de Sel—An interregional monitor for microplastics mass load and composition in European coastal waters? *Journal of analytical and applied pyrolysis*, 144: 104711. doi: 10.1016/j.jaap.2019.104711.

Fjeld, E. (2020). *Limnologiske undersøkelser i Padderudvannet og Dikemarksvatna* – Fjeld og Vann Rapport.

Fraissinet, S., Pennetta, A., Rossi, S., De Benedetto, G. E. & Malitesta, C. (2021). Optimization of a new multi-reagent procedure for quantitative mussel digestion in microplastic analysis. *Mar Pollut Bull*, 173 (Pt A): 112931-112931. doi: 10.1016/j.marpolbul.2021.112931.

Freinkel, S. (2011). *Pastic: a Toxic Love Story*: Houghton Mifflin Harcourt.

GESAMP. (2016). *Sources, fate and effects of microplastics in the marine environment: part two of a global assessment*: IMO London. p. 220.

Hann, S., Sherrington, C., Darrah, C., Cole, G. & Corbin, M. (2016). *Study to support the development of measures to combat a range of marine litter sources*.

Hartmann, N. B., Hüffer, T., Thompson, R. C., Hassellöv, M., Verschoor, A., Daugaard, A. E., Rist, S., Karlsson, T., Brennholt, N., Cole, M., et al. (2019). Are We Speaking the Same Language? Recommendations for a Definition and Categorization Framework for Plastic Debris. *Environ. Sci. Technol*, 53 (3): 1039-1047. doi: 10.1021/acs.est.8b05297.

Haschke, M. (2015). *Analytical performance of the M4 TORNADO*.

Hongve, D., Riise, G. & Kristiansen, J. F. (2004). Increased colour and organic acid concentrations in Norwegian forest lakes and drinking water – a result of increased precipitation? *Aquatic sciences*, 66 (2): 231-238. doi: 10.1007/s00027-004-0708-7.

Horikoshi, M. & Tang, Y. (2016). ggfortify: Data Visualization Tools for Statistical Analysis Results.

Hurley, R. R., Lusher, A. L., Olsen, M. & Nizzetto, L. (2018). Validation of a Method for Extracting Microplastics from Complex, Organic-Rich, Environmental Matrices. *Environ. Sci. Technol*, 52 (13): 7409-7417. doi: 10.1021/acs.est.8b01517.

Inkscape. (2020). *Inkscape*. Available at: https://nkscape.org.

IUCN. (2021). *Marine plastic pollution*: IUCN. Available at: https://www.iucn.org/resources/issues-briefs/marine-plastic-pollution (accessed: 30.11.2021).

Jekel, M. (2019). *Scientific Report on Tyre and Road Wear Particles, TRWP, in the aquatic environment*.

JEOL. (no date). *ZAF correction*. Available at: https://www.jeol.co.jp/en/words/semterms/search_result.html?keyword=ZAF%20correction (accessed: 15.01.2022).

Jung, U. & Choi, S.-S. (2022). Classification and Characterization of Tire-Road Wear Particles in Road Dust by Density. *Polymers (Basel)*, 14 (5): 1005. doi: 10.3390/polym14051005.

Kayhanian, M., McKenzie, E. R., Leatherbarrow, J. E. & Young, T. M. (2012). Characteristics of road sediment fractionated particles captured from paved surfaces, surface run-off and detention basins. *Sci Total Environ*, 439: 172-186. doi: 10.1016/j.scitotenv.2012.08.077.

Klöckner, P., Reemtsma, T., Eisentraut, P., Braun, U., Ruhl, A. S. & Wagner, S. (2019). Tire and road wear particles in road environment – Quantification and assessment of particle dynamics by Zn determination after density separation. *Chemosphere*, 222: 714-721. doi: 10.1016/j.chemosphere.2019.01.176.

Klöckner, P., Seiwert, B., Weyrauch, S., Escher, B. I., Reemtsma, T. & Wagner, S. (2021). Comprehensive characterization of tire and road wear particles in highway tunnel road dust by use of size and density fractionation. *Chemosphere*, 279: 130530. doi: 10.1016/j.chemosphere.2021.130530.

Kole, P. J., Löhr, A. & Ragas, A. (2015). Autobandenslijtstof: een verwaarloosde bron van microplastics? *Milieu*.

Kole, P. J., Löhr, A. J., Van Belleghem, F. G. A. J. & Ragas, A. M. J. (2017). Wear and Tear of Tyres: A Stealthy Source of Microplastics in the Environment. *Int J Environ Res Public Health*, 14 (10): 1265. doi: 10.3390/ijerph14101265.

Kovochich, M., Parker, J. A., Oh, S. C., Lee, J. P., Wagner, S., Reemtsma, T. & Unice, K. M. (2021). Characterization of Individual Tire and Road Wear Particles in Environmental Road Dust, Tunnel Dust, and Sediment. *Environmental science & technology letters*. doi: 10.1021/acs.estlett.1c00811.

Kreider, M. L., Panko, J. M., McAtee, B. L., Sweet, L. I. & Finley, B. L. (2009). Physical and chemical characterization of tire-related particles: Comparison of particles generated using different methodologies. *Science of The Total Environment*, 408 (3): 652-659. doi: https://doi.org/10.1016/j.scitotenv.2009.10.016.

La Nasa, J., Biale, G., Fabbri, D. & Modugno, F. (2020). A review on challenges and developments of analytical pyrolysis and other thermoanalytical techniques for the quali-quantitative determination of microplastics. *Journal of analytical and applied pyrolysis*, 149: 104841. doi: 10.1016/j.jaap.2020.104841.

Lambert, S. (2013). *Environmental risk of polymers and their degradation products*: University of York.

Lassen, C., Hansen, S. F., Magnusson, K., Hartmann, N. B., Rehne Jensen, P., Nielsen, T. & Brinch, A. (2015). *Microplastics - Occurrence, effects and sources of releases to the environment in Denmark*.

Leslie, H. A., J. M. van Velzen, M., Brandsma, S. H., Vethaak, D., Garcia-Vallejo, J. J. & Lamoree, M. H. (2022). Discovery and quantification of plastic particle pollution in human blood. *Environment International*: 107199. doi: https://doi.org/10.1016/j.envint.2022.107199.

Lusher, A., Welden, N., A., Sobral, P. & Cole, M. (2017). Sampling, isolating and identifying microplastics ingested by fish and invertebrates. *Analytical Methods*, 9.

Lutro, O., Graversen, O., Larsen, B. T., Naterstad, J., Bockelie, J. F. & Bockelie, T. (2017). *Berggrunnskart (bedrock map) Asker 1814-1, M 1:50 000*: Norges geologiske undersøkelse.

Marwood, C., McAtee, B., Kreider, M., Ogle, R. S., Finley, B., Sweet, L. & Panko, J. (2011). Acute aquatic toxicity of tire and road wear particles to alga, daphnid, and fish. *Ecotoxicology*, 20 (8): 2079-2089. doi: 10.1007/s10646-011-0750-x.

McIntyre, J. K., Prat, J., Cameron, J., Wetzel, J., Mudrock, E., Peter, K. T., Tian, Z., Mackenzie, C., Lundin, J., Stark, J. D., et al. (2021). Treading Water: Tire Wear Particle Leachate Recreates an Urban Runoff Mortality Syndrome in Coho but Not Chum Salmon. *Environ. Sci. Technol*, 55 (17): 11767-11774. doi: 10.1021/acs.est.1c03569.

Michnowicz, C. J. & Weaks, T. E. (1984). Effects of pH on toxicity of As, Cr, Cu, Ni and Zn to Selenastrum capricornutum Printz. *Hydrobiologia*, 118 (3): 299-305. doi: 10.1007/BF00046627.

NPRA. (2014a). *Håndbok R610 Standard for drift og vedlikehold av riksveger*. Oslo: Statens vegvesen.

NPRA. (2014b). Veg- og gateutforming, Håndbok N100.

NPRA. (2022). Vegkart. In *Statens Vegvesen*. Available at: https://vegkart.atlas.vegvesen.no/ (accessed: 12.01.2021).

Ogonowski, M., Schür, C., Jarsén, Å. & Gorokhova, E. (2016). The Effects of Natural and Anthropogenic Microparticles on Individual Fitness in Daphnia magna. *PLoS One*, 11 (5): e0155063-e0155063. doi: 10.1371/journal.pone.0155063.

Oliveira, M., Ribeiro, A., Hylland, K. & Guilhermino, L. (2013). Single and combined effects of microplastics and pyrene on juveniles (0+ group) of the common goby Pomatoschistus microps (Teleostei, Gobiidae). *Ecological indicators*, 34: 641-647. doi: 10.1016/j.ecolind.2013.06.019.

Padoan, E. & Amato, F. (2018). Non-Exhaust Emissions, Chapter 2 - Vehicle Non-Exhaust Emissions: Impact on Air Quality. In Amato, F. (ed.) *Non-Exhaust Emissions*, pp. 21-65: Academic Press.

Palarea-Albaladejo, J. & Martin-Fernandez, J. A. (2015). zCompositions -- R package for multivariate imputation of left-censored data under a compositional approach. *Chemom. Intell. Lab. Syst.*, 143: 85-96.

Pedersen, T. L. (2021). *ggforce: Accelerating 'ggplot2'*. Available at: https://CRAN.R-project.org/package=ggforce.

PlasticsEurope. (2019). *Plastics - the Facts*. Available at: https://plasticseurope.org/knowledge-hub/plastics-the-facts-2019/ (accessed: 30.11.2021).

R. (2021). *R: A language and environment for statistical computing*. Vienna, Austria: R Foundation for Statistical Computing. Available at: https://www.R-project.org/.

Rochman, C. M., Hoh, E., Hentschel, B. T. & Kaye, S. (2013a). Long-Term Field Measurement of Sorption of Organic Contaminants to Five Types of Plastic Pellets: Implications for Plastic Marine Debris. *Environ. Sci. Technol*, 47 (3): 1646-1654. doi: 10.1021/es303700s.

Rochman, C. M., Hoh, E., Kurobe, T. & Teh, S. J. (2013b). Ingested plastic transfers hazardous chemicals to fish and induces hepatic stress. *Sci Rep*, 3 (1): 3263. doi: 10.1038/srep03263.

Rochman, C. M., Brookson, C., Bikker, J., Djuric, N., Earn, A., Bucci, K., Athey, S., Huntington, A., McIlwraith, H., Munno, K., et al. (2019). Rethinking microplastics as a diverse contaminant suite. *Environ Toxicol Chem*, 38 (4): 703-711. doi: 10.1002/etc.4371.

Rstudio. (2021). *Integrated Development Environment for R,*. Boston, MA: PBC. Available at: http://www.rstudio.com/.

Rødland, E. S., Lind, O. C., Reid, M., Heier, L. S., Skogsberg, E., Snilsberg, B., Gryteselv, D. & Meland, S. (2022a). Characterization of Tire and Road Wear Microplastic Particle Contamination in a Road Tunnel: From Surface to Release. *Journal of Hazardous Materials*: 129032. doi: https://doi.org/10.1016/j.jhazmat.2022.129032.

Rødland, E. S., Lind, O. C., Reid, M. J., Heier, L. S., Okoffo, E. D., Rauert, C., Thomas, K. V. & Meland, S. (2022b). Occurrence of tire and road wear particles in urban and peri-urban snowbanks, and their potential environmental implications. doi: https://doi.org/10.1016/j.scitotenv.2022.153785.

Rødland, E. S., Samanipour, S., Rauert, C., Okoffo, E. D., Reid, M. J., Heier, L. S., Lind, O. C., Thomas, K. V. & Meland, S. (2022c). A novel method for the quantification of tire and polymer-modified bitumen particles in environmental samples by pyrolysis gas chromatography mass spectroscopy. *J Hazard Mater*, 423 (Pt A): 127092-127092. doi: 10.1016/j.jhazmat.2021.127092.

Saba, R. G., Uthus, N. & Aurstad, J. (2012). *Long-term performance of asphalt surfacings containing polymer modified binders*. 5th Eurasphalt & Eurobitume Congress.

SAPEA, A. (2019). Scientific Perspective on Microplastics in Nature and Society. *Science Advice for Policy by European Academies, Berlin*.

Schirinzi, G. F., Pérez-Pomeda, I., Sanchís, J., Rossini, C., Farré, M. & Barceló, D. (2017). Cytotoxic effects of commonly used nanomaterials and microplastics on cerebral and epithelial human cells. *Environ Res*, 159: 579-587. doi: 10.1016/j.envres.2017.08.043.

Schuyler, Q. A., Wilcox, C., Townsend, K. A., Wedemeyer-Strombel, K. R., Balazs, G., van Sebille, E. & Hardesty, B. D. (2016). Risk analysis reveals global hotspots for marine debris ingestion by sea turtles. *Glob Change Biol*, 22 (2): 567-576. doi: 10.1111/gcb.13078.

Sommer, F., Dietze, V., Baum, A., Sauer, J., Gilge, S., Maschowski, C. & Gieré, R. (2018). Tire Abrasion as a Major Source of Microplastics in the Environment. *Aerosol and air quality research*, 18 (8): 2014-2028. doi: 10.4209/aaqr.2018.03.0099.

Suaria, G., Avio, C. G., Mineo, A., Lattin, G. L., Magaldi, M. G., Belmonte, G., Moore, C. J., Regoli, F. & Aliani, S. (2016). The Mediterranean Plastic Soup: synthetic polymers in Mediterranean surface waters. *Sci Rep*, 6 (1): 37551-37551. doi: 10.1038/srep37551.

Sundt, P., Schulze, P.-E. & Syversen, F. (2014). *Sources of microplastic pollution to the marine environment*. In Mepex (ed.).

Sundt, P., Syversen, F., Skogesal, O. & Schulze, P.-E. (2016). *Primary microplasticpollution: Measures and reduction potentials in Norway*.

Sundt, P., Haugesdal, S., Rem, T. & Schulze, P.-E. (2020). *Norske landbaserte kilder til mikroplast*, M-1910.

Tang, Y., Horikoshi, M. & Li, W. (2016). ggfortify: Unified Interface to Visualize Statistical Result of Popular R Packages. *The R Journal*, 8.2: 478-489.

Thompson, A. (2018). *From fish to humans, a microplastic invasion may be taking a toll*. Scientific american. Available at: https://www.scientificamerican.com/article/from-fish-to-humans-a-microplastic-invasion-may-be-taking-a-toll/ (accessed: 8.12.2021).

Thompson, R. C., Olsen, Y., Mitchell, R. P., Davis, A., Rowland, S. J., John, A. W. G., McGonigle, D. & Russell, A. E. (2004). Lost at Sea: Where Is All the Plastic? *Science*, 304 (5672): 838-838. doi: 10.1126/science.1094559.

Tian, Z., Zhao, H., Peter, K. T., Gonzalez, M., Wetzel, J., Wu, C., Hu, X., Prat, J., Mudrock, E., Hettinger, R., et al. (2021). A ubiquitous tire rubber-derived chemical induces acute mortality in coho salmon. *Science*, 371 (6525): 185-189. doi: 10.1126/science.abd6951.

Tjomsland, T., Selvik, J. R. & Faafeng, B. (2012). *Modellert påvirkning av vegsalt i Padderudvann*.

Tsakona, M., Baker, E., Rucevska, I., Maes, T., Rosendahl Appelquist, L., Macmillan-Lawler, M., Harris, P., Raubenheimer, K., Langeard, R., Savelli-Soderberg, H., et al. (2021). *Drowning in Plastics: Marine Litter and Plastic Waste Vital Graphics*.

UN. (2015). *Transforming Our World: The 2030 Agenda for Sustainable Development*. New York: UN Publishing.

Van Cauwenberghe, L., Claessens, M., Vandegehuchte, M. B. & Janssen, C. R. (2015). Microplastics are taken up by mussels (Mytilus edulis) and lugworms (Arenicola marina) living in natural habitats. *Environ Pollut*, 199: 10-17. doi: 10.1016/j.envpol.2015.01.008.

Vogelsang, C., Lusher, A. L., Dadkah, M. E., Sundvor, I., Umar, M., Ranneklev, S. B., Eidsvoll, D. & Meland, S. (2020). *Microplastics in road dust pathways and measures– characteristics, pathways and measures*, 1894-7948: NIVA.

Wagner, M., Engwall, M. & Hollert, H. (2014). Editorial: (Micro)Plastics and the environment. *Environ Sci Eur*, 26 (1): 1-3. doi: 10.1186/s12302-014-0016-3.

Wagner, S., Hüffer, T., Klöckner, P., Wehrhahn, M., Hofmann, T. & Reemtsma, T. (2018). Tire wear particles in the aquatic environment - A review on generation, analysis, occurrence, fate and effects. *Water Res*, 139: 83-100. doi: 10.1016/j.watres.2018.03.051.

Walker, T. R. (2021). (Micro)plastics and the UN Sustainable Development Goals. *Current Opinion in Green and Sustainable Chemistry*, 30: 100497. doi: https://doi.org/10.1016/j.cogsc.2021.100497.

Westerlund, C. & Viklander, M. (2006). Particles and associated metals in road runoff during snowmelt and rainfall. *Sci Total Environ*, 362 (1): 143-156. doi: 10.1016/j.scitotenv.2005.06.031.

Wickham, H. (2016). *ggplot2: Elegant Graphics for Data Analysis*: Springer-Verlag New York.

Wilcox, C., Puckridge, M., Schuyler, Q. A., Townsend, K. & Hardesty, B. D. (2018). A quantitative analysis linking sea turtle mortality and plastic debris ingestion. *Sci Rep*, 8 (1): 12536-11. doi: 10.1038/s41598-018-30038-z.

XOS. (no date). *Micro X-ray Fluorescence (μXRF)*. Available at: https://www.xos.com/Micro-XRF.

Zhang, S., Wang, J., Liu, X., Qu, F., Wang, X., Wang, X., Li, Y. & Sun, Y. (2019). Microplastics in the environment: A review of analytical methods, distribution, and biological effects. *TrAC, Trends in analytical chemistry (Regular ed.)*, 111: 62-72. doi: 10.1016/j.trac.2018.12.002.

Økland, J. (1963). Notes on population density, age distribution, growth, and habitat of Anodonta piscinalis Nilss. (Moll., Lamellibr.) in a eutrophic Norwegian lake. *Nytt Mag. Zool.*, 11.

Appendices

Appendix A: Analysis of TP_{ref} from ICP-MS

Table 1: Measured concentrations of elements from ICP-MS (mg/Kg). Explanatory variables are found in the last columns.

Sample	Li	Be	Na	Mg	Al	P
S1-A	0,180	0,170	1500,000	200,000	680,000	0,000
S1-B	0,160	0,000	1200,000	160,000	620,000	0,000
S1-C	0,160	0,230	1200,000	160,000	660,000	2200,000
S2-A	10,000	0,000	1600,000	110,000	1000,000	1300,000
S2-B	8,300	0,000	1030,000	89,000	700,000	4600,000
S2-C	12,000	0,000	1800,000	91,000	1100,000	0,000
S3-A	1,200	0,000	430,000	120,000	210,000	0,000
S3-B	1,300	0,000	460,000	120,000	260,000	1300,000
S3-C	1,200	0,000	560,000	140,000	270,000	0,000
C1-A	15,000	0,000	2200,000	88,000	1100,000	0,000
C1-B	15,000	0,000	2100,000	82,000	1000,000	2100,000
C1-C	15,000	0,000	2100,000	77,000	980,000	0,000
C2-A	0,440	0,000	870,000	180,000	490,000	0,000
C2-B	0,420	0,000	890,000	170,000	350,000	0,000
C2-C	0,470	0,000	1360,000	140,000	340,000	0,000
C3-A	8,900	0,000	1900,000	79,000	420,000	0,000
C3-B	9,400	0,000	1900,000	77,000	450,000	2000,000
C3-C	8,500	0,000	2000,000	60,000	410,000	19000,000
T1-A	0,230	0,000	1200,000	91,000	260,000	0,000
T1-B	0,091	0,000	500,000	100,000	190,000	0,000
T1-C	0,083	0,000	490,000	96,000	180,000	1300,000
T2-A	0,110	0,000	440,000	81,000	280,000	0,000
T2-B	0,100	0,000	440,000	77,000	270,000	0,000
T2-C	0,120	0,190	440,000	88,000	330,000	4800,000
T3-A	0,230	0,000	1620,000	88,000	280,000	7200,000
T3-B	0,095	0,000	660,000	58,000	260,000	3900,000
T3-C	0,083	0,000	550,000	53,000	190,000	1800,000
NH4-A	6,700	0,000	2300,000	58,000	1200,000	6800,000
NH4-B	7,000	0,000	2300,000	67,000	1300,000	4600,000
NH4-C	7,400	0,000	2600,000	58,000	1300,000	0,000
B1-A	0,380	0,090	2000,000	63,000	380,000	2100,000
B1-B	0,370	0,050	2000,000	60,000	370,000	0,000
B1-C	0,370	0,070	1900,000	64,000	400,000	2600,000
B2-A	2,000	0,100	1300,000	93,000	490,000	0,000
B2-B	1,900	0,070	1300,000	91,000	480,000	0,000
B2-C	1,600	0,120	1100,000	120,000	430,000	0,000
B3-A	0,170	0,000	270,000	75,000	260,000	0,000
B3-B	0,190	0,000	320,000	82,000	250,000	0,000
B3-C	0,170	0,000	270,000	85,000	250,000	0,000

S	K	Ca	Sc	Ti	V	Cr
14000,000	0,000	650,000	0,093	57,000	2,000	4,900
14000,000	0,000	950,000	0,083	48,000	0,000	0,000
14000,000	0,000	660,000	0,065	47,000	2,600	0,000
18000,000	0,000	620,000	0,060	6800,000	1,600	3,900
18000,000	0,000	520,000	0,051	910,000	0,000	0,000
18000,000	0,000	610,000	0,048	42,000	2,500	6,200
13000,000	0,000	360,000	0,017	23,000	0,000	3,300
13000,000	0,000	360,000	0,020	24,000	1,400	3,500
13000,000	0,000	380,000	0,028	26,000	0,000	7,300
13000,000	0,000	1200,000	0,039	55,000	0,000	8,300
13000,000	0,000	1100,000	0,039	50,000	0,000	6,100
13000,000	0,000	1100,000	0,034	49,000	2,700	6,700
17000,000	0,000	640,000	0,037	57,000	0,000	7,400
16000,000	0,000	680,000	0,046	57,000	0,000	7,500
16000,000	0,000	630,000	0,068	81,000	0,000	310,000
13000,000	0,000	1200,000	0,060	86,000	0,000	0,000
13000,000	0,000	1400,000	0,038	2400,000	0,000	5,900
12000,000	0,000	1100,000	0,038	69,000	0,000	0,000
16000,000	0,000	1400,000	0,000	15,000	0,000	19,000
15000,000	0,000	1400,000	0,013	5,600	1,200	0,000
15000,000	0,000	1300,000	0,014	6,800	0,000	3,800
15000,000	0,000	1600,000	0,017	7,200	1,200	2,300
16000,000	0,000	1600,000	0,011	6,600	1,100	2,500
18000,000	0,000	1500,000	0,021	7,600	2,200	5,400
20000,000	0,000	1500,000	0,000	22,000	0,000	0,000
15000,000	0,000	1500,000	0,000	9,400	0,000	0,000
15000,000	0,000	1400,000	0,000	7,400	1,600	0,000
17000,000	0,000	920,000	0,000	47,000	0,000	0,000
18000,000	0,000	1000,000	0,000	52,000	0,000	13,600
19000,000	0,000	1000,000	0,000	45,000	0,000	13,000
17000,000	0,000	560,000	0,044	56,000	1,000	2,500
17000,000	0,000	470,000	0,051	130,000	0,850	1,400
17000,000	0,000	570,000	0,038	320,000	0,870	45,000
16000,000	2000,000	1100,000	0,039	35,000	1,300	4,300
17000,000	0,000	1100,000	0,045	36,000	1,300	2,100
16000,000	0,000	980,000	0,048	55,000	1,300	3,400
13000,000	0,000	280,000	0,023	21,000	3,600	2,900
14000,000	0,000	330,000	0,025	20,000	4,000	4,200
14000,000	1700,000	280,000	0,021	21,000	3,600	2,300

Mn	Fe	Co	Ni	Cu	Zn	Ge
5,400	290,000	1,100	5,800	19,000	15000,000	0,220
5,400	200,000	1,100	7,800	0,000	15000,000	0,420
4,300	190,000	1,100	6,000	11,500	15000,000	0,460
2,400	190,000	0,170	3,300	500,000	13000,000	0,280
4,700	175,000	0,210	0,000	67,000	17000,000	0,520
3,200	190,000	0,260	5,300	10,900	11000,000	0,220
2,300	110,000	0,590	5,800	8,500	11000,000	0,620
2,200	96,000	0,630	3,300	6,000	11000,000	0,800
2,500	120,000	5,200	6,200	12,900	11000,000	0,690
2,900	107,000	0,170	0,000	0,000	8800,000	0,000
2,100	94,000	0,190	18,000	16,000	9300,000	0,220
2,300	94,000	0,180	7,300	11,700	9300,000	0,240
2,600	120,000	0,840	6,300	0,000	11000,000	0,260
2,600	110,000	1,000	6,400	0,000	11000,000	0,000
6,200	230,000	1,800	1300,000	0,000	11000,000	0,000
2,600	110,000	0,130	6,400	0,000	9200,000	0,270
28,000	77,000	0,250	6,800	10,500	9800,000	0,000
3,500	130,000	0,127	8,500	17,600	9300,000	0,350
5,500	203,000	2,000	57,000	30,000	16000,000	0,000
2,600	70,000	0,140	3,500	5,300	17000,000	0,000
2,800	96,000	0,150	3,200	6,700	16000,000	0,130
2,300	80,000	0,280	2,000	4,500	16000,000	0,080
2,100	79,000	0,210	9,000	4,900	15000,000	0,000
2,400	160,000	0,190	4,600	9,500	15000,000	0,000
7,400	0,000	0,270	18,100	0,000	16000,000	0,000
3,000	112,000	0,240	0,000	0,000	16000,000	0,000
2,700	130,000	0,170	3,400	7,100	15000,000	0,000
3,800	170,000	0,220	0,000	19,200	8900,000	0,390
4,700	240,000	0,310	11,600	0,000	10000,000	0,000
4,500	168,000	0,280	11,100	0,000	10000,000	0,000
1,300	110,000	0,490	2,500	11,000	9400,000	0,090
1,200	110,000	0,490	2,500	30,000	10000,000	0,053
1,400	110,000	0,700	2,900	3,300	11000,000	0,070
2,000	130,000	2,500	11,000	110,000	7200,000	0,000
1,300	100,000	2,700	2,200	55,000	7400,000	0,070
1,900	160,000	2,300	29,000	34,000	8200,000	0,120
2,700	140,000	0,180	2,700	5,100	9000,000	0,000
2,300	76,000	0,220	5,800	7,400	9300,000	0,150
2,200	73,000	0,220	5,600	6,000	9200,000	0,080

As	Se	Rb	Sr	Y	Zr	Nb	Mo
0,380	0,000	2,300	2,400	0,590	7,500	0,190	0,000
0,440	1,320	2,600	3,000	0,860	6,600	0,150	0,000
0,340	0,000	2,000	2,300	0,370	6,200	0,150	0,000
0,200	0,560	1,100	36,000	0,400	18,000	0,230	0,940
0,660	0,000	1,200	7,100	0,300	11,000	0,174	0,000
0,300	0,000	0,900	3,800	0,600	18,000	0,190	0,000
0,480	0,600	1,100	1,500	0,240	7,100	0,055	0,000
0,450	1,200	1,500	1,700	0,270	3,800	0,075	0,000
0,480	1,060	1,400	1,700	0,450	9,900	0,094	0,000
0,000	0,000	0,700	1,600	0,340	11,000	0,140	0,000
0,300	0,000	0,700	1,400	0,370	11,000	0,150	0,000
0,320	0,000	0,660	1,400	0,330	11,000	0,150	0,000
0,360	1,070	1,300	1,500	0,170	9,500	0,130	0,000
0,360	0,000	0,960	1,600	0,210	9,200	0,130	1,350
0,000	0,000	1,500	1,600	0,620	13,000	8,300	43,000
0,000	0,000	0,660	3,700	0,460	12,000	0,210	0,000
0,290	0,000	0,580	310,000	0,490	14,000	0,730	1,200
0,000	0,000	1,100	2,300	0,360	12,000	0,190	0,000
0,760	0,000	1,330	2,800	0,150	0,000	0,000	13,000
0,450	0,000	0,250	2,700	0,120	2,000	0,038	0,000
0,410	0,550	0,440	2,700	0,170	2,600	0,049	1,400
0,330	0,000	0,200	3,700	0,110	1,600	0,030	0,590
0,340	0,000	0,210	3,600	0,140	1,700	0,032	0,440
0,390	0,000	0,460	3,600	0,220	3,700	0,069	0,000
1,030	0,000	0,000	3,300	0,200	0,000	0,000	0,000
0,570	0,000	0,000	3,500	0,073	0,000	0,000	0,000
0,500	0,000	0,340	3,300	0,170	2,700	0,051	0,000
0,000	0,000	0,000	1,700	0,490	23,000	0,170	0,000
0,000	0,000	1,150	2,000	0,420	16,000	0,200	2,440
0,000	0,000	1,100	1,800	0,350	14,000	0,166	0,000
0,150	0,000	0,220	1,800	0,380	15,000	0,180	0,460
0,200	0,000	0,170	1,800	0,280	14,000	0,140	0,250
0,160	0,270	0,170	1,800	0,400	17,000	0,150	0,770
0,810	0,000	0,510	2,100	0,250	4,100	0,100	0,490
0,510	0,300	0,320	2,200	0,260	3,600	0,099	0,000
0,230	0,000	0,660	2,700	0,220	4,600	0,110	0,600
0,570	0,420	0,830	1,200	0,061	0,000	0,037	0,000
0,640	0,000	1,300	1,300	0,120	2,900	0,054	0,000
0,530	0,000	0,890	1,200	0,110	1,600	0,030	0,910

Ag	Cd	In	Sn	Sb	Te	Cs	Ba
0,047	0,150	0,020	2,200	4,700	0,000	0,310	6,800
0,086	0,180	0,015	1,080	1,800	0,000	0,330	5,000
0,062	0,150	0,017	1,400	2,200	0,000	0,320	4,500
0,047	0,290	0,055	1,200	0,640	0,000	0,024	12000,000
0,128	0,500	0,110	1,600	0,810	0,000	0,037	1500,000
0,061	0,210	0,033	1,000	0,850	0,000	0,025	25,000
0,032	0,680	0,180	2,400	0,940	0,041	0,034	9,300
0,032	0,690	0,190	1,200	0,660	0,050	0,041	10,000
0,069	0,700	0,180	2,600	1,500	0,091	0,046	10,000
0,078	1,500	0,009	2,600	0,450	0,000	0,013	6,600
0,058	0,750	0,008	6,300	0,220	0,000	0,013	5,500
0,000	0,750	0,006	4,100	0,130	0,000	0,013	5,600
0,070	0,410	0,007	1,400	0,800	0,000	0,022	7,100
0,071	0,390	0,007	1,200	0,770	0,000	0,023	8,800
0,000	0,380	0,016	2,100	1,800	0,000	0,027	5,600
0,071	0,130	0,007	15,000	0,510	0,000	0,044	17,000
0,056	0,110	0,006	10,000	0,360	0,000	0,037	20,000
0,000	0,079	0,000	16,000	1,300	0,000	0,041	16,000
0,000	0,115	0,018	8,000	0,128	0,000	0,017	1,200
0,220	0,083	0,016	1,600	0,039	0,000	0,010	0,950
0,036	0,077	0,015	0,470	0,068	0,000	0,008	0,940
0,022	0,073	0,025	0,310	0,430	0,000	0,010	1,100
0,023	0,069	0,028	2,200	0,360	0,000	0,010	1,000
0,000	0,080	0,024	0,640	0,510	0,000	0,013	0,970
0,000	0,155	0,020	2,900	0,173	0,000	0,023	1,320
0,000	0,083	0,021	1,020	0,130	0,000	0,009	3,600
0,000	0,072	0,022	0,730	0,066	0,000	0,007	1,000
0,103	0,130	0,160	1,400	0,560	0,000	0,012	8,500
0,000	0,160	0,170	1,610	0,260	0,000	0,015	8,700
0,123	0,140	0,190	1,530	0,240	0,000	0,014	8,400
0,034	0,075	0,020	2,000	1,200	0,000	0,011	9,200
0,048	0,079	0,019	2,600	0,960	0,000	0,013	9,100
0,036	0,092	0,017	0,900	0,690	0,000	0,013	8,700
0,044	0,680	0,003	14,000	0,870	0,034	0,026	4,500
0,027	0,730	0,005	5,700	0,570	0,000	0,025	4,100
0,032	1,400	0,004	10,000	1,100	0,000	0,028	54,000
0,045	0,092	0,003	0,340	0,240	0,000	0,047	1,200
0,000	0,100	0,004	2,100	0,210	0,000	0,045	1,600
0,022	0,079	0,002	1,500	0,190	0,000	0,042	1,300

La	Ce	Pr	Nd	Sm	Eu	Gd	Tb
0,460	0,840	0,089	0,310	0,062	0,012	0,056	0,008
0,420	0,740	0,082	0,300	0,059	0,015	0,044	0,009
0,350	0,590	0,063	0,230	0,041	0,009	0,039	0,006
0,410	0,770	0,081	0,310	0,058	0,340	0,044	0,008
0,340	0,660	0,070	0,250	0,041	0,046	0,052	0,007
0,480	0,880	0,093	0,340	0,059	0,007	0,068	0,008
0,180	0,310	0,034	0,180	0,034	0,005	0,018	0,003
0,240	0,450	0,048	0,260	0,031	0,005	0,028	0,005
0,200	0,340	0,035	0,190	0,026	0,000	0,018	0,002
0,420	0,880	0,098	2,000	0,075	0,010	0,057	0,011
0,430	0,910	0,096	2,000	0,070	0,007	0,078	0,010
0,470	0,980	0,099	1,900	0,073	0,009	0,069	0,008
0,310	0,590	0,062	16,000	0,042	0,009	0,038	0,004
0,330	0,600	0,060	16,000	0,041	0,009	0,030	0,009
0,300	0,600	0,068	16,000	0,041	0,021	0,021	0,004
0,520	0,920	0,095	0,930	0,074	0,009	0,049	0,007
0,520	0,930	0,093	0,960	0,066	0,010	0,063	0,008
0,550	1,100	0,120	0,980	0,078	0,013	0,055	0,008
0,180	0,170	0,018	16,000	0,008	0,000	0,007	0,002
0,170	0,120	0,019	17,000	0,007	0,000	0,007	0,001
0,190	0,130	0,020	17,000	0,005	0,000	0,009	0,001
1,200	0,250	0,026	19,000	0,013	0,004	0,009	0,001
1,700	0,260	0,025	19,000	0,013	0,003	0,012	0,001
1,700	0,520	0,055	19,000	0,034	0,000	0,028	0,005
0,200	0,240	0,031	19,000	0,015	0,000	0,010	0,000
0,160	0,170	0,028	19,000	0,004	0,000	0,005	0,000
0,160	0,110	0,021	18,000	0,005	0,005	0,006	0,001
0,420	0,710	0,075	0,300	0,045	0,013	0,041	0,004
0,420	0,790	0,085	0,300	0,043	0,016	0,043	0,007
0,430	0,790	0,076	0,310	0,061	0,000	0,046	0,006
1,800	0,720	0,090	16,000	0,066	0,013	0,050	0,006
1,700	0,660	0,083	15,000	0,053	0,009	0,052	0,006
1,800	0,700	0,088	15,000	0,045	0,018	0,046	0,006
1,500	0,760	0,091	35,000	0,054	0,009	0,044	0,006
1,500	0,750	0,088	36,000	0,054	0,008	0,037	0,007
1,100	0,660	0,076	29,000	0,053	0,009	0,042	0,005
0,760	0,160	0,026	2,600	0,017	0,003	0,009	0,002
0,650	0,150	0,025	2,800	0,013	0,005	0,014	0,002
0,700	0,160	0,026	2,600	0,015	0,003	0,016	0,001

Dy	Ho	Er	Tm	Yb	Lu	Hf	Ta
0,048	0,011	0,030	0,005	0,028	0,005	0,200	0,000
0,048	0,012	0,034	0,005	0,038	0,005	0,220	0,000
0,038	0,009	0,027	0,004	0,030	0,004	0,170	0,000
0,049	0,011	0,029	0,004	0,031	0,004	0,500	0,000
0,040	0,006	0,025	0,003	0,023	0,003	0,330	0,000
0,054	0,012	0,032	0,005	0,040	0,005	0,480	0,000
0,013	0,002	0,007	0,001	0,009	0,001	0,110	0,000
0,021	0,005	0,014	0,002	0,010	0,002	0,110	0,000
0,015	0,003	0,008	0,001	0,008	0,001	0,340	0,000
0,052	0,012	0,038	0,006	0,032	0,007	0,280	0,000
0,058	0,010	0,038	0,004	0,041	0,006	0,270	0,000
0,049	0,011	0,034	0,005	0,039	0,005	0,300	0,000
0,026	0,006	0,017	0,003	0,022	0,003	0,250	0,000
0,027	0,006	0,023	0,002	0,017	0,005	0,220	0,000
0,031	0,004	0,019	0,003	0,024	0,003	0,430	0,000
0,059	0,012	0,033	0,005	0,037	0,005	0,290	0,000
0,052	0,012	0,038	0,005	0,046	0,007	0,390	0,660
0,055	0,012	0,030	0,006	0,046	0,006	0,340	0,000
0,013	0,003	0,006	0,000	0,012	0,000	0,000	0,000
0,008	0,001	0,004	0,001	0,004	0,001	0,070	0,420
0,010	0,003	0,004	0,000	0,003	0,000	0,090	0,000
0,009	0,001	0,005	0,000	0,004	0,000	0,060	0,000
0,008	0,000	0,004	0,001	0,004	0,000	0,060	0,760
0,023	0,004	0,011	0,001	0,008	0,001	0,130	0,000
0,010	0,000	0,008	0,000	0,000	0,000	0,000	0,000
0,008	0,001	0,004	0,000	0,006	0,000	0,000	0,000
0,004	0,000	0,003	0,000	0,003	0,000	0,100	0,000
0,045	0,009	0,024	0,004	0,029	0,003	0,380	0,000
0,044	0,009	0,031	0,002	0,026	0,004	0,410	0,000
0,054	0,007	0,036	0,003	0,041	0,004	0,370	0,000
0,047	0,008	0,034	0,005	0,037	0,005	0,350	0,000
0,047	0,009	0,028	0,004	0,033	0,005	0,330	0,000
0,046	0,009	0,030	0,005	0,034	0,005	0,430	0,000
0,035	0,006	0,020	0,003	0,021	0,003	0,120	0,000
0,034	0,007	0,019	0,003	0,021	0,003	0,110	0,000
0,033	0,006	0,019	0,003	0,019	0,003	0,091	0,000
0,011	0,003	0,006	0,001	0,005	0,001	0,000	0,000
0,010	0,002	0,004	0,001	0,008	0,001	0,100	0,000
0,012	0,010	0,006	0,001	0,006	0,001	0,060	0,000

W	Tl	Pb	Bi	Th	Sample	types	brands
0,430	0,037	5,800	0,510	0,120	S1-A	Summer	Yokohama
0,300	0,037	5,100	0,520	0,100	S1-B	Summer	Yokohama
0,250	0,033	5,300	0,520	0,110	S1-C	Summer	Yokohama
0,120	0,200	13,000	0,690	0,200	S2-A	Summer	Kumho
0,470	0,280	21,000	1,400	0,150	S2-B	Summer	Kumho
0,280	0,180	9,100	0,520	0,230	S2-C	Summer	Kumho
0,310	0,180	26,000	2,800	0,062	S3-A	Winter studded	Kumho
0,240	0,190	26,000	3,000	0,100	S3-B	Winter studded	Kumho
0,790	0,180	28,000	3,100	0,074	S3-C	Winter studded	Kumho
0,250	0,030	33,000	0,320	0,170	C1-A	Winter studded	Continental
0,190	0,028	10,000	0,620	0,170	C1-B	Winter studded	Continental
0,680	0,019	9,900	0,300	0,180	C1-C	Winter studded	Continental
0,220	0,029	11,000	0,540	0,084	C2-A	Winter non-studded	Continental
1,800	0,033	12,000	2,500	0,096	C2-B	Winter non-studded	Continental
12,000	0,025	11,000	0,550	0,124	C2-C	Winter non-studded	Continental
0,230	0,026	9,900	0,230	0,230	C3-A	Summer	Continental
0,180	0,027	11,000	0,990	0,210	C3-B	Summer	Continental
0,300	0,024	9,500	0,310	0,200	C3-C	Summer	Continental
7,300	0,081	30,000	1,500	0,000	T1-A	Truck non-studded	Truck
0,140	0,088	31,000	1,400	0,021	T1-B	Truck non-studded	Truck
0,240	0,086	31,000	1,400	0,027	T1-C	Truck non-studded	Truck
0,710	0,075	4,400	0,410	0,029	T2-A	Truck unknown	Truck
0,070	0,073	4,400	0,320	0,029	T2-B	Truck unknown	Truck
0,160	0,067	4,500	0,440	0,073	T2-C	Truck unknown	Truck
0,000	0,160	5,800	0,660	0,000	T3-A	Truck unknown	Truck
0,260	0,160	6,100	0,320	0,000	T3-B	Truck unknown	Truck
1,400	0,160	5,300	5,200	0,000	T3-C	Truck unknown	Truck
0,330	0,061	8,700	0,620	0,140	NH4-A	Summer	Nokian
2,600	0,058	9,900	0,630	0,160	NH4-B	Summer	Nokian
0,390	0,057	8,900	0,630	0,150	NH4-C	Summer	Nokian
0,130	0,051	11,000	0,230	0,170	B1-A	Winter non-studded	Bridgestone
0,090	0,053	13,000	0,076	0,170	B1-B	Winter non-studded	Bridgestone
1,400	0,058	13,000	0,061	0,170	B1-C	Winter non-studded	Bridgestone
0,080	0,035	16,000	0,310	0,160	B2-A	Winter studded	Bridgestone
0,060	0,033	14,000	0,160	0,160	B2-B	Winter studded	Bridgestone
0,140	0,088	42,000	0,580	0,130	B2-C	Winter studded	Bridgestone
0,110	0,035	1,200	0,090	0,024	B3-A	Winter studded	Bridgestone
0,130	0,038	2,100	0,130	0,029	B3-B	Winter studded	Bridgestone
0,270	0,035	1,100	0,950	0,021	B3-C	Winter studded	Bridgestone

Figure 1: Box plot of most abundant elements found in TP_{ref}. Outliers are marked as “X”

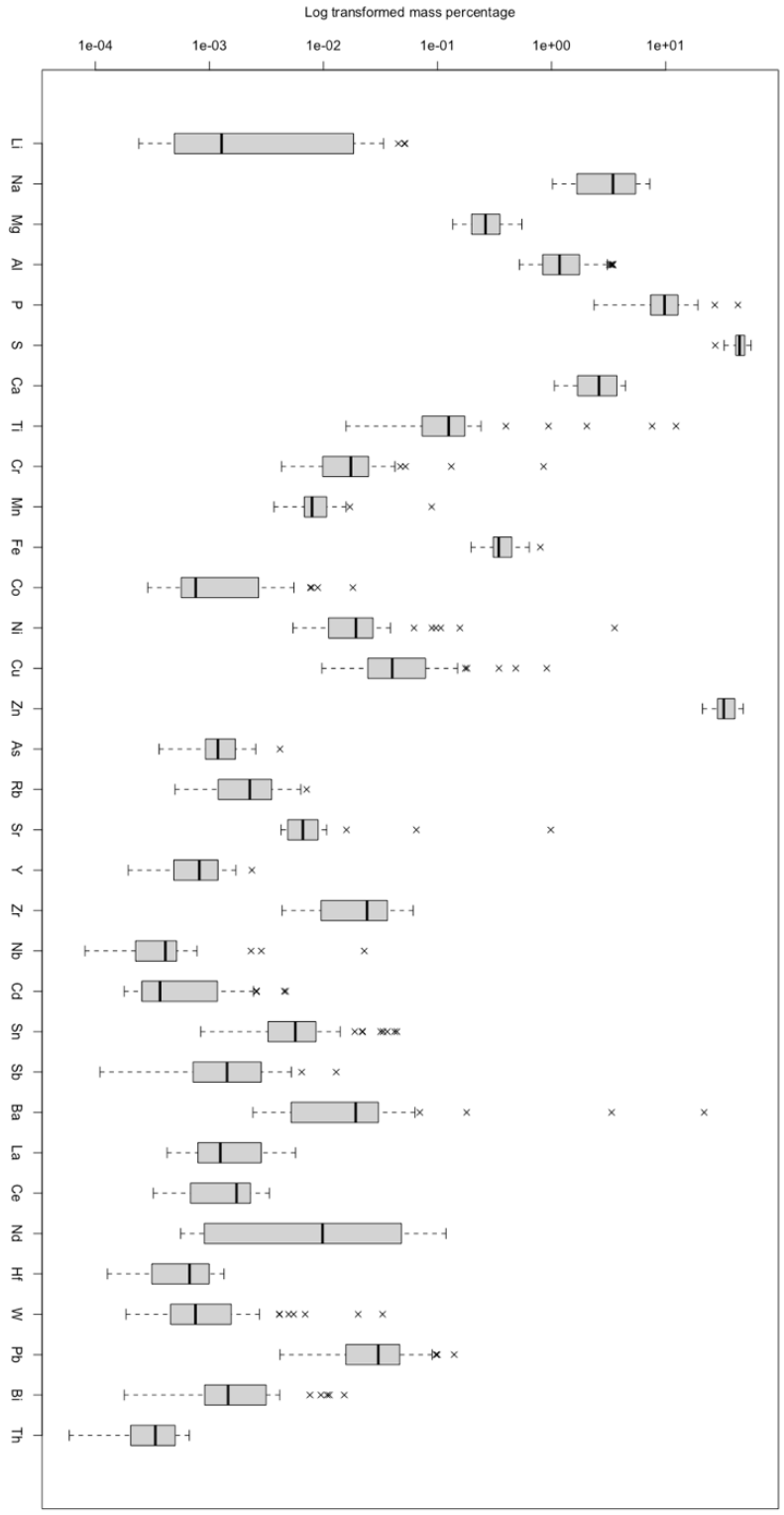

Figure 2: Plots of principal component analysis of TP_{ref}. A = Compositional differences found between all registered types of tires from the dataset. B = Compositional differences found between brands.

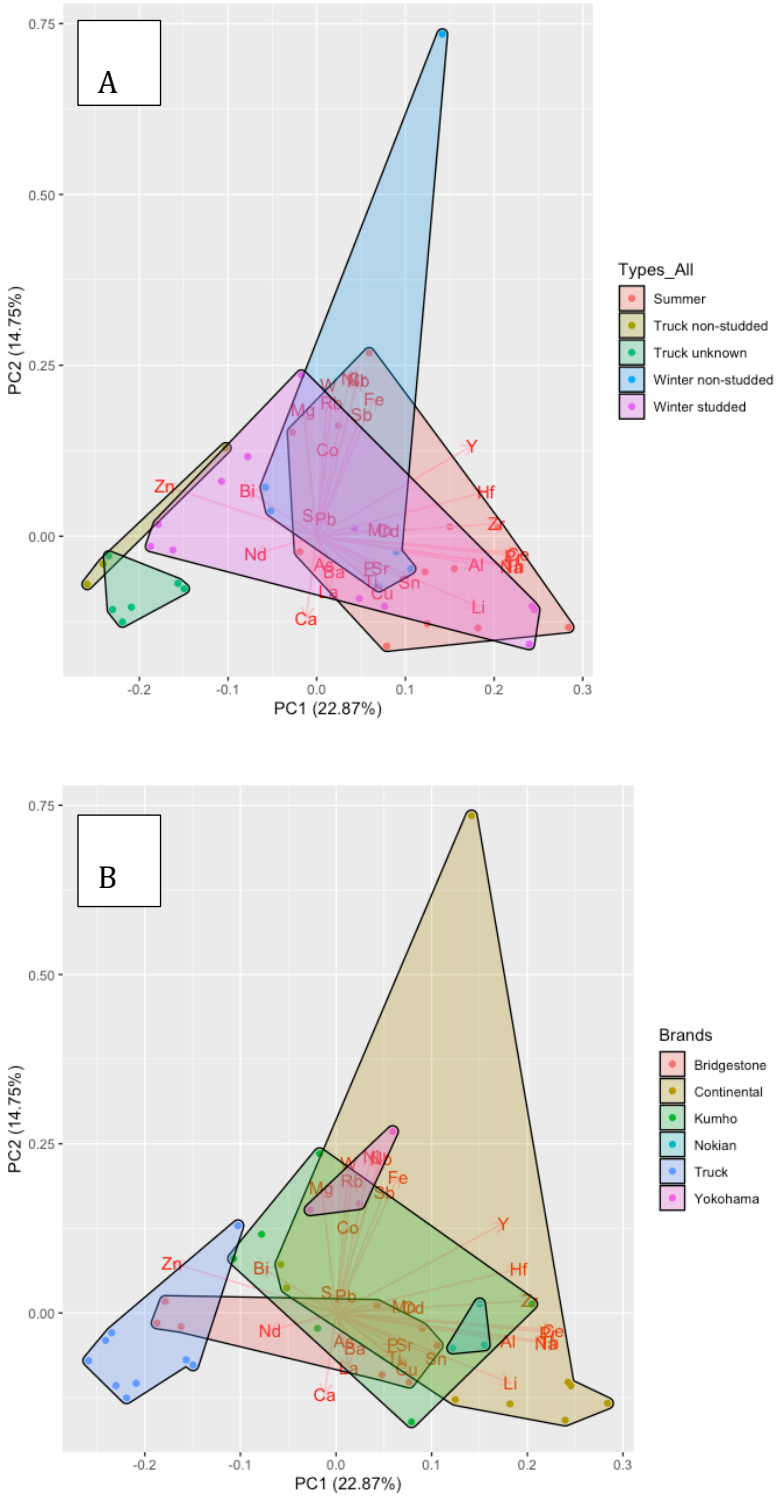

Appendix B: μ-XRF point scan measurements

Table 1: Normalized mass percentages measured with μ-XRF point scans of treated reference tire particles.

Spectrum	Na	Mg	Al	Si	P
TP_{ref} (treated)	5,565	0,070	0,175	2,071	0,108
TP_{ref} (treated)	6,647		0,006	2,996	
TP_{ref} (treated)	9,281		0,434	4,316	
TP_{ref} (treated)	5,107		0,176	10,178	
TP_{ref} (treated)	10,370		0,145	1,721	
TP_{ref} (treated)	8,408		0,220	2,280	0,085
TP_{ref} (treated)	8,252		0,199	4,127	
TP_{ref} (treated)	6,803		0,144	5,627	
TP_{ref} (treated)	10,157		0,081	1,380	0,006
TP_{ref} (treated)	9,598	0,124	0,150	1,128	0,014
TP_{ref} (treated)	7,503		0,272	1,436	
TP_{ref} (treated)	7,482	0,141	0,225	4,543	
TP_{ref} (treated)	6,080	0,040	0,086	1,399	0,013
TP_{ref} (treated)	5,538		0,272	13,821	
TP_{ref} (treated)	5,917	0,027	0,454	16,491	

S	Cl	K	Ca	Ti	Cr	Mn
15,318	68,230	0,304	2,646	0,049	0,025	0,043
6,843	77,649		2,912	0,073	0,043	
3,935	68,225	0,029	12,551	0,293	0,027	0,018
4,745	77,396		1,464	0,035	0,043	0,022
7,812	75,618		2,555	0,030	0,092	0,042
16,435	61,588	0,399	1,514	0,014		0,042
5,829	78,583	0,013	1,561	0,020	0,048	
4,532	80,091		1,477	0,064	0,029	0,016
2,411	84,377		1,077		0,039	0,007
11,157	71,701		2,387	0,070		
13,368	69,077		2,860	0,027		
8,756	74,702	0,034	2,520	0,049		
3,317	86,489		1,003	0,066	0,016	0,007
7,968	69,451		1,322	0,041	0,021	
7,123	64,606	0,084	1,465	0,059		0,014

Fe	Ni	Cu	Zn	Sr	Sm	Gd
0,388			5,011			
0,215			2,606	0,011		
0,125	0,008		0,638	0,026	0,053	0,039
0,118			0,703	0,012		
0,038			1,566	0,011		
0,092			8,919	0,005		
0,119			1,231	0,016		
0,102			1,101	0,015		
0,051		0,018	0,354	0,005		0,036
0,226			3,432	0,014		
0,078			5,377			
0,077			1,471			
0,097			1,388			
0,055			1,511			
0,122			3,639			

Table 2: Normalized mass percentages of untreated reference particles measured with µ-XRF point scans.

Spectrum	Al	Si	S	Cl	K	Ca
TP 1	0,59	75,26	18,48	0,94	0,08	2,54
TP 2	0,99	73,06	20,80	0,36	0,00	1,41
TP 3	0,93	71,87	20,83	0,61	0,00	1,97
TP 4	0,84	69,28	23,25	1,44	0,00	3,58
TP 5	0,15	53,22	32,11	3,94	0,00	8,24
TP 6	1,52	11,73	46,81	10,71	0,00	25,96
TP 7	0,96	61,82	26,33	3,43	0,00	5,87

Ti	Fe	Zn	Sr
0,09	0,09	1,88	0,05
0,04	0,09	3,22	0,03
0,06	0,12	3,58	0,04
0,00	0,13	1,41	0,07
0,26	0,37	1,51	0,20
0,01	0,62	1,98	0,65
0,02	0,13	1,32	0,13

Table 3: Normalized mass percentages of crystals found in mussel gills measured with μ-XRF point scans. One Particle were scanned on top of gill material, whilst four were removed and scanned separately.

Sample	Na	Mg	Al	Si	P
Crystal on Gill material	3,586	0,213	0,156	5,200	9,566
Crystal from gill 1	2,706	0,019	0,153	0,039	4,327
Crystal from gill 2	1,591	0,087	0,136	0,036	2,163
Crystal from gill 3	1,626	0,000	0,081		5,090
Crystal from gill 4	1,026	0,168	0,125		0,659

S	Cl	K	Ca	Ti	Cr	Mn
1,709	11,370		50,485	0,023		12,911
0,261	1,849		84,912	0,030	0,500	4,489
0,272	1,582		89,388	0,002		4,040
0,153	3,034		84,125			4,758
0,386	2,562	0,017	90,968			3,448

Fe	Ni	Cu	Zn	Br	Sr	Ba
2,924		0,012	1,180		0,402	0,264
0,258			0,405		0,052	
0,136		0,013	0,422		0,080	0,053
0,477	0,012		0,367	0,071	0,123	0,084
0,142			0,383		0,064	0,050

Table 4: Stomachs and mantles from duck mussels, digested with NaClO. Measurements are performed with µ-XRF point scans.

Sample	Na	Mg	Al	Si	P	S
L2-3	8,556	0,380	0,158	0,473	1,660	0,187
L2-3	11,417	0,179	0,098	0,019	1,457	0,295
L2-3	8,075	0,189	0,150	0,176	1,291	0,253
L2-3	10,054	0,060	0,073	1,347	1,032	0,231
L2-3	6,777	0,164	0,087	0,053	1,302	0,319
L2-2	8,859	0,158	0,211	1,417	1,635	0,360
L2-2	10,073	0,199	0,164	0,783	1,636	0,379
L2-2	7,676	0,146	1,066	2,910	1,919	0,367
L2-2	6,164	0,031	0,432	3,446	2,110	0,389
L2-2	8,296		0,347	1,602	1,667	0,365
L2-1	2,695	0,135	0,453	2,675	1,810	0,316
L2-1	3,732		0,240	1,279	1,949	0,320
L2-1	3,606		0,255	1,480	1,734	0,330
L2-1	3,478	0,108	0,747	4,671	1,929	0,317
L2-1	3,281	0,089	0,467	2,552	1,772	0,318
L1-3	27,611	0,154	0,065	0,122	0,355	0,186
L1-3	10,766	0,024	0,352	2,410	1,863	0,476
L1-3	14,043		0,129	0,709	1,824	0,452
L1-3	17,004	0,111	0,242	1,608	1,560	0,414
L1-3	13,119		0,100	0,872	2,384	0,482
L1-2	3,820	0,046	0,128	0,316	2,355	0,571
L1-2	4,015	0,152	0,456	3,709	2,386	0,381
L1-2	3,968	0,065	0,359	3,536	2,536	0,403
L1-2	3,207	0,128	0,039	0,445	2,703	0,545
L1-2	3,613	0,281	0,392	4,043	2,732	0,406
L1-1	7,097	0,036	0,252	1,893	1,815	0,589
L1-1	9,305	0,195	0,276	1,816	1,444	0,587
L1-1	11,020	0,110	0,407	5,098	1,972	0,505
L1-1	9,028	0,015	0,136	0,966	1,475	0,629
L1-1	10,851	0,134	0,207	1,516	1,253	0,472

Cl	K	Ca	Ti	Mn	Fe	Ni
83,598	0,009	2,990	0,090	0,317	1,087	
85,037		1,035	0,052	0,078	0,189	
87,679		1,608	0,009	0,068	0,290	
86,190		0,440	0,012	0,052	0,347	
90,358		0,517		0,066	0,173	
82,838	0,119	2,379	0,085	0,363	1,443	
83,341	0,042	2,242	0,039	0,234	0,770	0,006
79,693	1,363	2,799	0,083	0,702	1,113	
78,690	0,326	4,215	0,225	1,446	2,269	
81,443	0,214	4,113	0,101	0,544	1,183	
85,167	0,276	4,263	0,092	0,507	1,453	
86,822	0,133	3,827	0,087	0,426	1,051	
85,127	0,132	5,248	0,104	0,560	1,263	
78,373	0,863	6,544	0,209	0,737	1,846	
84,030	0,314	4,863	0,125	0,649	1,374	
68,272	0,006	1,030	0,011	0,345	0,380	
74,852	0,321	4,730	0,035	0,854	1,015	
74,561	0,006	4,217	0,036	0,786	0,838	
71,903	0,125	3,944	0,039	0,640	0,734	0,007
72,948		5,890	0,053	0,826	0,963	0,008
89,410		1,343	0,007	0,271	1,069	
80,118	0,219	4,468	0,151	0,751	2,043	
81,280	0,192	4,117	0,101	0,633	1,677	
87,248		2,213	0,035	0,628	1,398	
80,780	0,139	4,224	0,085	0,600	1,460	
82,793	0,083	1,804	0,086	0,338	1,409	
82,427	0,074	1,429	0,045	0,203	0,690	
73,756	0,203	2,989	0,089	0,528	1,529	
85,151	0,012	1,026	0,031	0,122	0,599	
83,104	0,036	0,918	0,018	0,122	0,362	

Cu	Zn	Br	Sr
0,010	0,485		
0,018	0,128		
0,012	0,199		
0,012	0,136	0,014	
0,025	0,160		
0,005	0,120		0,008
0,007	0,086		
0,010	0,153		
0,013	0,244		
0,009	0,116		
0,008	0,150		
0,013	0,121		
0,010	0,151		
0,018	0,161		
0,014	0,152		
0,046	1,408		0,010
0,077	2,182	0,013	0,007
0,063	2,300	0,020	0,014
0,054	1,592	0,015	0,008
0,079	2,262		0,013
0,049	0,615		
0,028	1,124		
0,030	1,103		
0,090	1,322		
0,030	1,215		
0,032	1,773		
0,028	1,457	0,023	
0,029	1,766		
0,029	0,767		
0,022	0,986		

Table 5: Normalized mass percentages of gills digested with NaClO measured with µ-XRF point scans.

Sample	Na	Mg	Al	Si	P	S
L2-3	6,818	0,147	0,397	1,923	8,135	0,069
L2-3	6,544	0,193	0,515	3,105	9,481	0,078
L2-3	6,221	0,243	0,626	2,945	9,023	0,093
L2-3	4,334	0,149	0,879	4,545	7,706	0,089
L2-3	5,669	0,130	1,306	5,685	9,037	0,068
L2-2	4,684	0,129	0,094	0,221	15,048	
L2-2	6,256	0,224	0,155	0,271	15,218	
L2-2	3,669	0,362	0,112	0,229	16,422	
L2-2	5,408	0,159	0,107	0,258	16,021	
L2-2	5,321	0,062	0,091	0,364	15,504	
L2-1	6,094	0,327	0,193	2,276	13,897	
L2-1	5,416	0,212	0,263	0,326	16,037	
L2-1	5,615	0,036	0,046	0,092	13,934	
L2-1	4,391	0,117	0,058	0,130	13,854	
L2-1	2,887	0,131	0,119	0,133	14,393	
L1-3	3,925	0,289	0,147	0,267	15,528	
L1-3	4,116	0,279	0,136	0,301	16,130	
L1-3	3,948	0,107	0,136	0,314	15,911	
L1-3	5,904	0,135	0,121	0,253	14,813	
L1-3	3,314		0,072	0,248	15,192	
L1-2	11,856	0,260	0,101	0,115	11,067	0,014
L1-2	6,515	0,298	0,101	0,116	13,511	
L1-2	17,274	0,265	0,094	0,102	5,920	0,047
L1-2	13,995	0,113	0,077	0,114	9,251	0,024
L1-2	5,890	0,284	0,084	0,110	14,377	
L1-1	3,099	0,150	0,086	0,368	14,898	
L1-1	1,204	0,253	0,083	0,251	15,112	
L1-1	1,598	0,179	0,081	0,466	14,587	
L1-1	1,648	0,319	0,120	0,503	13,490	
L1-1	1,979	0,181	0,096	0,262	15,063	

Cl	K	Ca	Ti	Mn	Fe	Cu
37,349	0,136	33,518	0,112	6,111	4,433	0,015
34,440	0,352	31,442	0,100	6,426	6,289	0,014
37,163	0,642	32,515	0,098	5,791	3,874	0,008
33,384	0,564	34,895	0,148	6,784	5,520	0,015
28,279	0,561	36,007	0,109	7,105	5,101	0,019
16,131		48,248	0,019	12,250	1,920	0,005
11,507		50,487	0,012	12,717	1,933	0,005
11,479		51,954	0,035	12,749	1,837	0,007
13,642		49,737	0,030	11,616	2,008	0,010
12,903		50,229	0,038	12,416	1,907	0,008
13,187	0,375	47,226	0,094	12,210	2,677	0,008
13,635	0,179	48,256	0,021	12,649	1,516	0,005
12,160		50,550	0,018	14,389	1,529	0,010
18,731		46,190	0,037	13,055	1,793	0,010
12,176		51,430	0,015	15,243	1,630	0,008
10,742		49,180	0,054	12,937	5,339	0,011
10,221		50,199	0,038	12,283	4,958	0,004
11,349		48,355	0,027	12,941	5,381	0,009
16,052		45,332	0,034	11,602	4,490	0,004
13,016		50,280	0,026	11,584	4,732	0,014
31,549		34,790	0,040	6,290	3,046	
21,667		43,231	0,047	8,861	4,176	0,010
48,774		21,258	0,024	3,722	1,919	0,005
36,237		30,530	0,028	5,817	2,926	
15,902		47,726	0,026	9,652	4,452	0,011
15,064		48,961	0,051	9,773	5,689	0,022
12,265		50,994	0,040	11,001	6,548	0,034
15,594		48,899	0,058	10,330	6,173	0,024
16,529		48,110	0,065	10,590	6,483	0,030
14,826		48,608	0,049	10,626	6,245	0,030

Zn	Br	Sr	Ba
0,597		0,068	0,171
0,735		0,116	0,169
0,534		0,062	0,164
0,689	0,031	0,075	0,193
0,650		0,067	0,207
0,731		0,250	0,270
0,709		0,216	0,290
0,671		0,199	0,276
0,570		0,169	0,264
0,681		0,203	0,272
0,962		0,224	0,252
1,006		0,208	0,271
1,113		0,239	0,270
1,148		0,260	0,227
1,255		0,296	0,283
0,899		0,320	0,362
0,752		0,221	0,362
0,883		0,265	0,374
0,700		0,197	0,364
0,885		0,282	0,354
0,513		0,130	0,229
0,955		0,214	0,300
0,374	0,014	0,088	0,119
0,551		0,119	0,219
0,892	0,019	0,192	0,382
1,341		0,150	0,348
1,661		0,173	0,379
1,520		0,176	0,314
1,607		0,182	0,322
1,533		0,148	0,355

Figure 1: Spectrum of different samples. Peaks illustrates which elements that is found in the samples. The y-axis gives the unit in counts second^{-1} eV^{-1}(CPS/eV) and the x-axis shows the energy of the received signals.

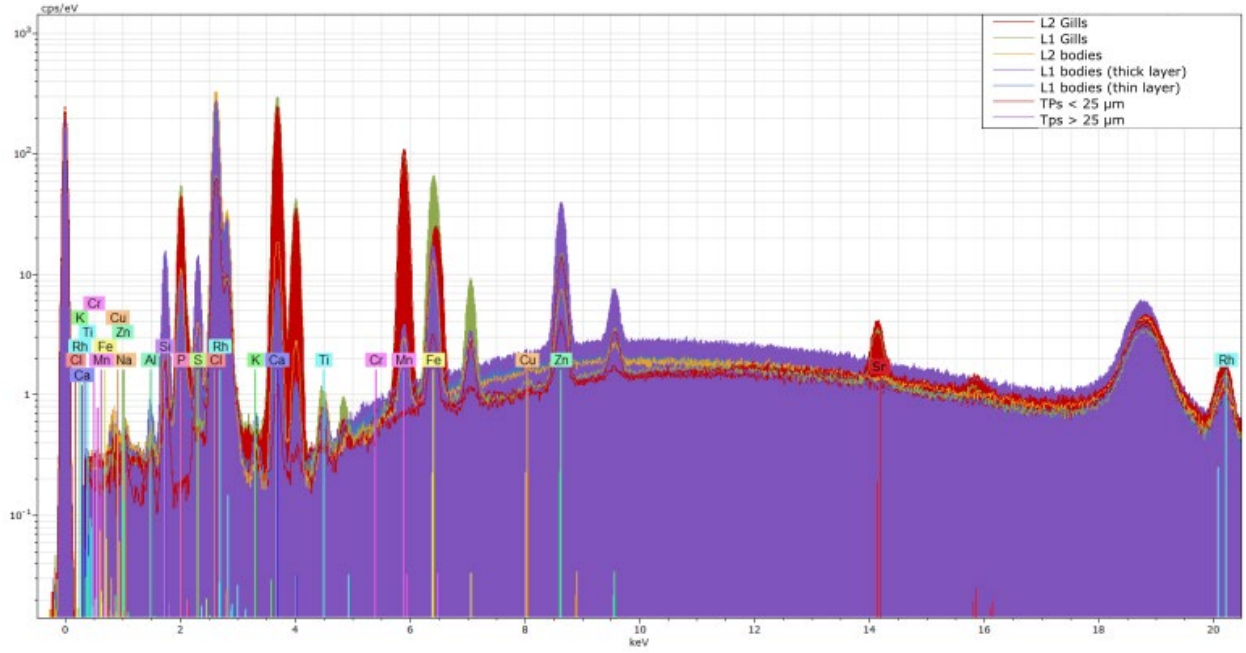

Appendix C: Counted potential particles in mussels

Table 1: Counted potential TRWP in from images captured with microscopy (table). Sample ID means location and image number, two Images were captured of each individual for each magnification level. Hence, L1-1 and L1-2 are different images from the same mussel.

SAMPLE ID	LOCATION	MAGNIFICATION LEVEL	POTENTIAL PARTICLES
L1-1	L1	Low	30
L1-2	L1	Low	22
L1-3	L1	Low	27
L1-4	L1	Low	22
L1-5	L1	Low	3
L1-6	L1	Low	0
L2-1	L2	Low	4
L2-2	L2	Low	3
L2-3	L2	Low	6
L2-4	L2	Low	6
L2-5	L2	Low	3
L2-6	L2	Low	1
L1-1	L1	High	15
L1-2	L1	High	14
L1-3	L1	High	17
L1-4	L1	High	26
L1-5	L1	High	3
L1-6	L1	High	5
L2-1	L2	High	5
L2-2	L2	High	4
L2-3	L2	High	3
L2-4	L2	High	8
L2-5	L2	High	2
L2-6	L2	High	2

Norges miljø- og biovitenskapelige universitet
Noregs miljø- og biovitskapelege universitet
Norwegian University of Life Sciences

Postboks 5003
NO-1432 Ås
Norway